RDECOM TR 10-D-108

**U.S. ARMY RESEARCH,
DEVELOPMENT AND
ENGINEERING COMMAND**

TITLE: The S407, S409, and S410 Airfoils

AUTHOR: **Dan M. Somers**

COMPANY NAME: **Airfoils, Incorporated**

COMPANY ADDRESS: **122 Rose Drive
Port Matilda PA 16870-7535**

DATE: **August 2010**

FINAL REPORT: **Contract Number W911W6-07-C-0047, SBIR Phase II,
Topic Number A06-006, Proposal Number A2-2972**

Prepared for:

U.S. ARMY RESEARCH, DEVELOPMENT AND ENGINEERING COMMAND, AVIATION APPLIED TECHNOLOGY DIRECTORATE, FORT EUSTIS, VA 23604-5577

AIRFOILS, INCORPORATED
122 ROSE DRIVE
PORT MATILDA, PA 16870-7535 USA
WEBSITE WWW.AIRFOILS.COM
TELEPHONE (814) 357-0500
FACSIMILE (814) 357-0357

THE S407, S409, AND S410 AIRFOILS

DAN M. SOMERS

AUGUST 2010

ABSTRACT

A family of airfoils, the S407, S409, and S410, intended for a high-altitude, tandem-rotor helicopter has been designed and analyzed theoretically. The two primary objectives of high maximum lift, relatively insensitive to roughness, and low profile drag have been achieved. The constraints on the pitching moments and airfoil thicknesses have been satisfied.

INTRODUCTION

Almost all airfoils in use on rotorcraft today were developed under the assumption that extensive laminar flow is not likely on a rotor. (See ref. 1, for example.) Because the airfoil family designed under the present effort is intended for a high-altitude, tandem-rotor helicopter with its attendant low Reynolds numbers, however, the achievement of laminar flow warrants exploration. To complement the design effort, the primary airfoil of this family was investigated in The Pennsylvania State University Low-Speed, Low-Turbulence Wind Tunnel (ref. 2). This family is part of an effort sponsored by the U.S. Army to design theoretically and verify experimentally several airfoils for rotorcraft applications.

SYMBOLS

C_p	pressure coefficient
c	airfoil chord, mm
c_d	section profile-drag coefficient
c_l	section lift coefficient
c_m	section pitching-moment coefficient about quarter-chord point
M	free-stream Mach number
R	Reynolds number based on free-stream conditions and airfoil chord
t	airfoil thickness, mm
x	airfoil abscissa, mm
α	angle of attack relative to x-axis, deg

Subscripts:

dd	drag divergence

ll	lower limit of low-drag range
max	maximum
min	minimum
S	separation
T	transition
ul	upper limit of low-drag range
0	zero lift

Abbreviations:

L.	lower surface
S.	boundary-layer separation location, x_S/c
T.	boundary-layer transition location, x_T/c
U.	upper surface

AIRFOIL DESIGN

OBJECTIVES AND CONSTRAINTS

The design specifications for the airfoil family are contained in table I. The family consists of three airfoils: primary, tip, and root.

Two primary objectives are evident from the specifications. The first objective is to achieve high maximum lift coefficients. A requirement related to this objective is that the maximum lift coefficients not decrease significantly with transition fixed near the leading edge on both surfaces. In addition, the airfoils should exhibit docile stall characteristics. The second objective is to obtain low profile-drag coefficients over the specified ranges of lift coefficients.

Two major constraints were placed on the design of the airfoil family. First, the zero-lift pitching-moment coefficients must be greater than or equal to the values specified. It should be noted that the positive pitching-moment coefficient of the root airfoil is used to balance the negative pitching-moment coefficient of the primary airfoil on the rotor. Second, the airfoil thicknesses must be greater than the values specified.

PHILOSOPHY

Given the above objectives and constraints, certain characteristics of the designs are apparent. The following sketch illustrates a drag polar that meets the goals for the primary airfoil. (The polars for the tip and root airfoils should be qualitatively similar.)

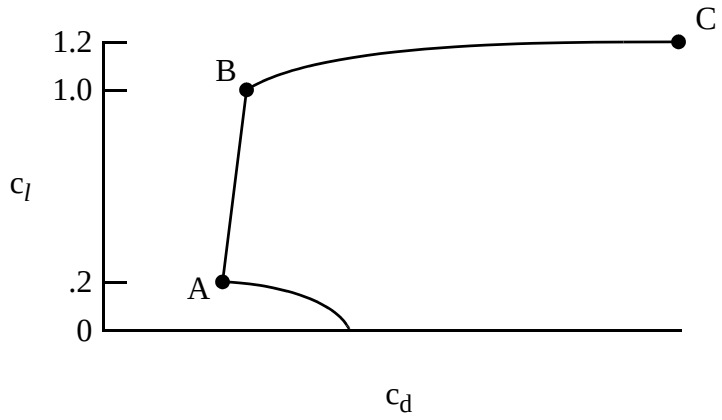

Sketch 1

The desired airfoil shape can be traced to the pressure distributions that occur at the various points in sketch 1. Point A is the lower limit of the low-drag range of lift coefficients; point B, the upper limit. The profile-drag coefficient at point B is not as low as at point A, unlike the polars of many laminar-flow airfoils where the drag coefficient within the laminar bucket is nearly constant. (See, for example, ref. 3.) This characteristic is related to the elimination of significant (i.e., drag-producing) laminar separation bubbles on the upper surface for the design range of Reynolds numbers. (See ref. 4.) The drag coefficient increases rapidly outside the low-drag, lift-coefficient range because boundary-layer transition moves quickly toward the leading edge with increasing (or decreasing) lift coefficient. This feature results in a leading-edge shape that produces a suction peak at higher lift coefficients, which ensures that transition on the upper surface will occur very near the leading edge. Thus, the maximum lift coefficient, point C, occurs with turbulent flow along the entire upper surface and, therefore, should be relatively insensitive to roughness at the leading edge.

From the preceding discussion, the pressure distributions along the polar can be deduced. The pressure distribution at point A for the primary airfoil should look something like sketch 2.

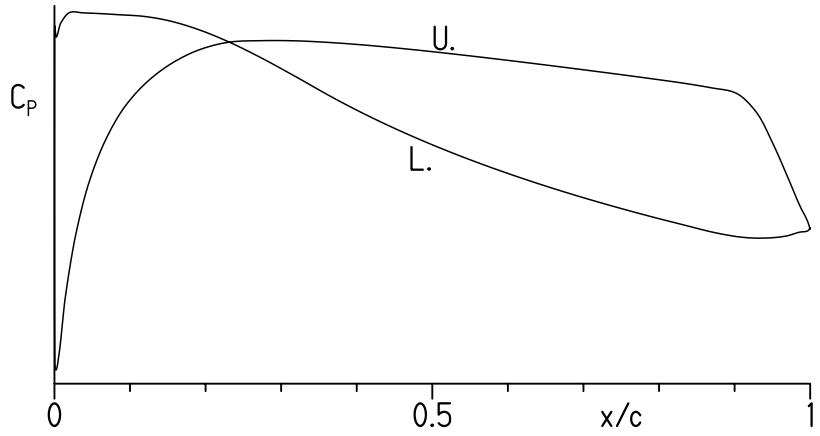

Sketch 2

To achieve low drag, a favorable pressure gradient is desirable along the upper surface to about 30-percent chord. This region is followed by a very slightly convex pressure recovery. The specific pressure recovery employed represents a compromise between maximum lift, drag, pitching moment, stall characteristics, and drag divergence. The steep, adverse pressure gradient aft of about 90-percent chord is a "separation ramp," originally proposed by F. X. Wortmann,[1] which confines turbulent separation to a small region near the trailing edge. By constraining the movement of the separation point at high angles of attack, higher lift coefficients can be achieved with little drag penalty. (See ref. 5.) This feature has the added benefit of promoting docile stall characteristics. (See ref. 6.)

Along the lower surface, the pressure gradient is briefly favorable and then slightly adverse to about 10-percent chord. Aft of this point, a short region having a shallow, adverse pressure gradient (i.e., a "transition ramp") promotes the efficient transition from laminar to turbulent flow (ref. 7). The curved transition ramp (ref. 4) is followed a concave pressure recovery, which exhibits lower drag and has less tendency to separate than the corresponding linear or convex pressure recovery (ref. 7). The pressure recovery must begin much farther forward than optimum for low drag to alleviate separation at lower lift coefficients, especially with transition fixed near the leading edge.

The amounts of pressure recovery on the upper and lower surfaces are determined by the airfoil-thickness and pitching-moment constraints.

---

[1]Director, Institute for Aerodynamics and Gas Dynamics, University of Stuttgart, Germany, 1974–1985.

At point B, the pressure distribution should look like sketch 3.

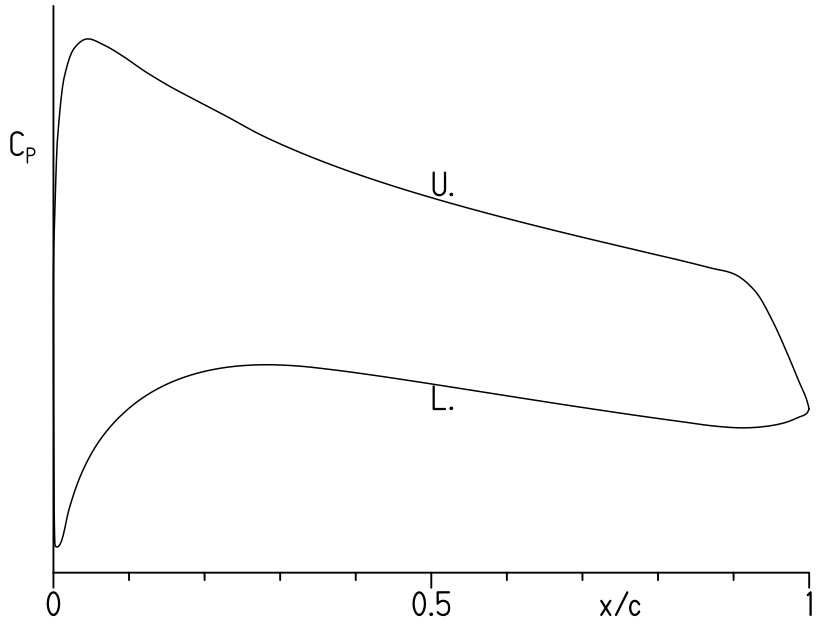

Sketch 3

No suction peak exists at the leading edge. Instead, a rounded peak occurs aft of the leading edge, which allows some laminar flow, although not to the extent of point A. Because the pressure gradient along the lower surface is favorable farther aft, the extent of laminar flow is greater than at point A.

EXECUTION

Given the pressure distributions previously discussed, the design of the airfoils is reduced to the inverse problem of transforming the pressure distributions into airfoil shapes. The Eppler Airfoil Design and Analysis Code (refs. 8 and 9) was used because of its unique capability for multipoint design and because of confidence gained during the design, analysis, and experimental verification of many other airfoils. (See ref. 10, for example.)

The primary airfoil is designated the S407. The tip and root airfoils, the S409 and S410, respectively, were derived from the S407 airfoil to assure the aerodynamic and geometric compatibilities of the three airfoils. The airfoil shapes and coordinates are available from Airfoils, Incorporated. The S407 airfoil thickness is 11.43-percent chord; the S409, 9.89-percent chord; and the S410, 8.51-percent chord, which satisfy the design constraints.

THEORETICAL PROCEDURE

The results are predicted using the method of references 8 and 9 (PROFIL07), commonly known as the Eppler code, and the method of reference 11 (MSES 3.0). Critical amplification factors of 11 and 9 were specified for the boundary-layer transition computations using the method of references 8 and 9 and the method of reference 11, respectively. It should be noted that the compressibility correction (ref. 12) incorporated in the method of references 8 and 9 is invalid if the local flow is supersonic.

Computations were performed over the range of operational conditions in table I with transition free (smooth) and with transition fixed near the leading edge, 5-percent chord on the upper surface and 10-percent chord on the lower surface, to simulate full-chord, turbulent flow. It should be noted that the S409 and S410 airfoils require a turbulator (i.e., a trip) on the lower surface at 90- and 83-percent chord, respectively, to prevent laminar separation without turbulent reattachment.

DISCUSSION OF RESULTS

S407 AIRFOIL

Pressure Distributions

The pressure distributions for the S407 airfoil predicted using the method of reference 11 at various angles of attack at a Mach number of 0.20 and a Reynolds number of 147,000 with transition free are shown in figure 1. At an angle of attack of −3.00° (fig. 1(a)), laminar separation, without turbulent reattachment, occurs forward of the trailing edge on the upper surface and a short laminar separation bubble is evident on the lower surface around 50-percent chord. As the angle of attack is increased, the bubble moves aft (fig. 1(a)). At an angle of attack of −1.00° (fig. 1(a)), a short laminar separation bubble is evident on the upper surface just forward of the trailing edge. As the angle of attack is increased, the bubble on the upper surface moves forward, whereas the bubble on the lower surface continues to move aft, eventually disappearing by an angle of attack of 4.00° (fig. 1(b)). At an angle of attack of 9.00° (fig. 1(d)), turbulent, trailing-edge separation is evident on the upper surface. The amount of separation increases with increasing angle of attack (fig. 1(d)). The maximum lift coefficient occurs at an angle of attack of approximately 12° (fig. 1(d)). As the angle of attack is increased further, the separation point continues to move forward, but the leading-edge peak does not collapse (fig. 1(e)).

The pressure distributions predicted at various angles of attack at a Mach number of 0.50 and a Reynolds number of 368,000 with transition free are shown in figure 2. At an angle of attack of −1.00° (fig. 2(a)), a short laminar separation bubble is evident on the upper surface just forward of the trailing edge and on the lower surface around 50-percent chord. As the angle of attack is increased, the bubble on the upper surface moves forward, whereas the bubble on the lower surface moves aft (figs. 2(a)–2(c)). At an angle of attack of 6.00° (fig. 2(c)), the flow near the leading edge on the upper surface is supersonic and the bubble on

the lower surface has disappeared. At an angle of attack of 7.00° (fig. 2(c)), turbulent, trailing-edge separation is evident on the upper surface, but no wave drag is predicted.

The pressure distributions predicted at various angles of attack at a Mach number of 0.70 and a Reynolds number of 552,000 with transition free are shown in figure 3. At an angle of attack of −4.00° (fig. 3(a)), a short laminar separation bubble is evident on the upper surface just forward of the trailing edge and on the lower surface around 25-percent chord, where the flow is supersonic. As the angle of attack is increased, the bubble on the upper surface moves forward, whereas the bubble on the lower surface moves aft (figs. 3(a) and 3(b)). At an angle of attack of −2.50° (fig. 3(b)), the flow is subsonic everywhere and remains subsonic up to an angle of attack of about −1.5°.

Section Characteristics

The section characteristics of the S407 airfoil with transition free predicted using the method of references 8 and 9 (PROFIL07) and the method of reference 11 (MSES 3.0) are shown in figure 4. The results are in reasonable agreement, especially considering the low Reynolds numbers. The method of reference 11 generally predicts lower profile-drag coefficients probably because it predicts transition farther aft. At a Mach number of 0.20 and a Reynolds number of 147,000 (fig. 4(a)), both methods predict a maximum lift coefficient that exceeds the design objective of 1.20. At a Mach number of 0.70 and a Reynolds number of 552,000 (fig. 4(c)), the method of references 8 and 9 predicts the lower limit of the low-drag, lift-coefficient range is about 0.2, which meets the design objective; the method of reference 11 predicts about 0.3, which is above the objective. At a Mach number of 0.50 and a Reynolds number of 368,000 (fig. 4(b)), both methods predict the maximum lift-to-drag ratio occurs at a lift coefficient of about 1.0, which meets the design objective. (Because the upper limit of the low-drag range is not sharply defined, a precise value for the upper limit cannot be given.) At a Mach number of 0.70 and a Reynolds number of 552,000 (fig. 4(c)), the method of reference 11 predicts a zero-lift pitching-moment coefficient of −0.15, which satisfies the design constraint.

The effect of fixing transition on the section characteristics predicted using the method of references 8 and 9 is shown in figure 5. The maximum lift coefficient is unaffected by fixing transition (fig. 5(a)), whereas the drag coefficients are adversely affected.

The effect of fixing transition on the section characteristics predicted using the method of reference 11 is shown in figure 6. The maximum lift coefficient increases with transition fixed (fig. 6(a)), which is an atypical result for high Reynolds numbers, but not uncommon for low Reynolds numbers. This result is probably caused by the elimination of the upper-surface laminar separation bubble. The drag coefficients are adversely affected by fixing transition. The magnitude of the zero-lift pitching-moment coefficient at a Mach number of 0.70 and a Reynolds number of 552,000 decreases slightly with transition fixed (fig. 6(c)).

Based on the predictions, all the design objectives and constraints for the S407 airfoil have essentially been met.

S409 AIRFOIL

Pressure Distributions

The pressure distributions for the S409 airfoil predicted using the method of reference 11 at various angles of attack at a Mach number of 0.55 and a Reynolds number of 303,000 with transition free are shown in figure 7. At an angle of attack of −1.00° (fig. 7(a)), a short laminar separation bubble is evident on the upper surface around 70-percent chord. (It should be remembered that the S409 airfoil requires a turbulator on the lower surface at 90-percent chord to prevent laminar separation without turbulent reattachment.) As the angle of attack is increased, the bubble on the upper surface moves forward (figs. 7(a)–7(c)). At an angle of attack of 5.00° (fig. 7(c)), the flow near the leading edge on the upper surface is supersonic. The maximum lift coefficient occurs at an angle of attack of approximately 8° (fig. 7(d)), although the local Mach number exceeds 1.3.

The pressure distributions predicted at various angles of attack at a Mach number of 0.58 and a Reynolds number of 319,000 with transition free are shown in figure 8. At an angle of attack of −1.00° (fig. 8(a)), a short laminar separation bubble is evident on the upper surface around 65-percent chord. As the angle of attack is increased, the bubble moves forward (figs. 8(a)–8(c)). At an angle of attack of 5.00° (fig. 8(c)), the flow near the leading edge on the upper surface is supersonic. At an angle of attack of 8.00° (fig. 8(c)), the local Mach number exceeds 1.3 and significant wave drag is predicted.

The pressure distributions predicted at various angles of attack at a Mach number of 0.76 and a Reynolds number of 409,000 with transition free are shown in figure 9. At an angle of attack of −1.50° (fig. 9(a)), a short laminar separation bubble is evident on the upper surface around 55-percent chord. The flow is locally supersonic on both surfaces. As the angle of attack is increased, the bubble on the upper surface moves forward to about 45-percent chord, where it remains relatively stationary (figs. 9(a) and 9(b)).

Section Characteristics

The section characteristics of the S409 airfoil with transition free predicted using the method of references 8 and 9 (PROFIL07) and the method of reference 11 (MSES 3.0) are shown in figure 10. The results are in good agreement, especially considering the low Reynolds numbers. (It should be remembered that the compressibility correction incorporated in the method of refs. 8 and 9 is invalid if the local flow is supersonic and, accordingly, only subsonic results are shown.) The method of reference 11 generally predicts lower drag coefficients probably because it predicts transition farther aft on the upper surface. At a Mach number of 0.55 and a Reynolds number of 303,000 (fig. 10(a)), the method of reference 11 predicts a maximum lift coefficient that exceeds the design objective of 1.00. At a Mach number of 0.76 and a Reynolds number of 409,000 (fig. 10(c)), the method of reference 11 predicts the lower limit of the low-drag range is below 0, which surpasses the design objective of 0.10, and the zero-lift pitching-moment coefficient is 0.00, which meets the design constraint. At a Mach number of 0.58 and a Reynolds number of 319,000 (fig. 10(b)), the method of ref-

erence 11 predicts the maximum lift-to-drag ratio occurs at a lift coefficient of about 0.8, which is below the design objective of 0.90. The drag-divergence Mach number at a lift coefficient of 0.00 and a Reynolds number of 420,000 is predicted to be 0.77, which is below the design goal of 0.78.

The effect of fixing transition on the section characteristics predicted using the method of references 8 and 9 is shown in figure 11. The drag coefficients are adversely affected by fixing transition.

The effect of fixing transition on the section characteristics predicted using the method of reference 11 is shown in figure 12. The maximum lift coefficient is essentially unaffected by fixing transition (fig. 12(a)), whereas the drag coefficients are adversely affected. The pitching-moment coefficients at a Mach number of 0.76 and a Reynolds number of 409,000 are more negative with transition fixed (fig. 12(c)) and the drag-divergence Mach number increases to 0.78.

Based on the predictions, all the design objectives and constraints for the S409 airfoil have essentially been met.

S410 AIRFOIL

Pressure Distributions

The pressure distributions for the S410 airfoil predicted using the method of reference 11 at various angles of attack at a Mach number of 0.18 and a Reynolds number of 185,000 with transition free are shown in figure 13. At an angle of attack of –1.00° (fig. 13(a)), a short laminar separation bubble is evident on the upper surface around 65-percent chord and on the lower surface near the leading edge. As the angle of attack is increased, the bubble on the upper surface moves forward, whereas the bubble on the lower surface moves aft, until laminar flow extends to the turbulator at 83-percent chord at an angle of attack of 1.00° (fig. 13(a)). At an angle of attack of 11.00° (fig. 13(d)), turbulent, trailing-edge separation is evident on the upper surface. The maximum lift coefficient occurs at an angle of attack of about 12° (fig. 13(d)). As the angle of attack is increased further, the separation point moves forward, but the leading-edge peak does not collapse (fig. 13(d)).

The pressure distributions predicted at various angles of attack at a Mach number of 0.425 and a Reynolds number of 437,000 with transition free are shown in figure 14. At an angle of attack of –1.00° (fig. 14(a)), a short laminar separation bubble is evident on the upper surface around 55-percent chord and on the lower surface near the leading edge. As the angle of attack is increased, the bubble on the upper surface moves forward, whereas the bubble on the lower surface moves aft, until laminar flow extends to the turbulator at 83-percent chord at an angle of attack of 2.00° (fig. 14(b)). The flow is subsonic at all angles of attack shown.

Section Characteristics

The section characteristics of the S410 airfoil with transition free predicted using the method of references 8 and 9 (PROFIL07) and the method of reference 11 (MSES 3.0) are shown in figure 15. The results are in reasonable agreement, especially considering the low Reynolds numbers. The method of reference 11 generally predicts lower drag coefficients probably because it predicts transition farther aft on the upper surface. At a Mach number of 0.18 and a Reynolds number of 185,000 (fig. 15(a)), the method of references 8 and 9 and the method of reference 11 predict maximum lift coefficients of about 1.0 and 1.2, respectively, which meets the design objective. At a Mach number of 0.425 and a Reynolds number of 437,000 (fig. 15(c)), both methods predict the lower limit of the low-drag range is below 0.2, which meets the design objective. At a Mach number of 0.20 and a Reynolds number of 206,000 (fig. 15(b)), the method of references 8 and 9 predicts the maximum lift-to-drag ratio occurs at a lift coefficient of about 0.65, which is below the design objective of 0.80; the method of reference 11 predicts the design objective is met. At a Mach number of 0.425 and a Reynolds number of 437,000 (fig. 15(c)), the method of references 8 and 9 and the method of reference 11 predict the zero-lift pitching-moment coefficient is 0.07 and 0.05, respectively, which satisfies the design constraint.

The effect of fixing transition on the section characteristics predicted using the method of references 8 and 9 and the method of reference 11 is shown in figures 16 and 17, respectively. The maximum lift coefficient (figs. 16(a) and 17(a)) and the zero-lift pitching-moment coefficient (figs. 16(c) and 17(c)) are essentially unaffected by fixing transition, whereas the drag coefficients are adversely affected.

Based on the predictions, all the design objectives and constraints for the S410 airfoil have essentially been met.

CONCLUDING REMARKS

A family of airfoils, the S407, S409, and S410, intended for a high-altitude, tandem-rotor helicopter has been designed and analyzed theoretically. The two primary objectives of high maximum lift coefficients, relatively insensitive to roughness, and low profile-drag coefficients have been achieved. The constraints on the zero-lift pitching-moment coefficients and airfoil thicknesses have been satisfied.

ACKNOWLEDGMENTS

This effort was sponsored by the U.S. Army. Preston B. Martin served as the technical monitor.

REFERENCES

1. Noonan, Kevin W.: Aerodynamic Characteristics of Two Rotorcraft Airfoils Designed for Application to the Inboard Region of a Main Rotor Blade. NASA TP-3009, 1990.

2. Somers, Dan M.; and Maughmer, Mark D.: Design and Experimental Results for the S407 Airfoil. U.S. Army RDECOM TR 10-D-109, 2010. (Available from DTIC.)

3. Abbott, Ira H.; Von Doenhoff, Albert E.; and Stivers, Louis S., Jr.: Summary of Airfoil Data. NACA Rep. 824, 1945. (Supersedes NACA WR L-560.)

4. Eppler, Richard; and Somers, Dan M.: Airfoil Design for Reynolds Numbers Between 50,000 and 500,000. Proceedings of the Conference on Low Reynolds Number Airfoil Aerodynamics, UNDAS-CP-77B123, Univ. of Notre Dame, June 1985, pp. 1–14.

5. Eppler, R.: Comparison of Theoretical and Experimental Profile Drags. NASA TT F-16981, 1976. (Translated from Schweizer Aero-Revue, vol. 38, no. 10, Oct. 1963, pp. 593–595.)

6. Maughmer, Mark D.; and Somers, Dan M.: Design and Experimental Results for a High-Altitude, Long-Endurance Airfoil. J. Aircr., vol. 26, no. 2, Feb. 1989, pp. 148–153.

7. Wortmann, F. X.: Experimental Investigations on New Laminar Profiles for Gliders and Helicopters. TIL/T.4906, British Minist. Aviat., Mar. 1960. (Translated from Z. Flugwissenschaften, Bd. 5, Heft 8, Aug. 1957, S. 228–243.)

8. Eppler, Richard: Airfoil Design and Data. Springer-Verlag (Berlin), 1990.

9. Eppler, Richard: Airfoil Program System “PROFIL07.” User’s Guide. Richard Eppler, c.2007.

10. Somers, Dan M.: Subsonic Natural-Laminar-Flow Airfoils. Natural Laminar Flow and Laminar Flow Control, R. W. Barnwell and M. Y. Hussaini, eds., Springer-Verlag New York, Inc., 1992, pp. 143–176.

11. Drela, M.: Design and Optimization Method for Multi-Element Airfoils. AIAA Paper 93-0969, Feb. 1993.

12. Labrujere, Th. E.; Loeve, W.; and Sloof, J. W.: An Approximate Method for the Determination of the Pressure Distribution on Wings in the Lower Critical Speed Range. Transonic Aerodynamics. AGARD CP No. 35, Sept. 1968, pp. 17-1–17-10.

TABLE I.- AIRFOIL DESIGN SPECIFICATIONS

(a) Primary airfoil

Parameter	Objective/ Constraint	Mach Number M	Reynolds Number R	Priority
Minimum lift coefficient $c_{l,min}$	0.15	0.70	552,000	Low
Maximum lift coefficient $c_{l,max}$	1.20	0.20	147,000	High
Lower limit of low-drag, lift-coefficient range $c_{l,ll}$	0.20	0.70	552,000	High
Upper limit of low-drag, lift-coefficient range $c_{l,ul}$	1.00	0.50	368,000	Medium
Zero-lift pitching-moment coefficient $c_{m,0}$	≥ -0.15	0.70	552,000	Low
Thickness t/c	> 0.06			Low
Other requirements: Maximum lift coefficient $c_{l,max}$ independent of leading-edge roughness Docile stall characteristics				

TABLE I.- Continued

(b) Tip airfoil

Parameter	Objective/ Constraint	Mach Number M	Reynolds Number R	Priority
Minimum lift coefficient $c_{l,min}$	0.00	0.76	409,000	Low
Maximum lift coefficient $c_{l,max}$	1.00	0.55	303,000	High
Lower limit of low-drag, lift-coefficient range $c_{l,ll}$	0.10	0.76	409,000	High
Upper limit of low-drag, lift-coefficient range $c_{l,ul}$	0.90	0.58	319,000	Medium
Zero-lift pitching-moment coefficient $c_{m,0}$	≥ 0.00	0.76	409,000	Medium
Thickness t/c	> 0.05			Low
Other requirements: Maximum lift coefficient $c_{l,max}$ independent of leading-edge roughness Docile stall characteristics Drag-divergence Mach number $M_{dd} > 0.78$ at $c_l = 0.00$				

TABLE I.- Concluded

(c) Root airfoil

Parameter	Objective/ Constraint	Mach Number M	Reynolds Number R	Priority
Minimum lift coefficient $c_{l,min}$	0.10	0.425	437,000	Low
Maximum lift coefficient $c_{l,max}$	1.00	0.18	185,000	High
Lower limit of low-drag, lift-coefficient range $c_{l,ll}$	0.20	0.425	437,000	High
Upper limit of low-drag, lift-coefficient range $c_{l,ul}$	0.80	0.20	206,000	Low
Zero-lift pitching-moment coefficient $c_{m,0}$	≥ 0.05	0.425	437,000	Medium
Thickness t/c	> 0.05			Low
Other requirements: Maximum lift coefficient $c_{l,max}$ independent of leading-edge roughness Docile stall characteristics				

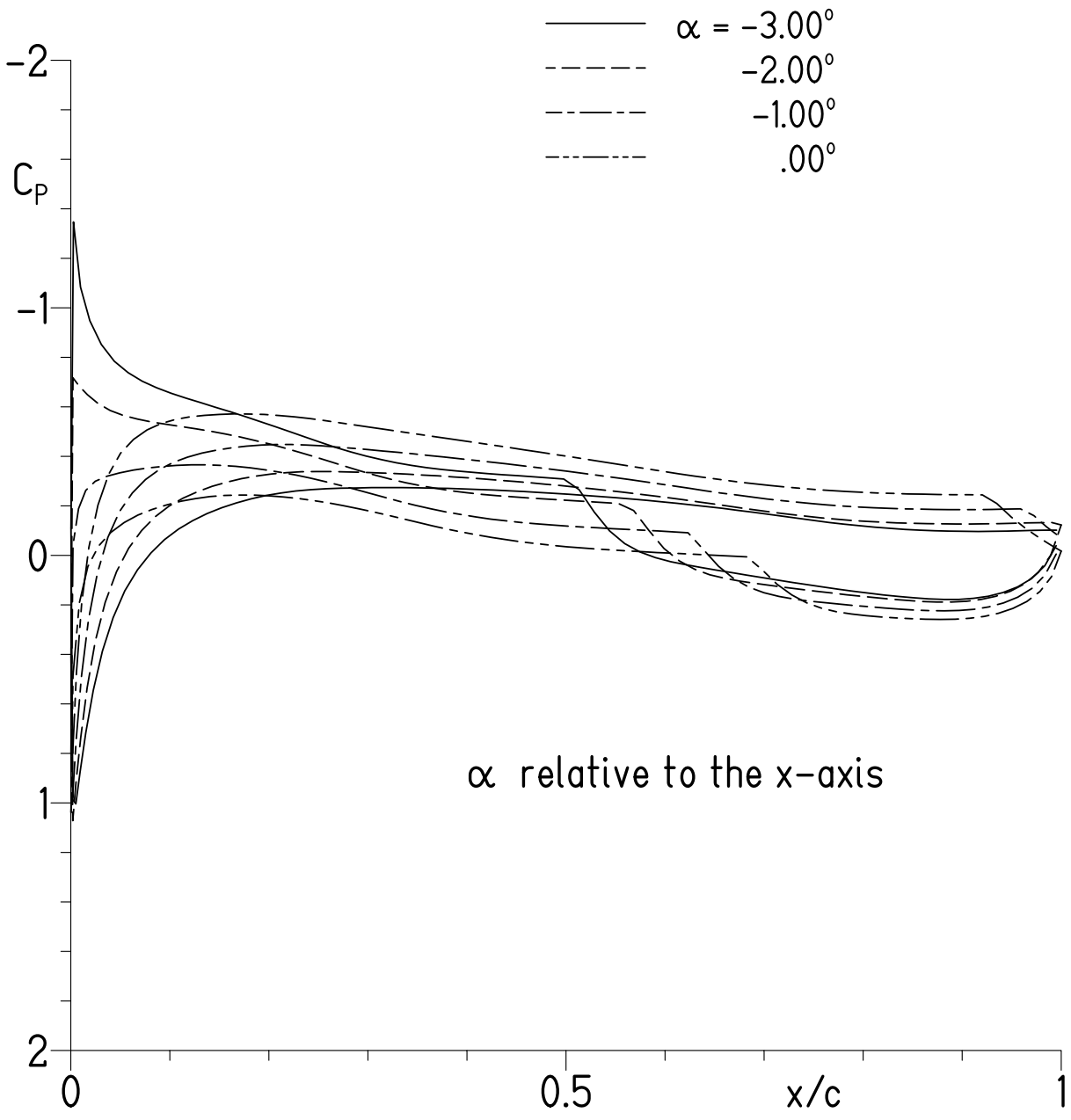

(a) $\alpha = -3.00°, -2.00°, -1.00°$, and $0.00°$.

Figure 1.- Pressure distributions for S407 airfoil at M = 0.20 and R = 147,000 with transition free.

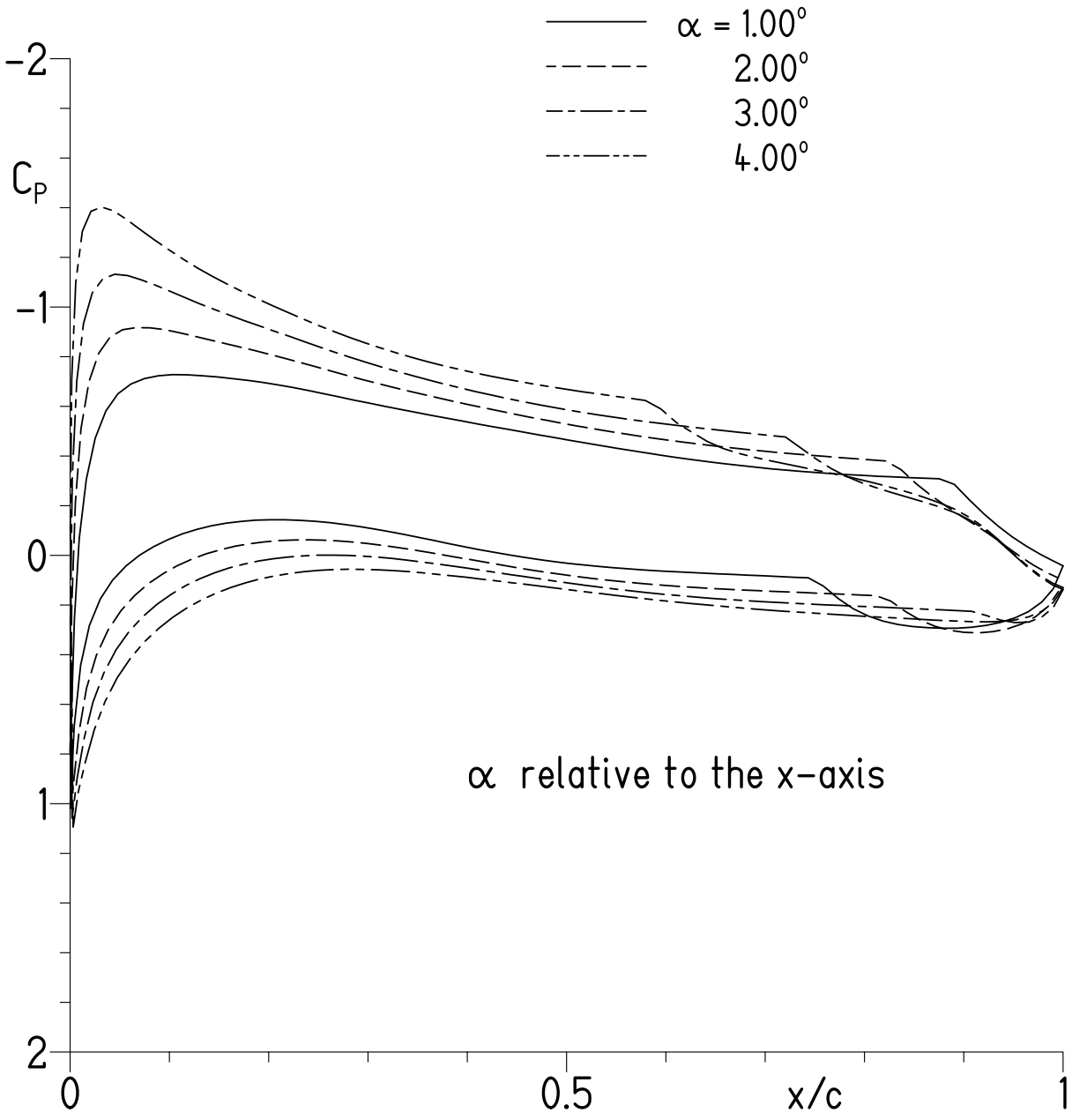

(b) $\alpha = 1.00°, 2.00°, 3.00°$, and $4.00°$.

Figure 1.- Continued.

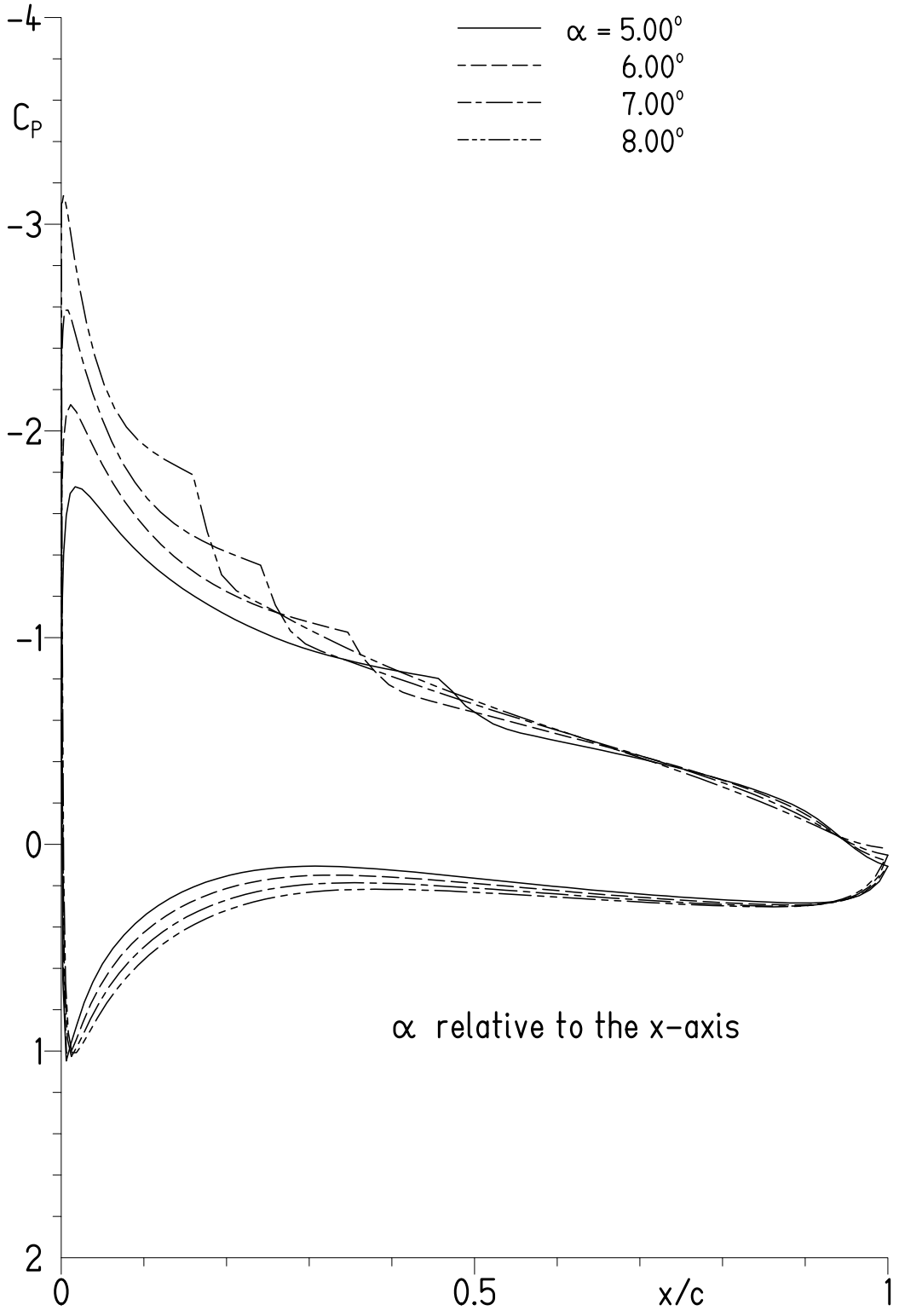

(c) $\alpha = 5.00°$, 6.00°, 7.00°, and 8.00°.

Figure 1.- Continued.

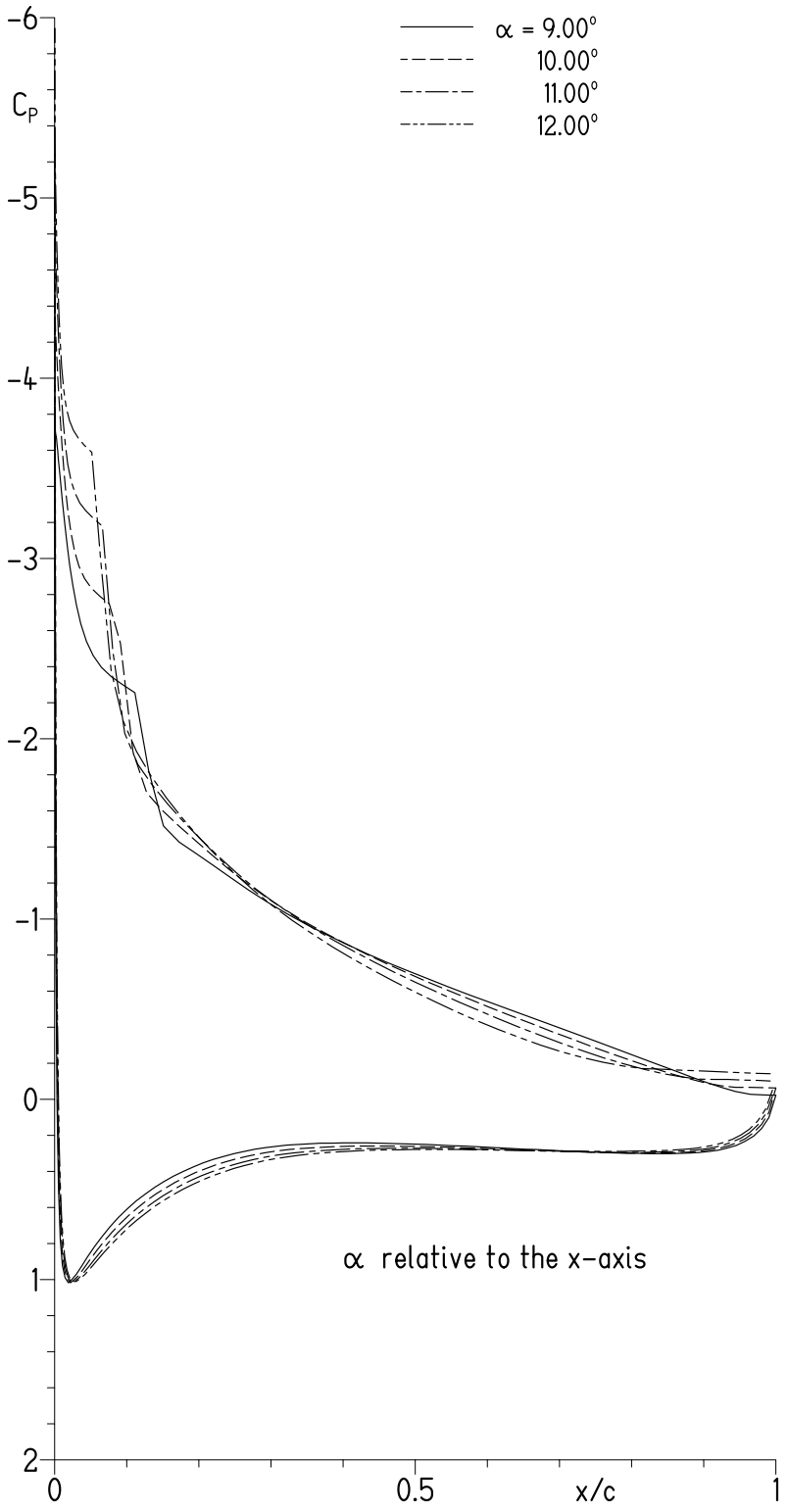

(d) $\alpha = 9.00°$, 10.00°, 11.00°, and 12.00°.

Figure 1.- Continued.

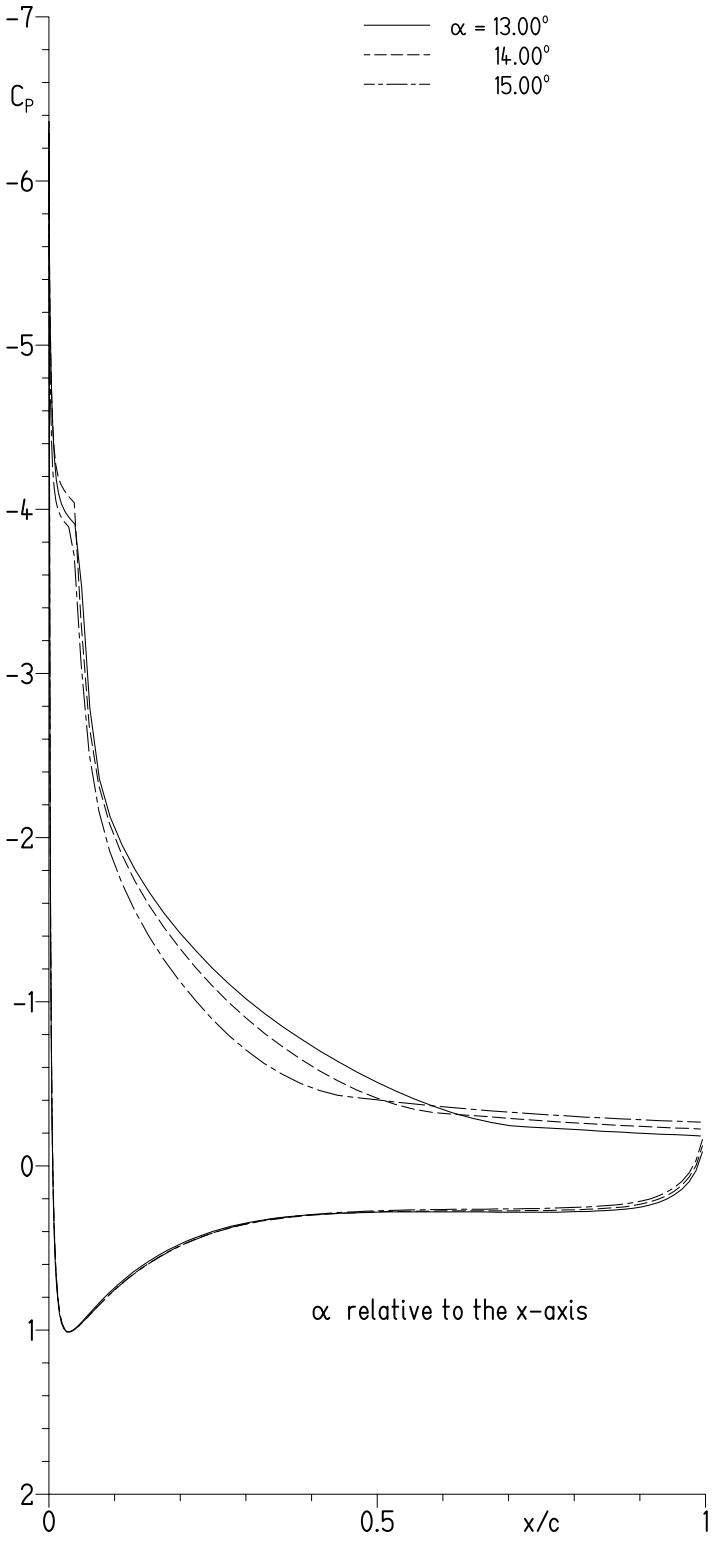

(e) $\alpha = 13.00°$, 14.00°, and 15.00°.

Figure 1.- Concluded.

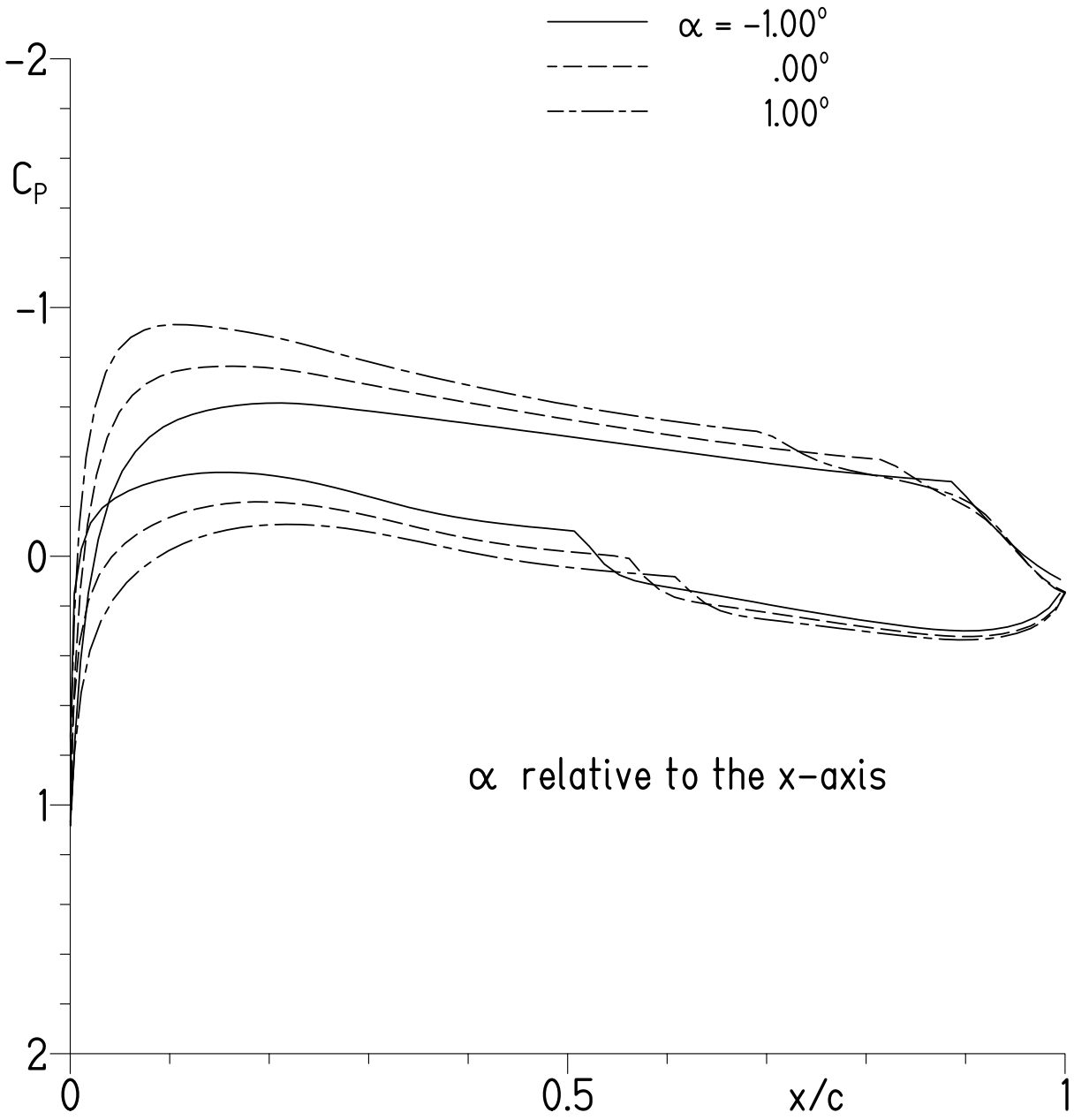

(a) $\alpha = -1.00°$, 0.00°, and 1.00°.

Figure 2.- Pressure distributions for S407 airfoil at M = 0.50 and R = 368,000 with transition free.

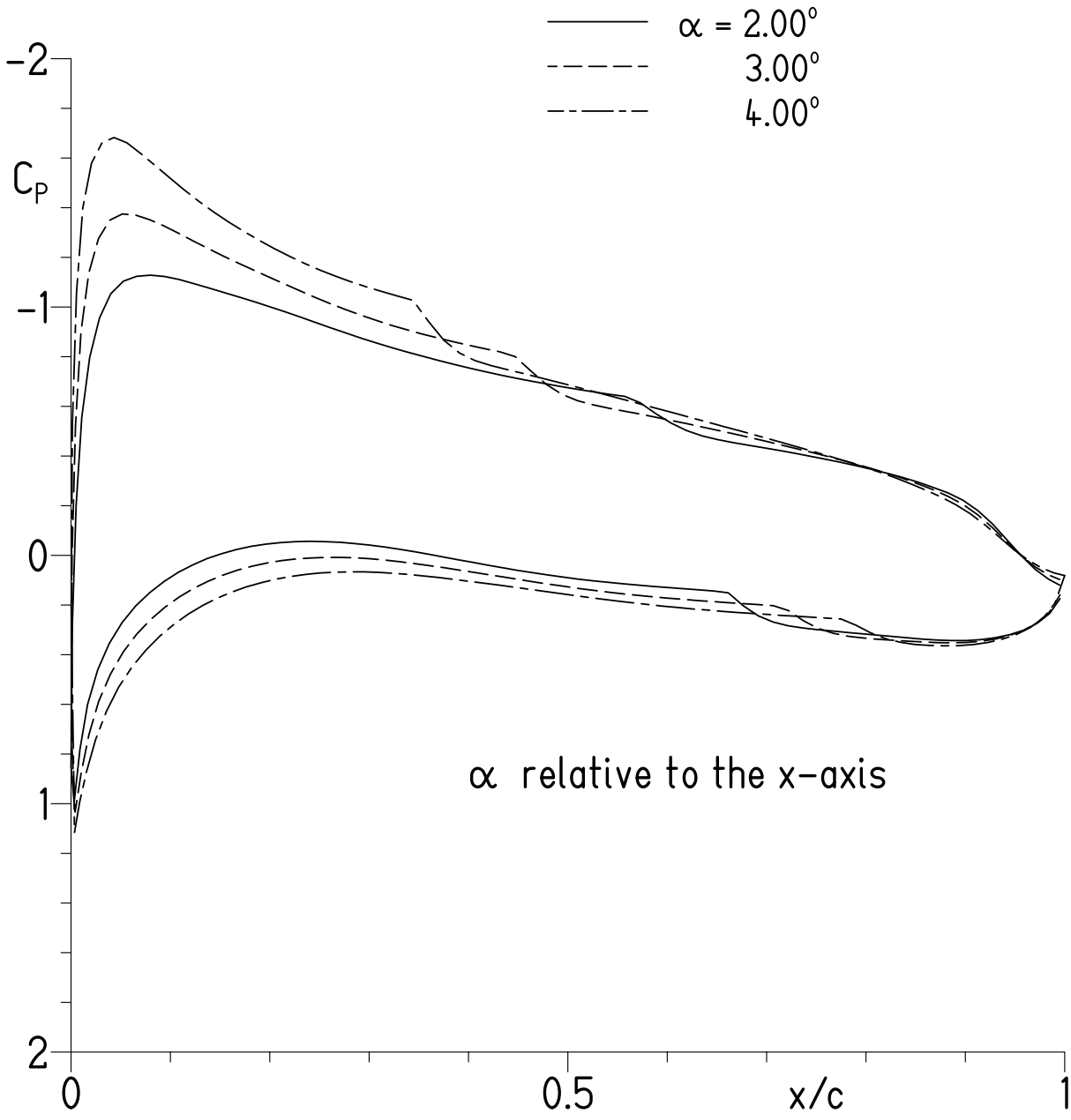

(b) $\alpha = 2.00°$, 3.00°, and 4.00°.

Figure 2.- Continued.

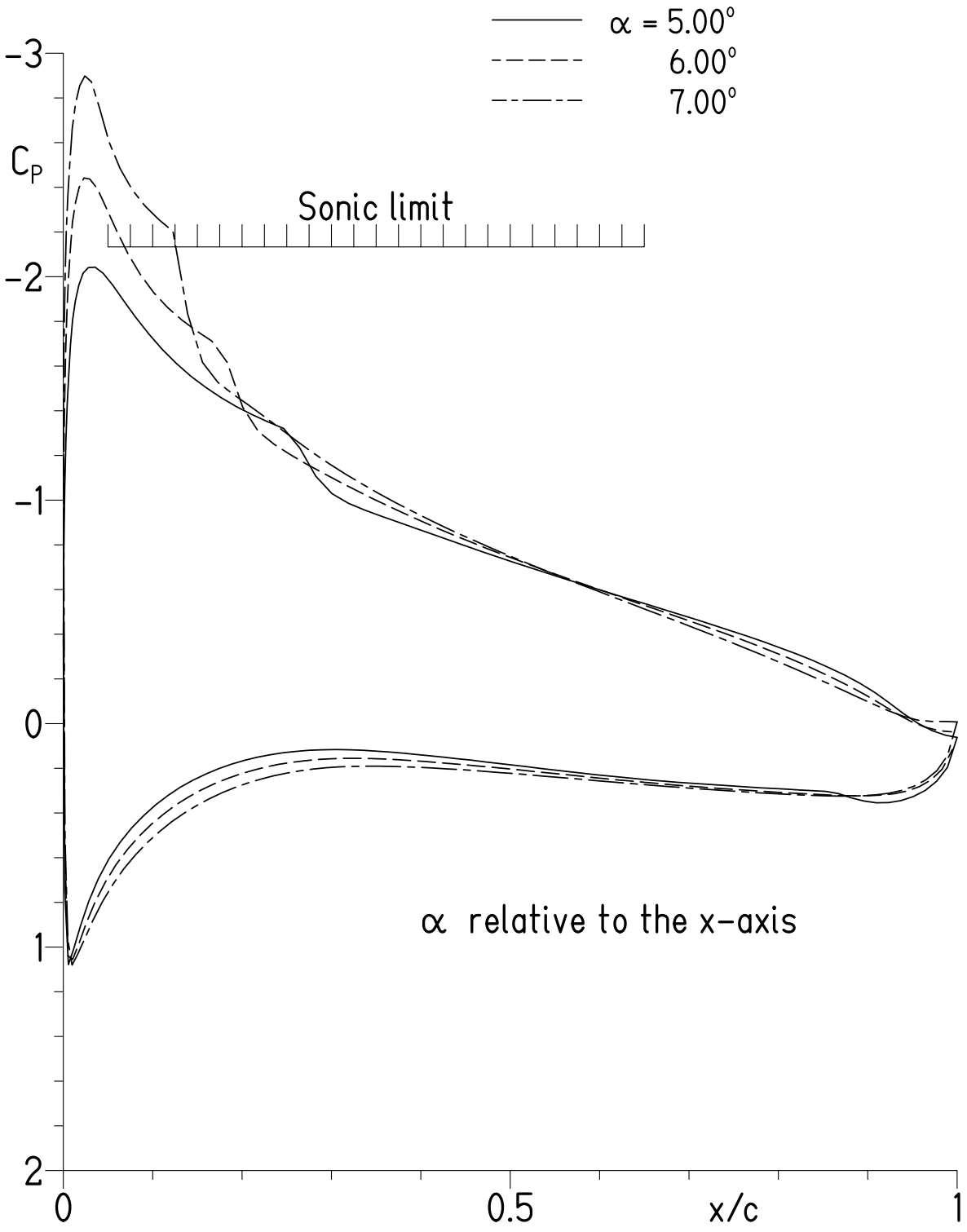

(c) $\alpha = 5.00°$, 6.00°, and 7.00°.

Figure 2.- Concluded.

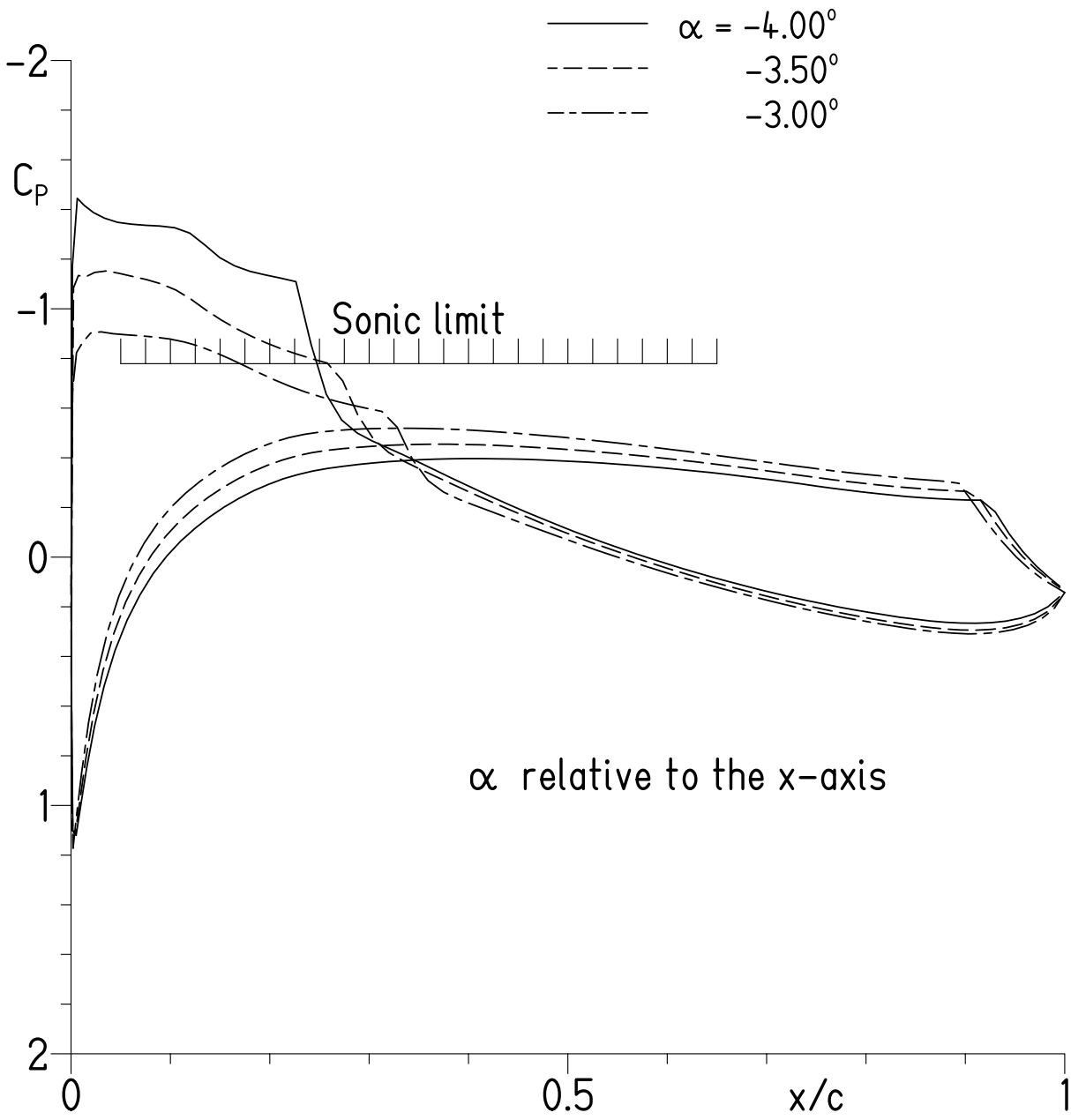

(a) $\alpha = -4.00°, -3.50°$, and $-3.00°$.

Figure 3.- Pressure distributions for S407 airfoil at M = 0.70 and R = 552,000 with transition free.

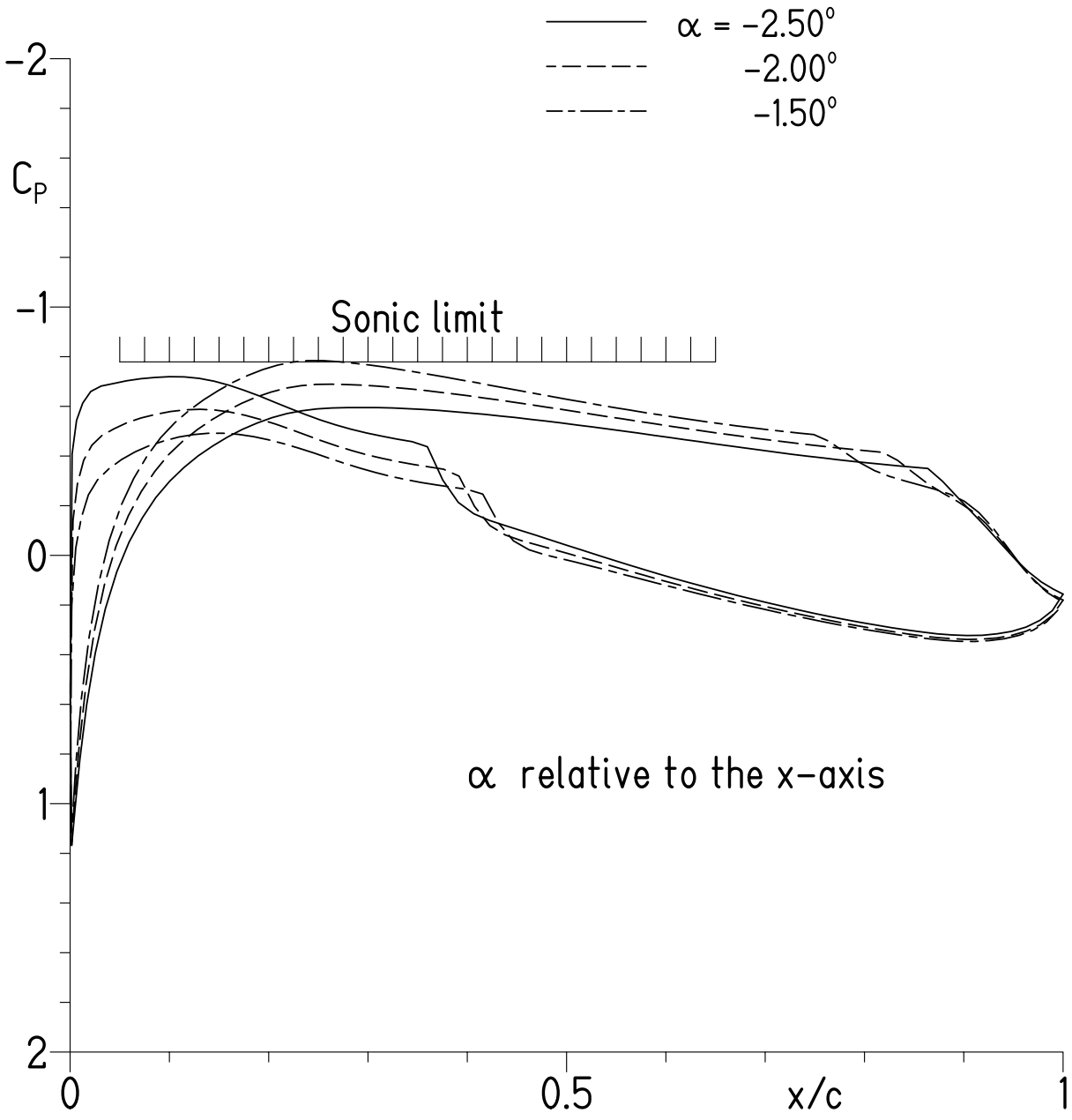

(b) $\alpha = -2.50°$, $-2.00°$, and $-1.50°$.

Figure 3.- Concluded.

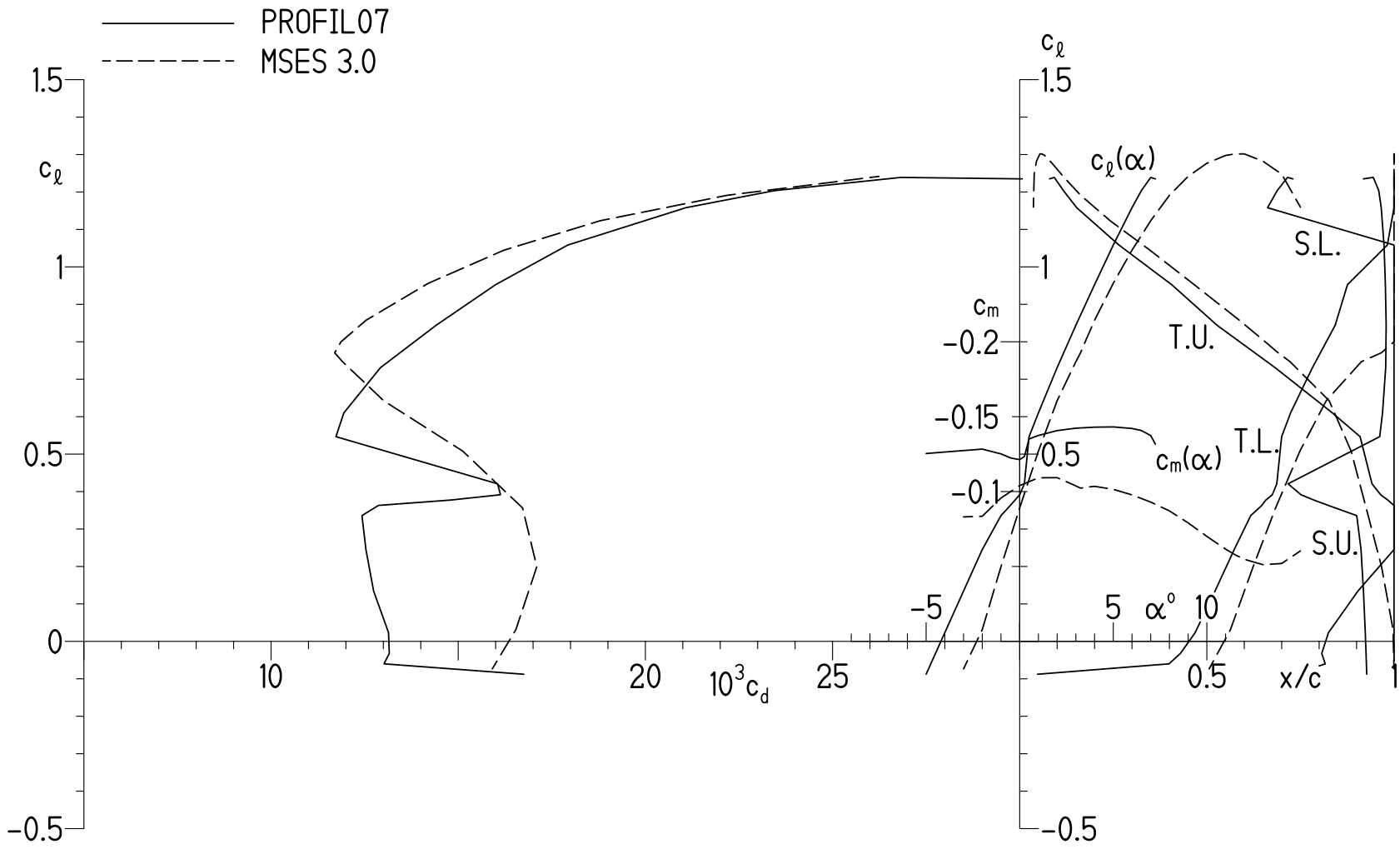

(a) M = 0.20 and R = 147,000.

Figure 4.- Section characteristics of S407 airfoil with transition free.

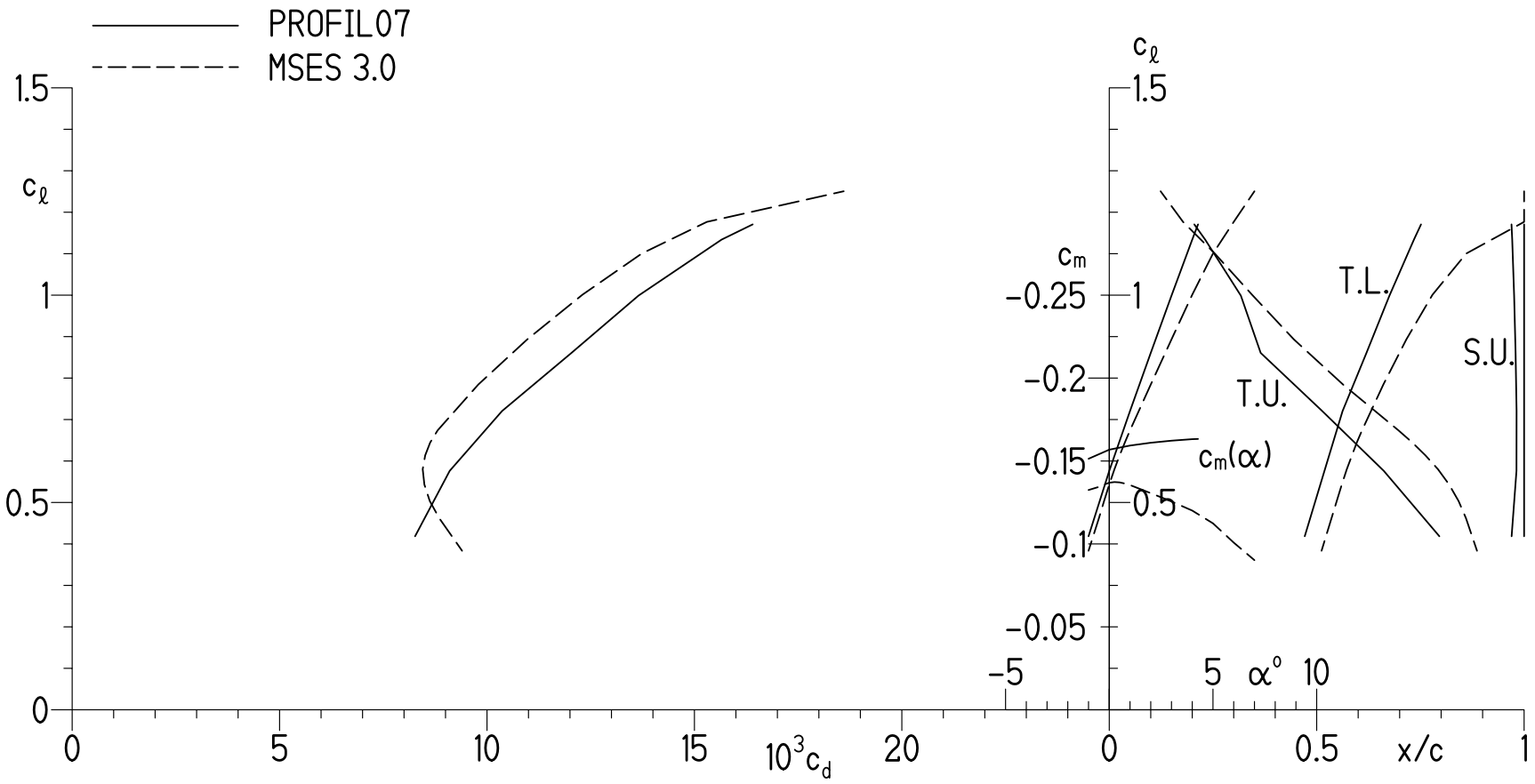

(b) M = 0.50 and R = 368,000.

Figure 4.- Continued.

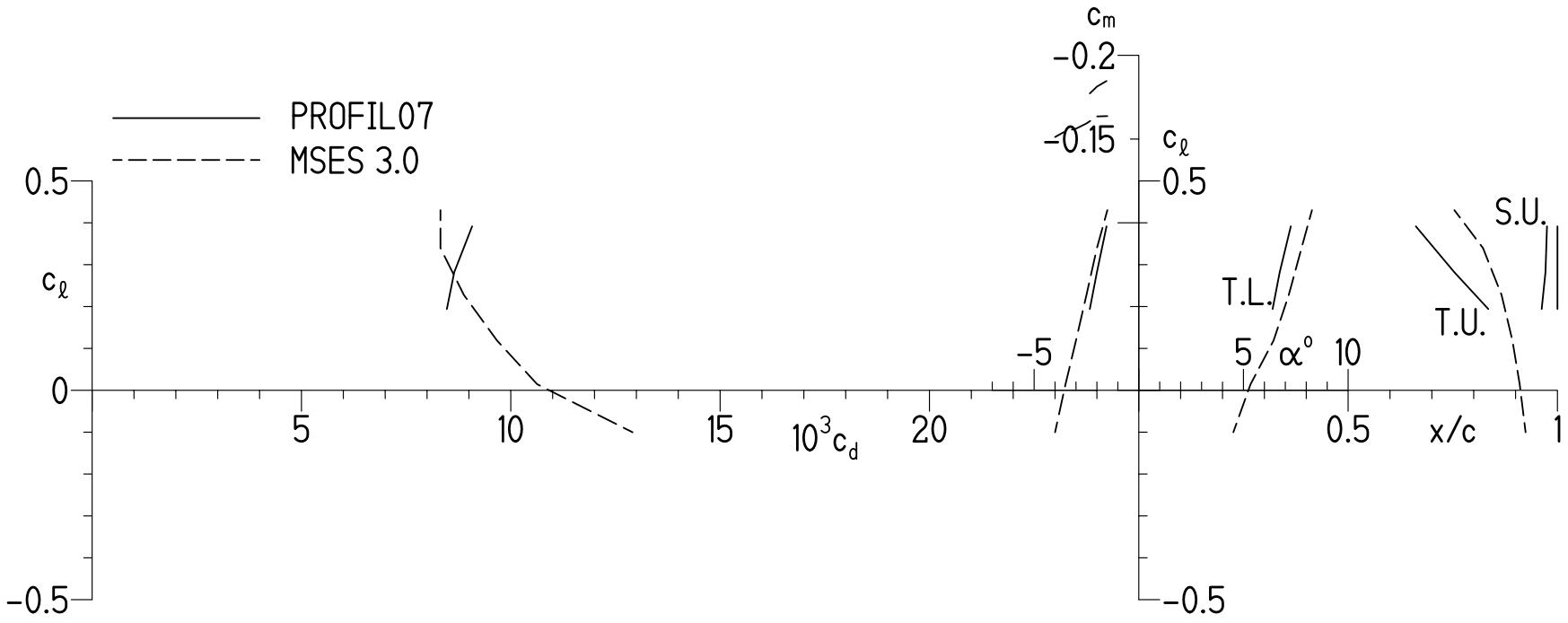

(c) M = 0.70 and R = 552,000.

Figure 4.- Concluded.

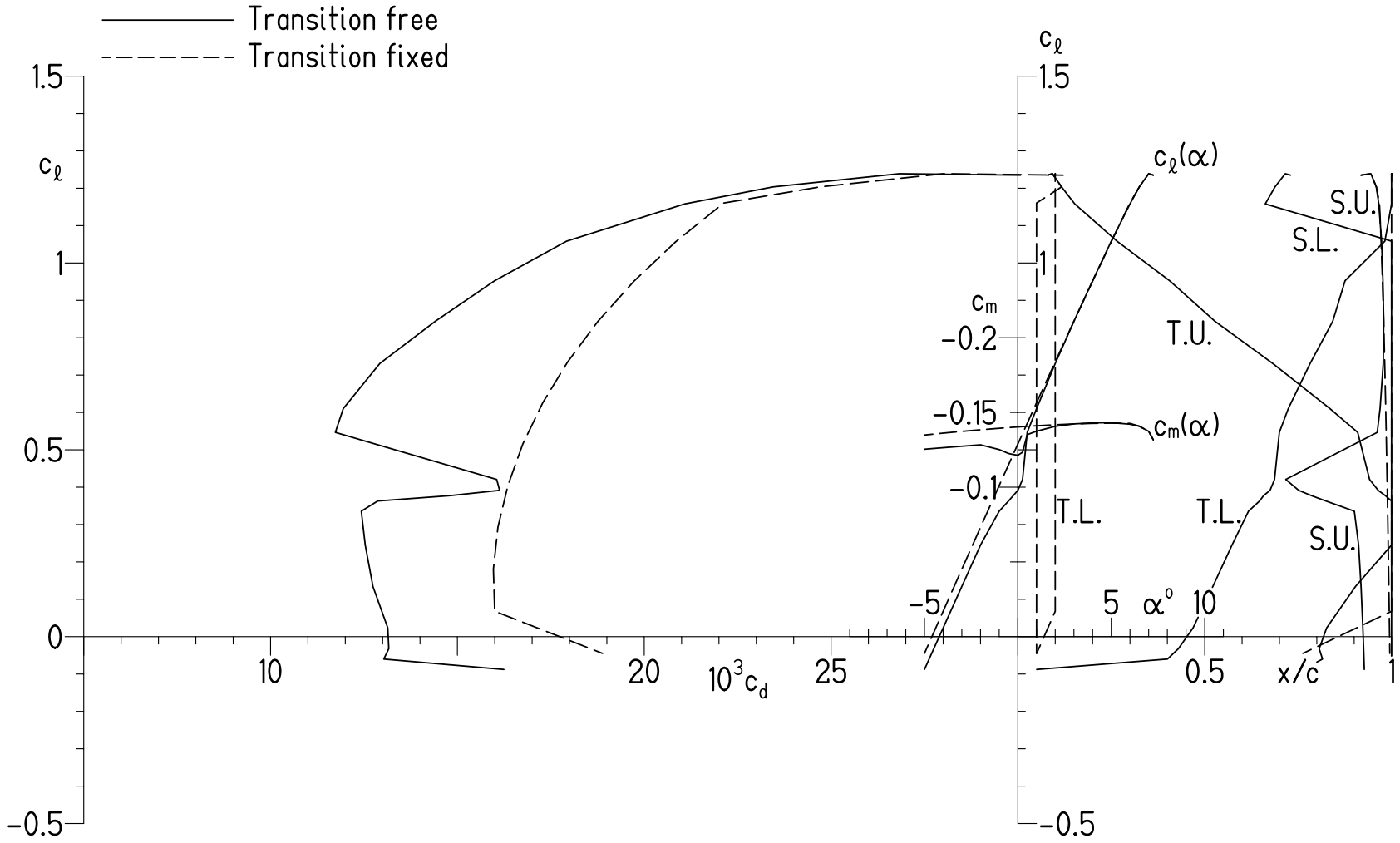

(a) M = 0.20 and R = 147,000.

Figure 5.- Effect of fixing transition on section characteristics of S407 airfoil predicted using method of references 8 and 9.

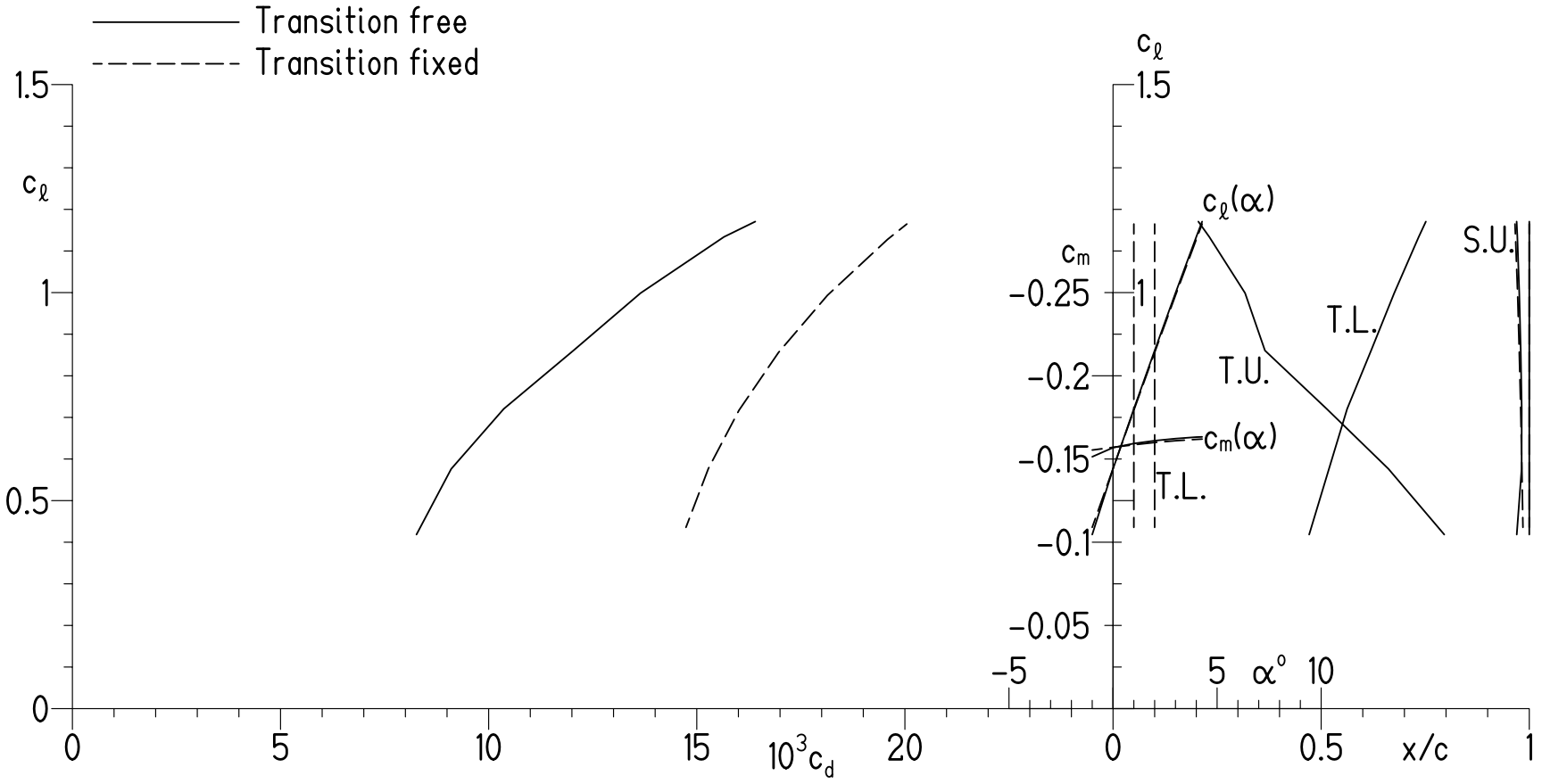

(b) M = 0.50 and R = 368,000.

Figure 5.- Continued.

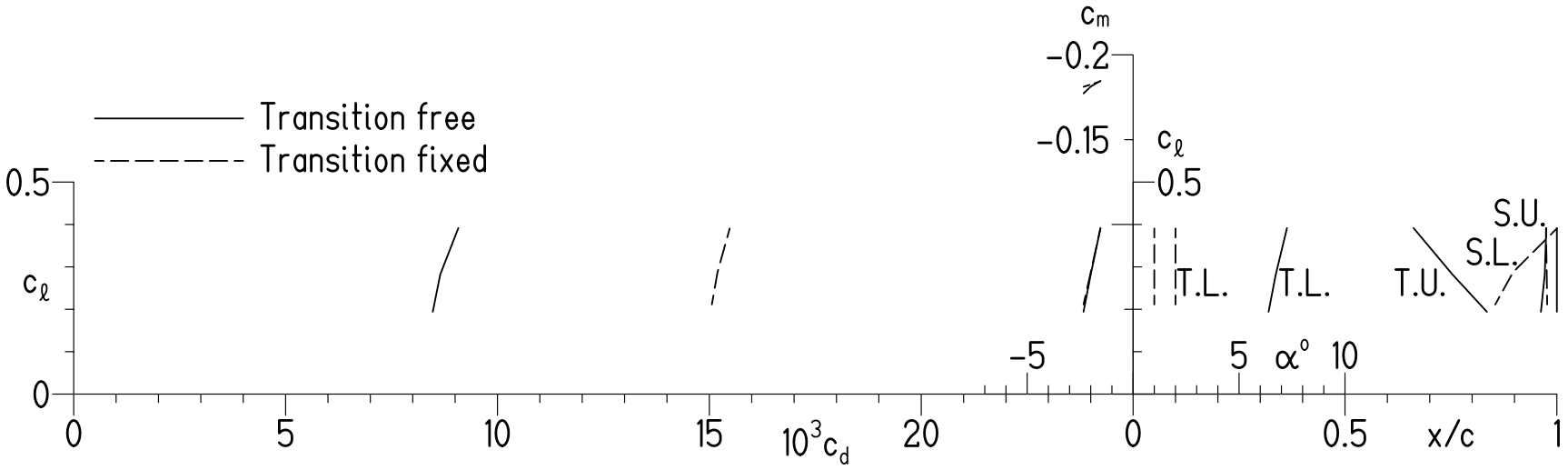

(c) M = 0.70 and R = 552,000.

Figure 5.- Concluded.

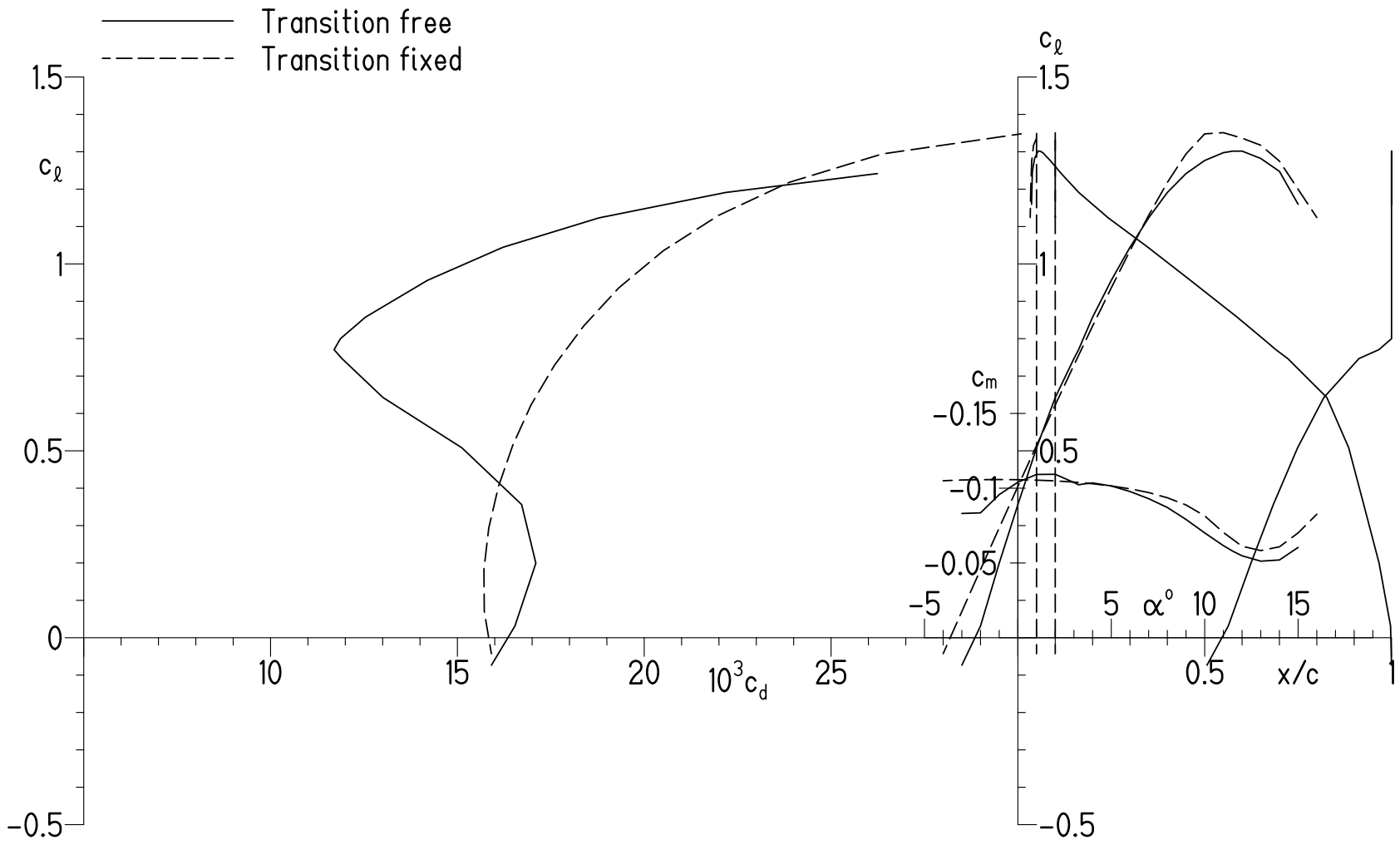

(a) M = 0.20 and R = 147,000.

Figure 6.- Effect of fixing transition on section characteristics of S407 airfoil predicted using method of reference 11.

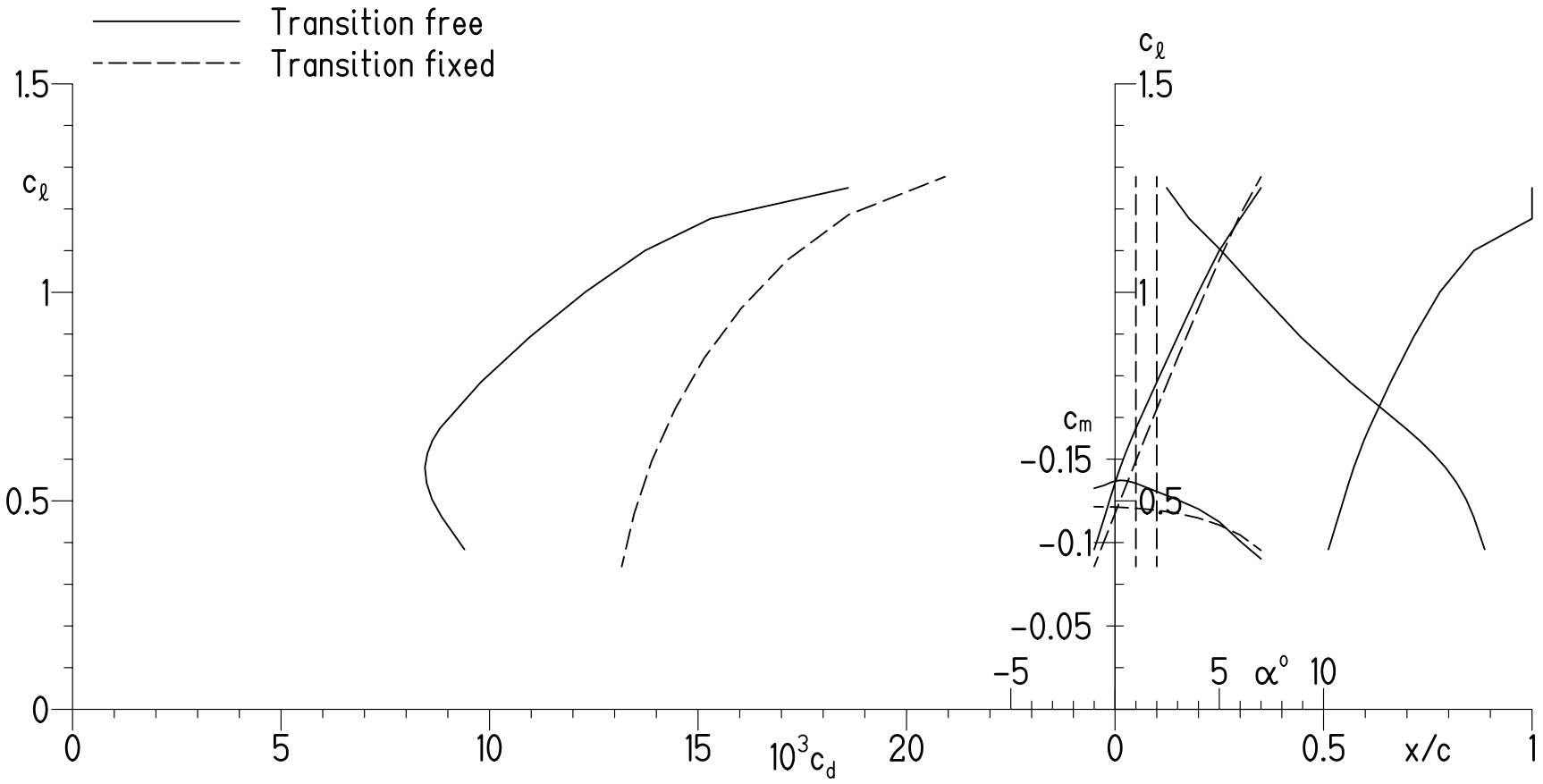

(b) M = 0.50 and R = 368,000.

Figure 6.- Continued.

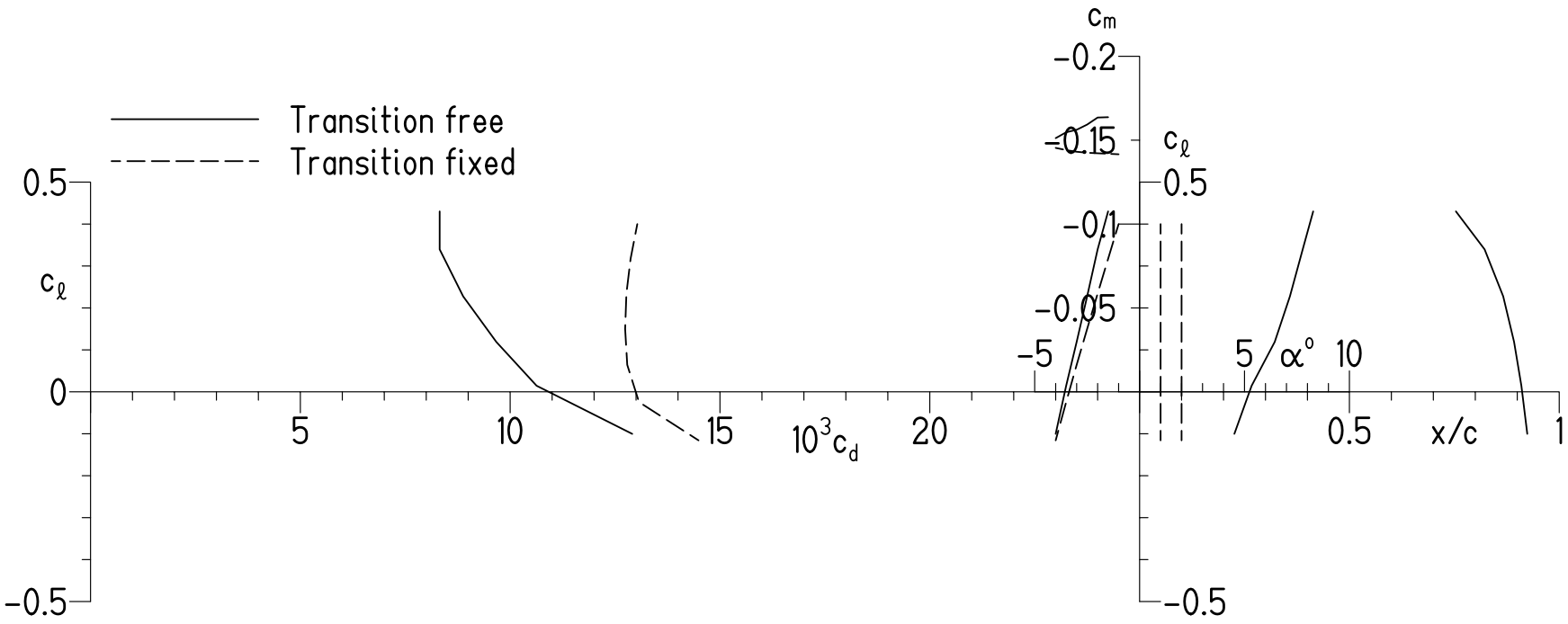

(c) M = 0.70 and R = 552,000.

Figure 6.- Concluded.

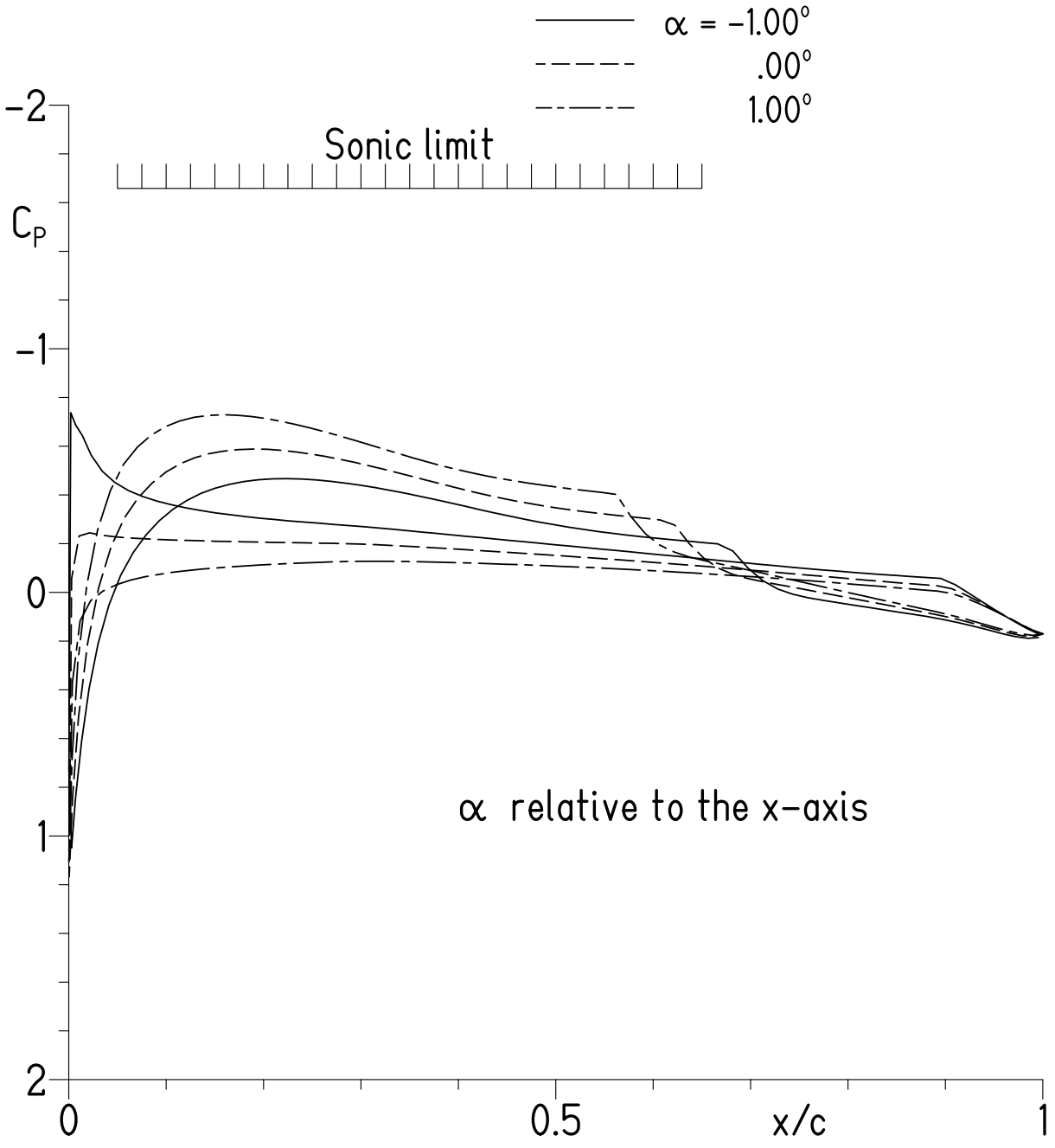

(a) $\alpha = -1.00°$, 0.00°, and 1.00°.

Figure 7.- Pressure distributions for S409 airfoil at M = 0.55 and R = 303,000 with transition free.

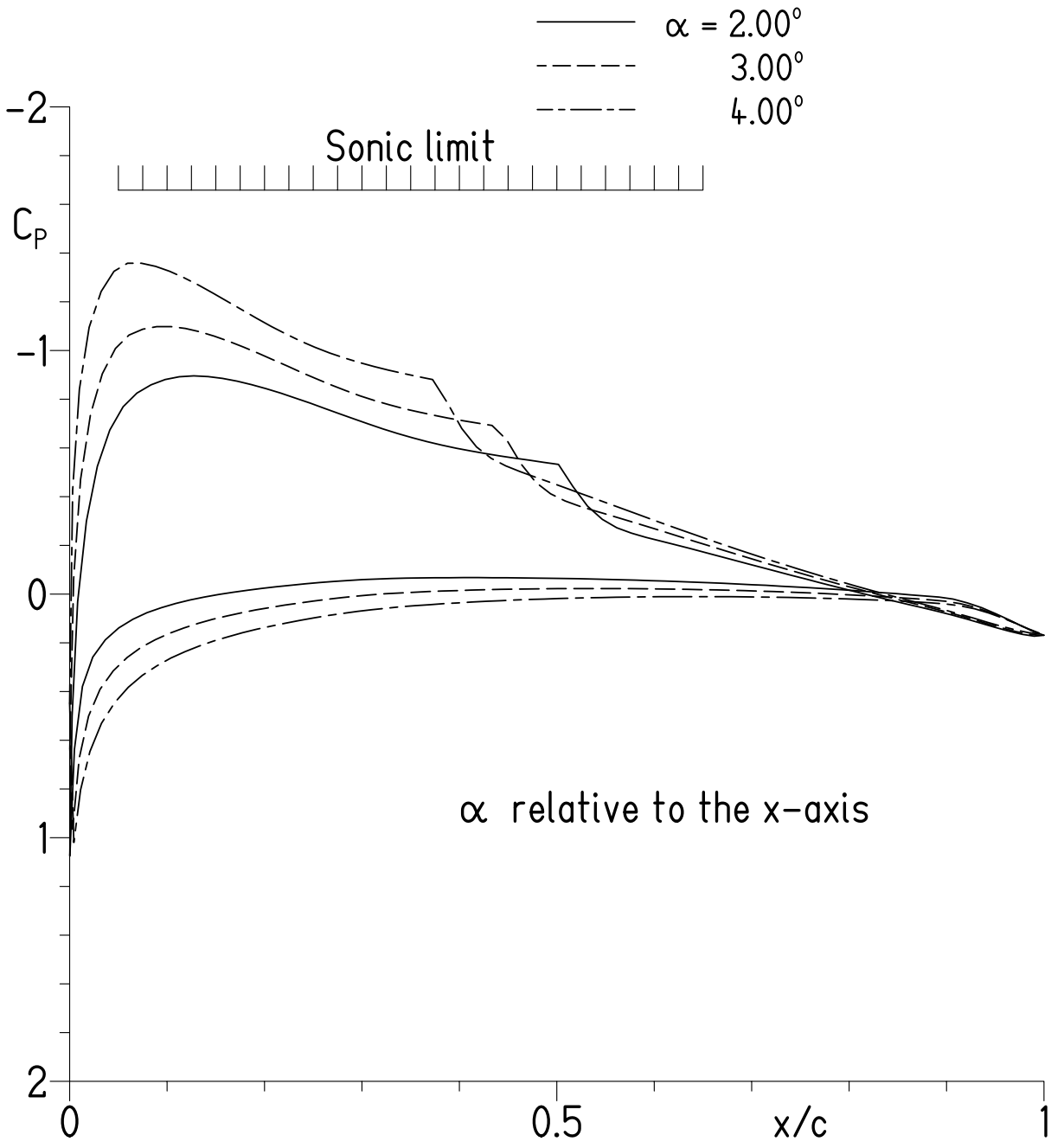

(b) $\alpha = 2.00°$, 3.00°, and 4.00°.

Figure 7.- Continued.

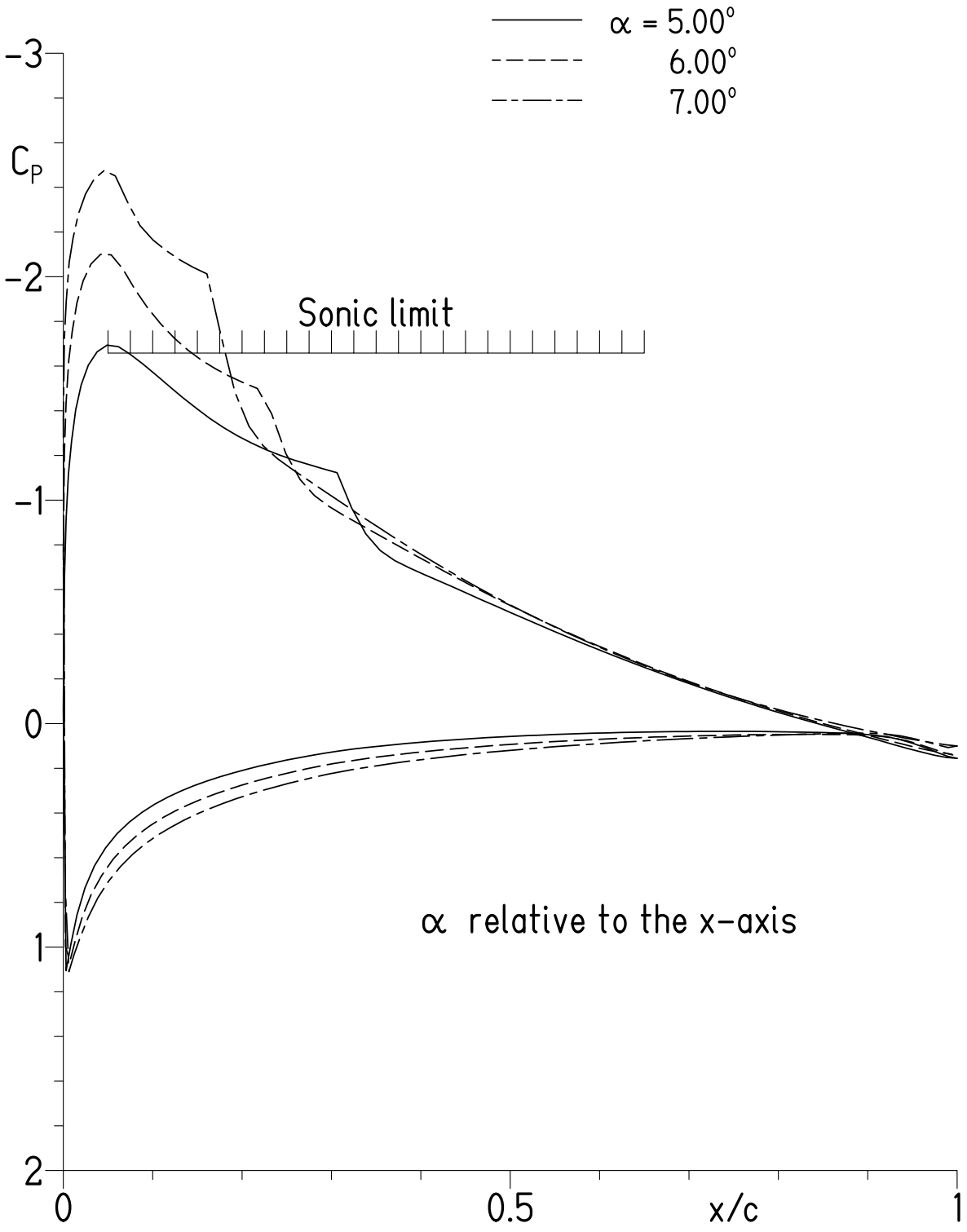

(c) $\alpha = 5.00°$, 6.00°, and 7.00°.

Figure 7.- Continued.

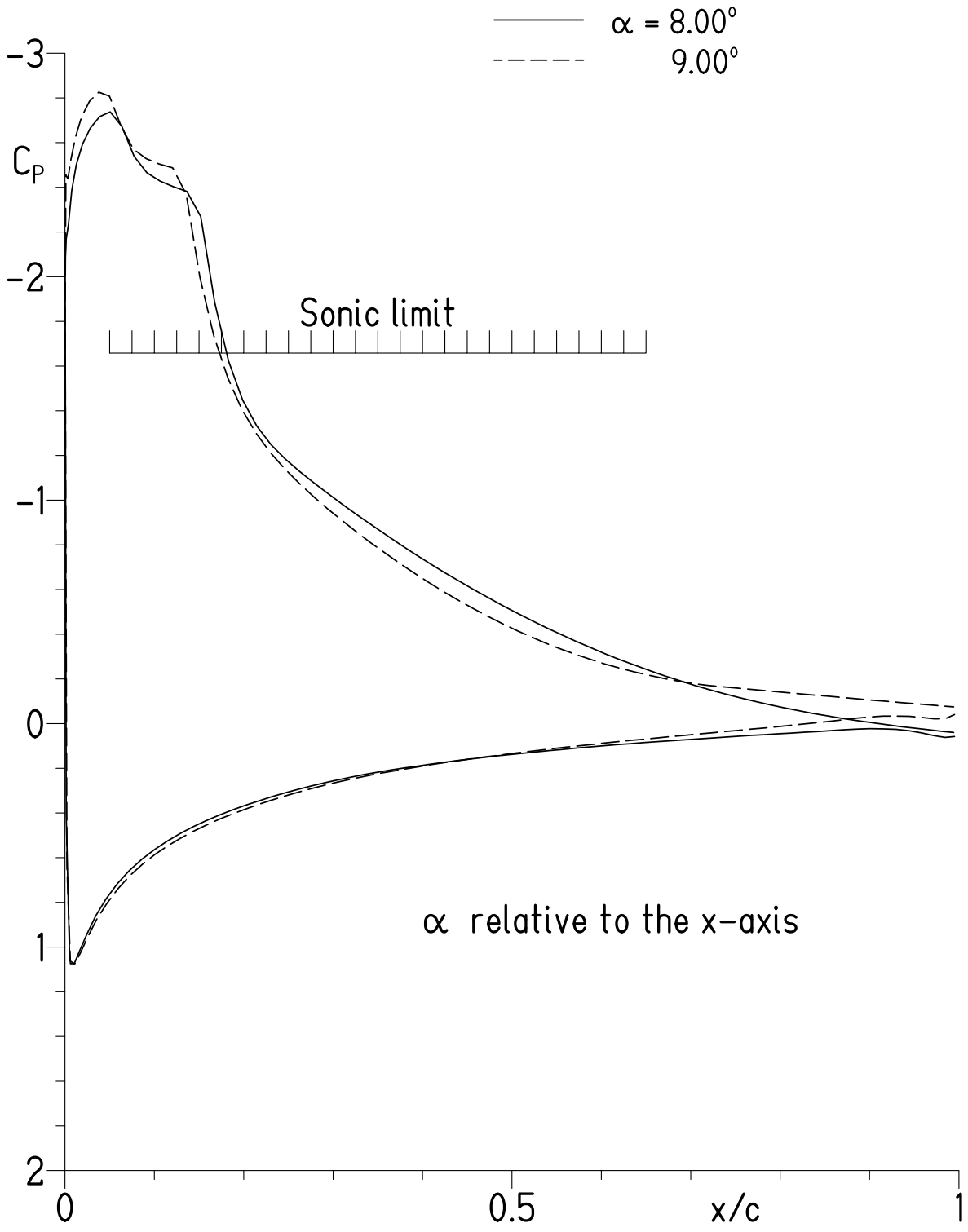

(d) $\alpha = 8.00°$ and $9.00°$.

Figure 7.- Concluded.

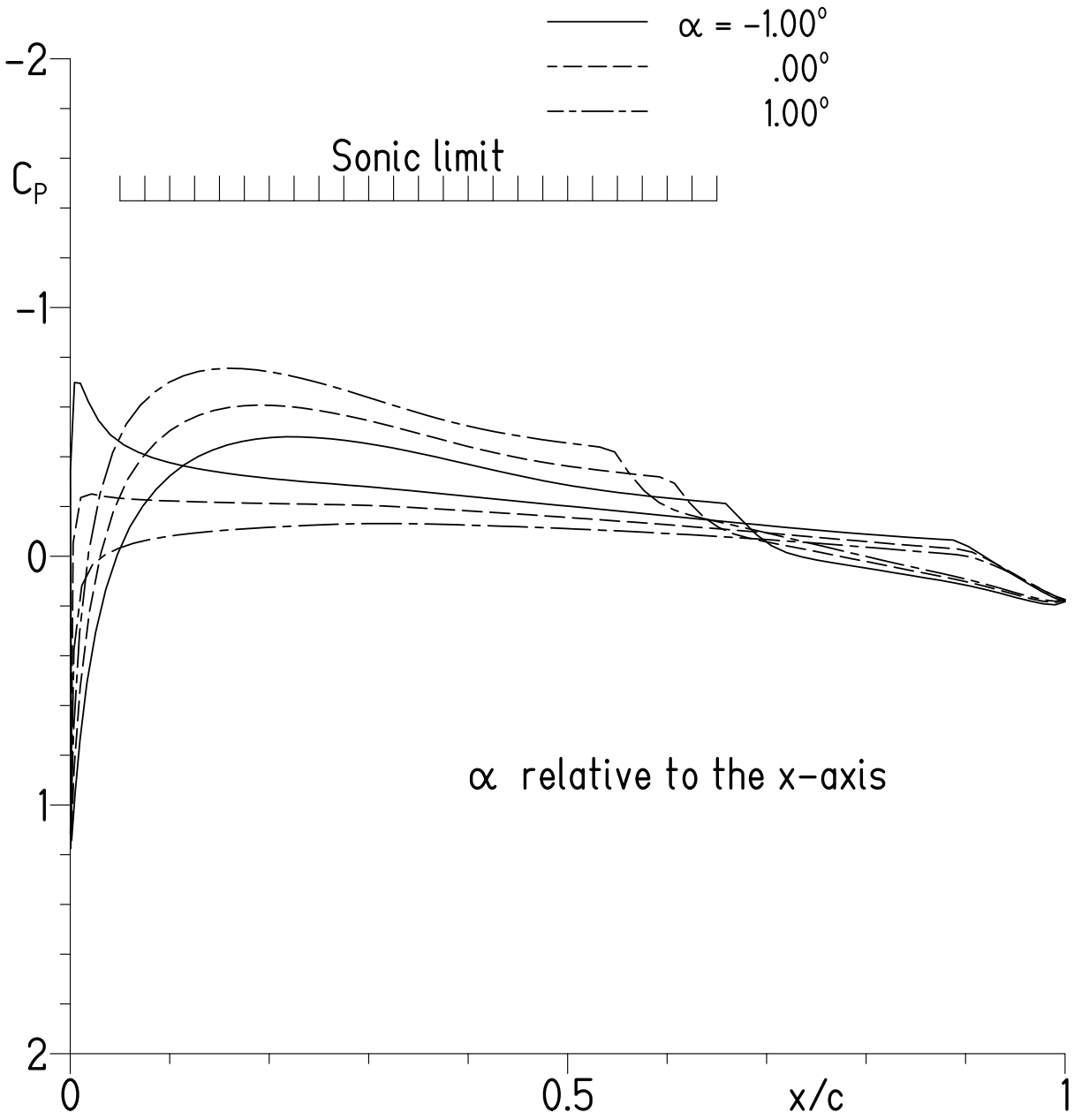

(a) $\alpha = -1.00°$, 0.00°, and 1.00°.

Figure 8.- Pressure distributions for S409 airfoil at M = 0.58 and R = 319,000 with transition free.

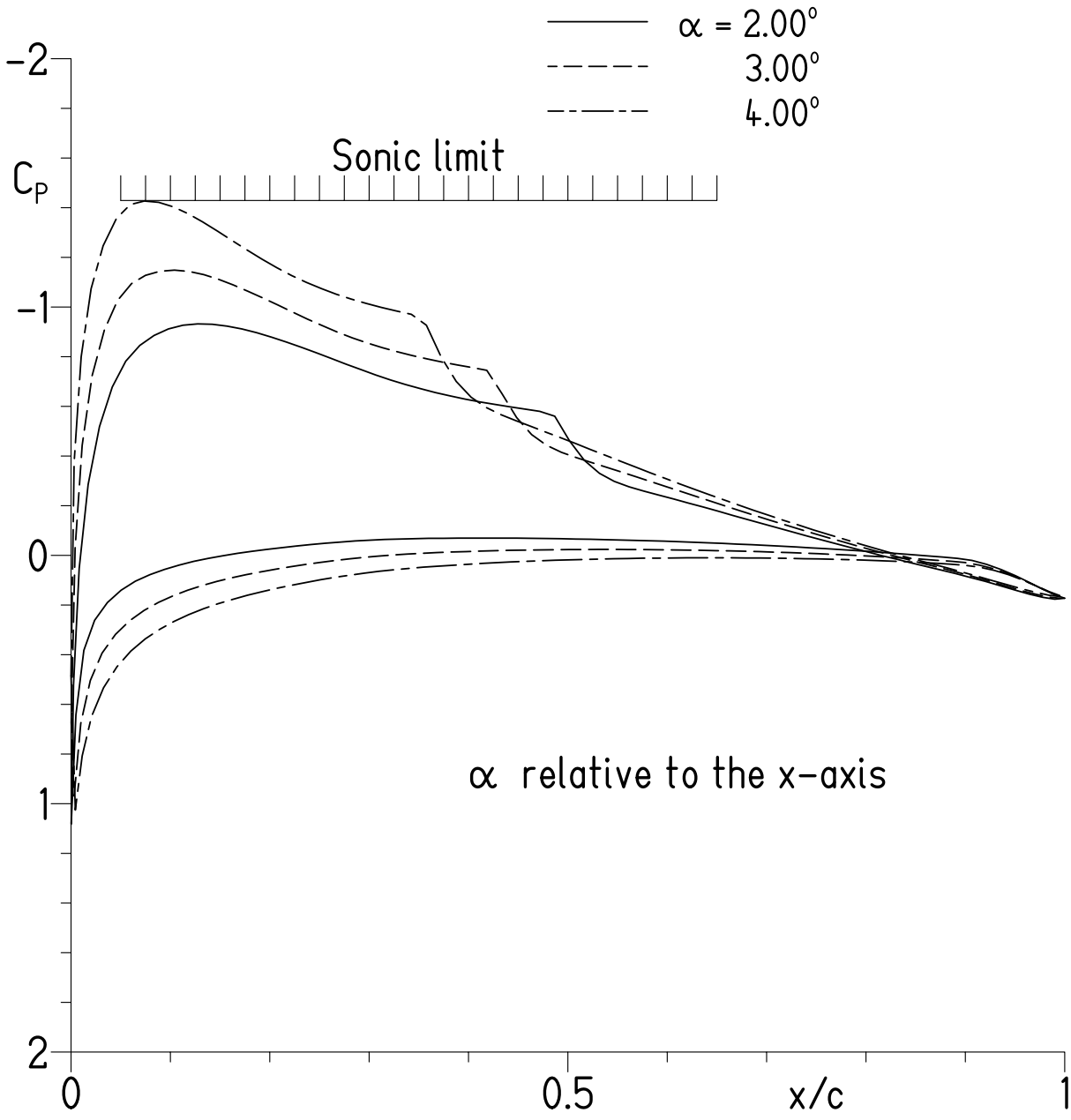

(b) $\alpha = 2.00°$, 3.00°, and 4.00°.

Figure 8.- Continued.

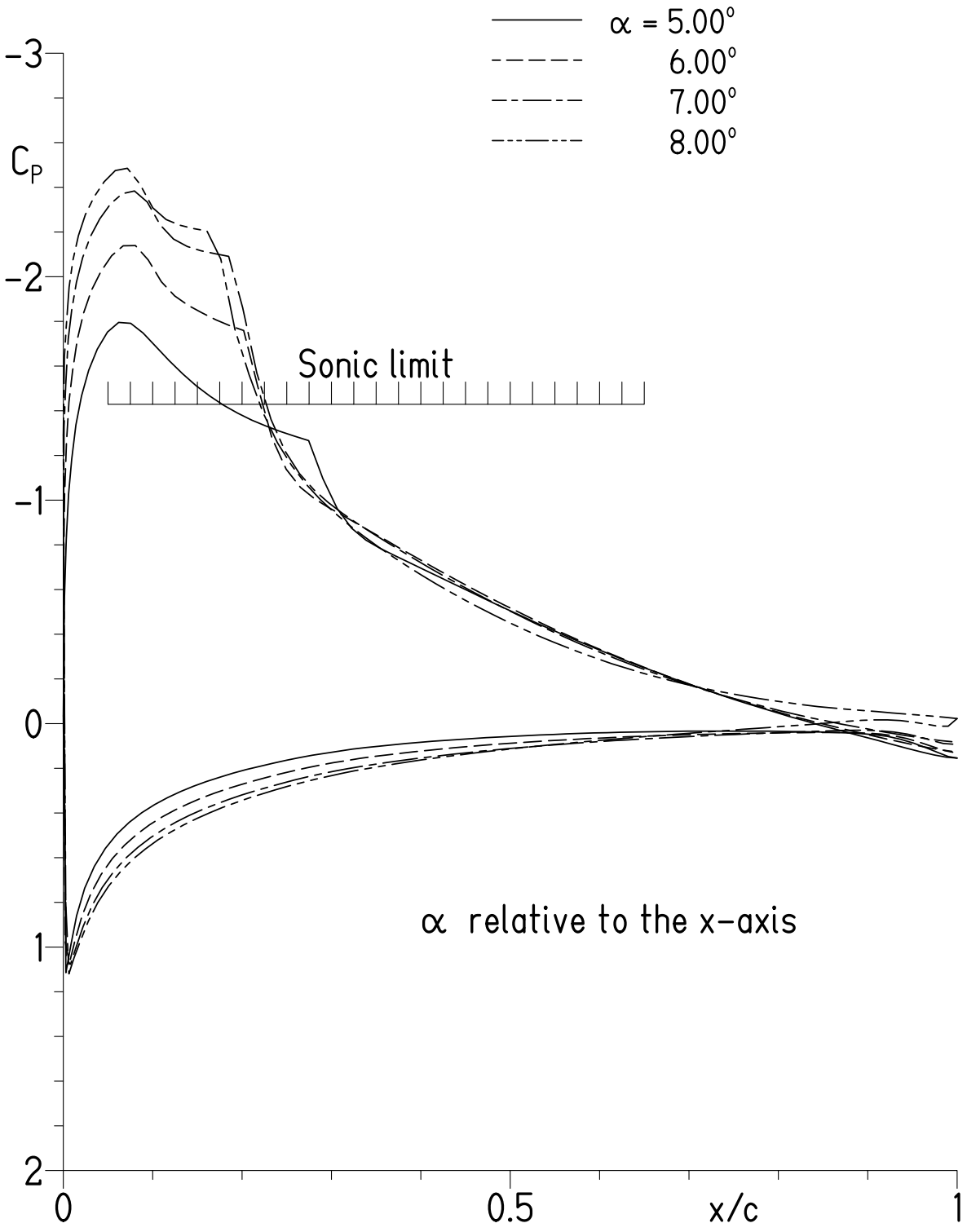

(c) $\alpha = 5.00°$, 6.00°, 7.00°, and 8.00°.

Figure 8.- Concluded.

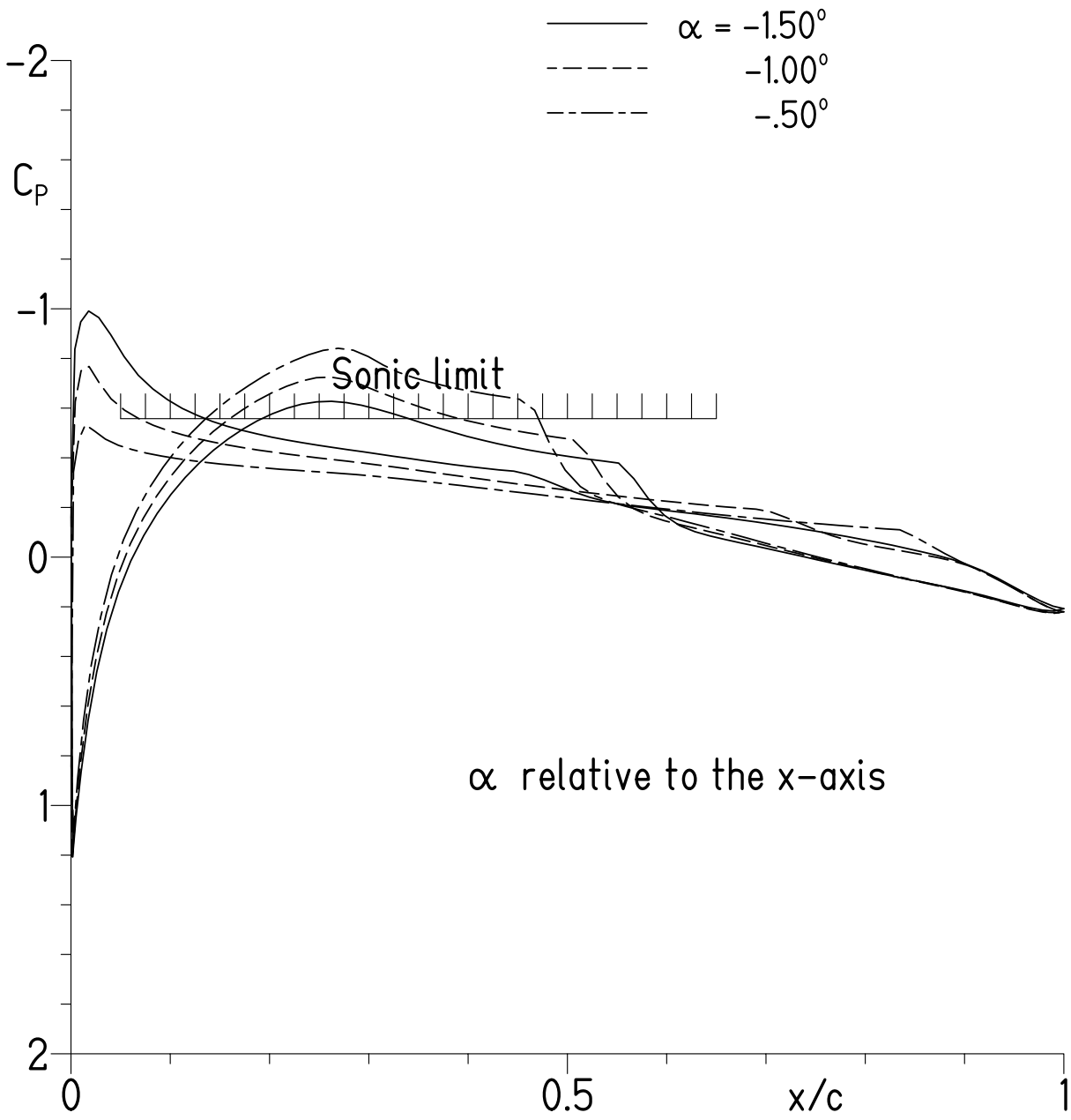

(a) $\alpha = -1.50°, -1.00°$, and $-0.50°$.

Figure 9.- Pressure distributions for S409 airfoil at M = 0.76 and R = 409,000 with transition free.

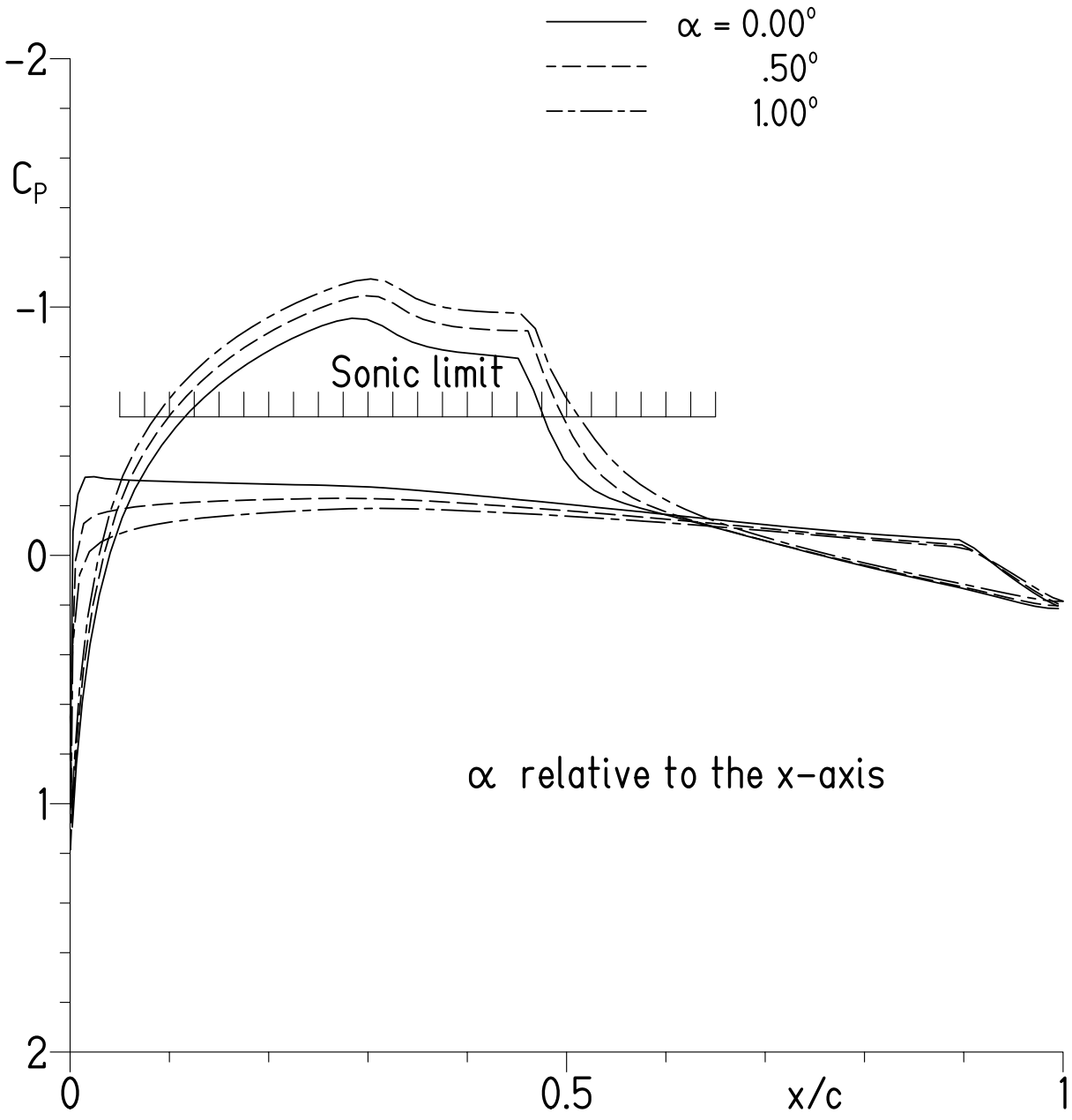

(b) $\alpha = 0.00°$, 0.50°, and 1.00°.

Figure 9.- Concluded.

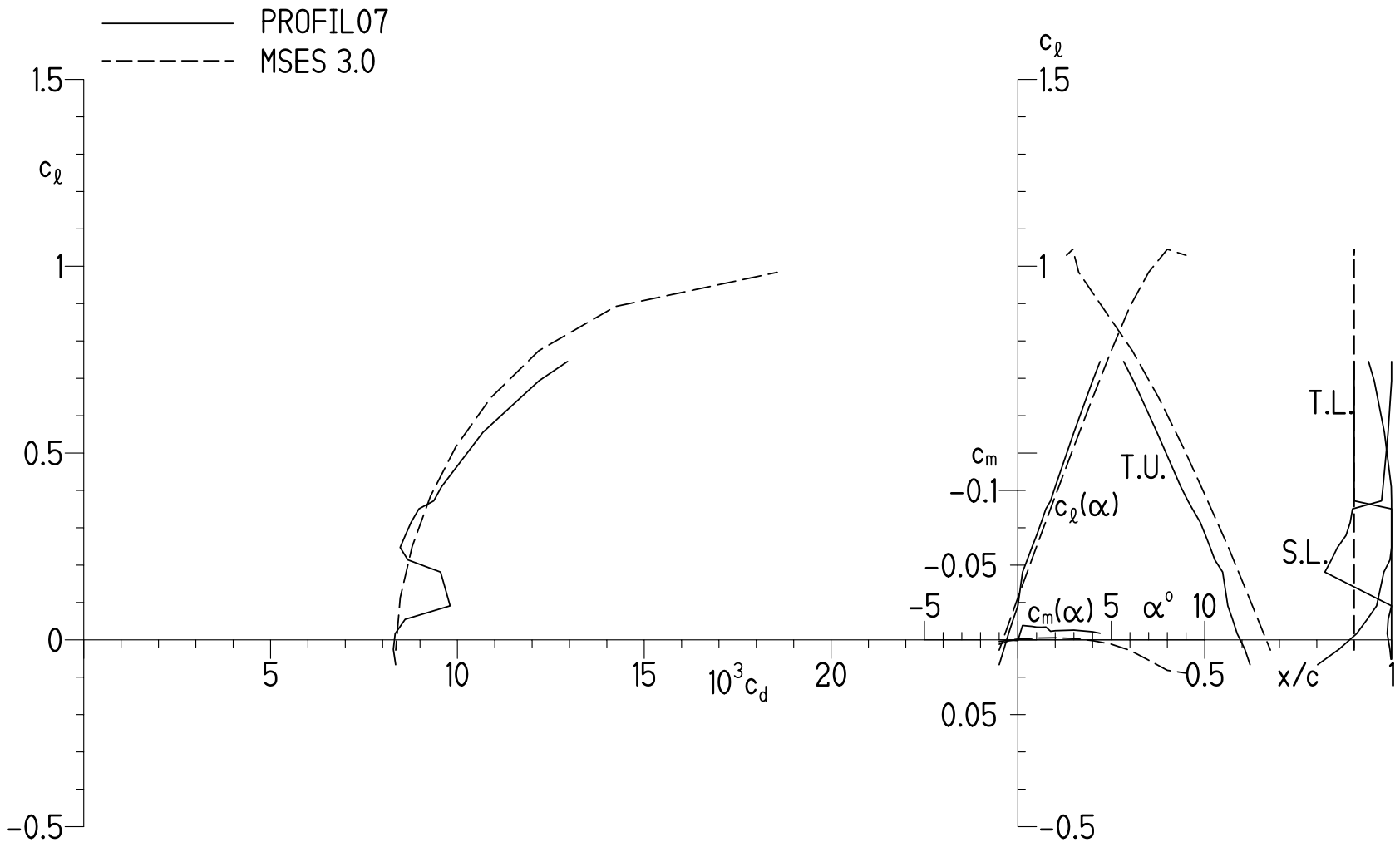

(a) M = 0.55 and R = 303,000.

Figure 10.- Section characteristics of S409 airfoil with transition free.

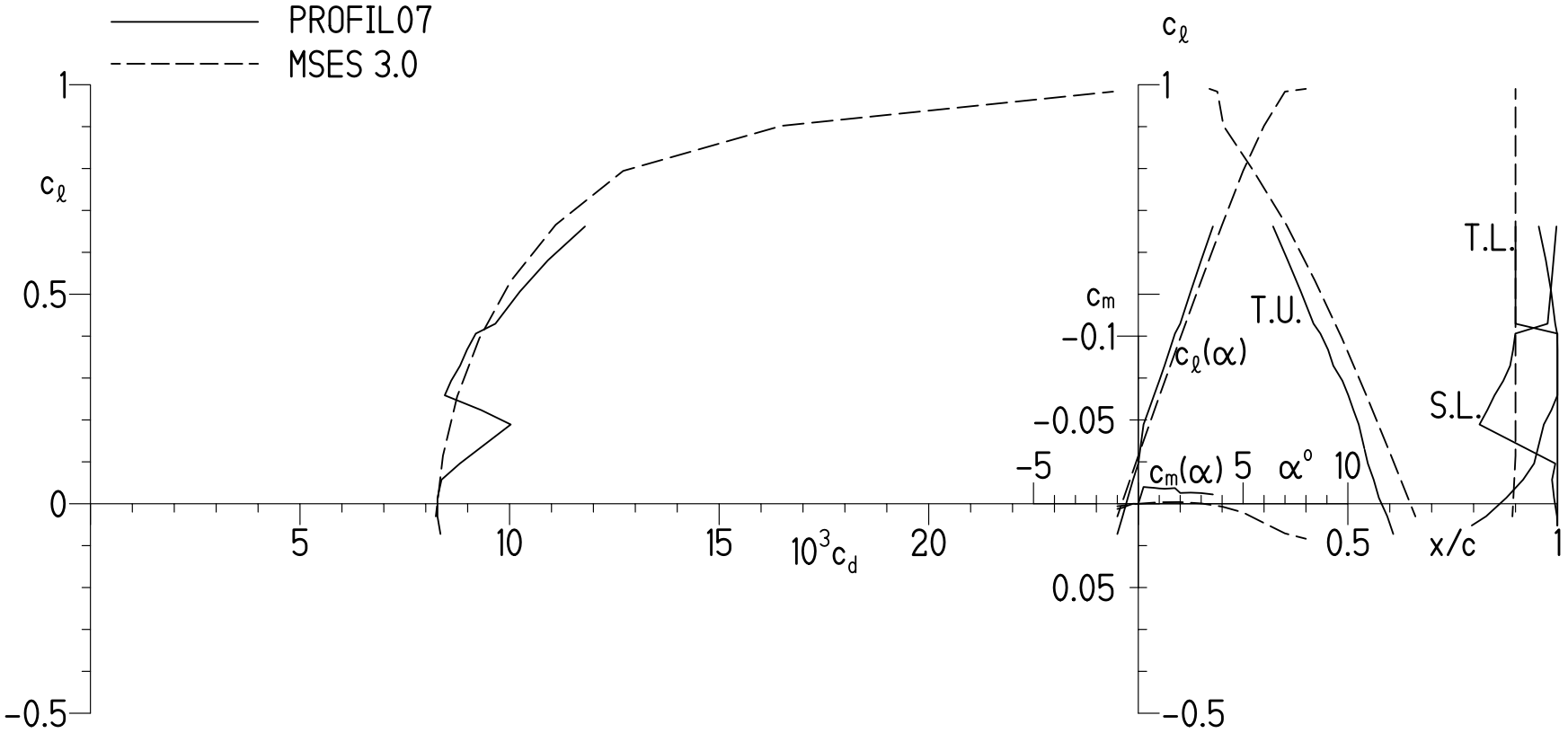

(b) M = 0.58 and R = 319,000.

Figure 10.- Continued.

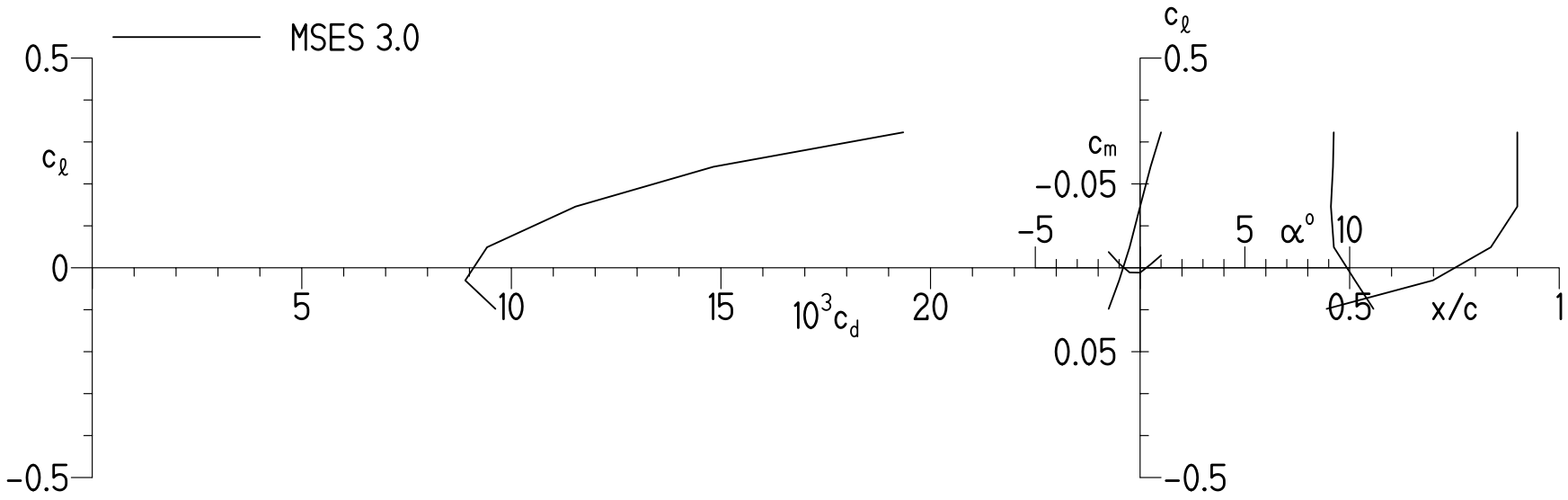

(c) M = 0.76 and R = 409,000.

Figure 10.- Concluded.

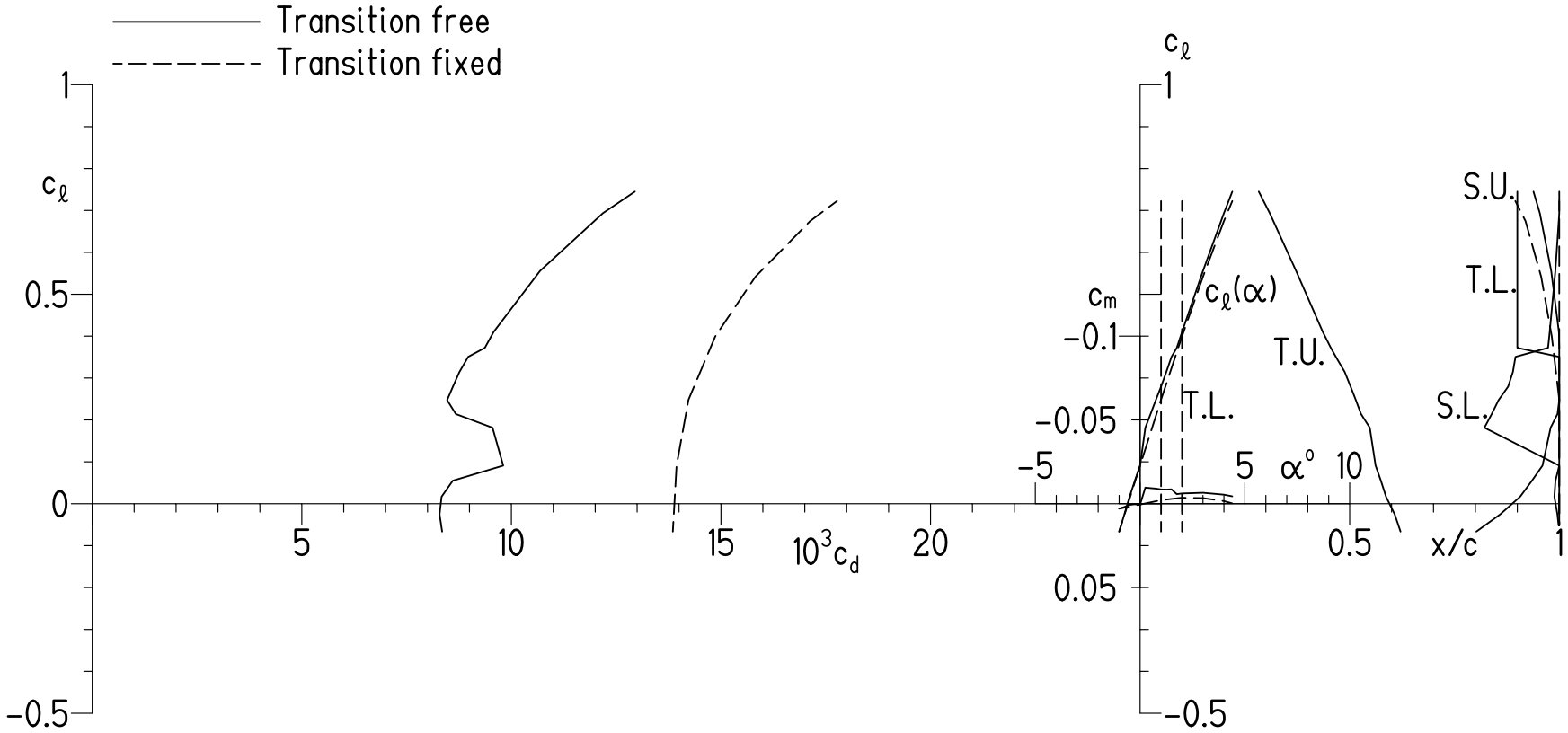

(a) M = 0.55 and R = 303,000.

Figure 11.- Effect of fixing transition on section characteristics of S409 airfoil predicted using method of references 8 and 9.

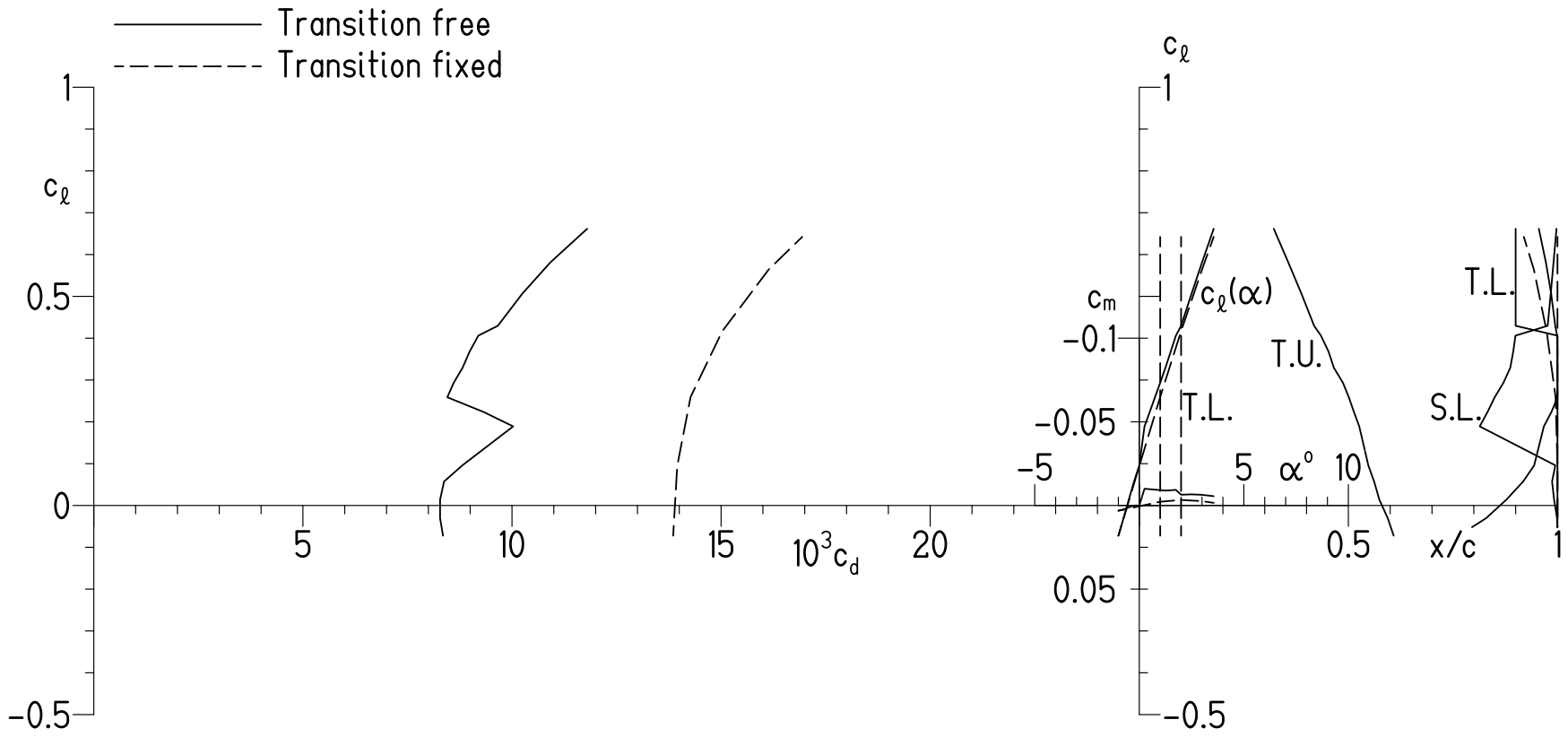

(b) M = 0.58 and R = 319,000.

Figure 11.- Concluded.

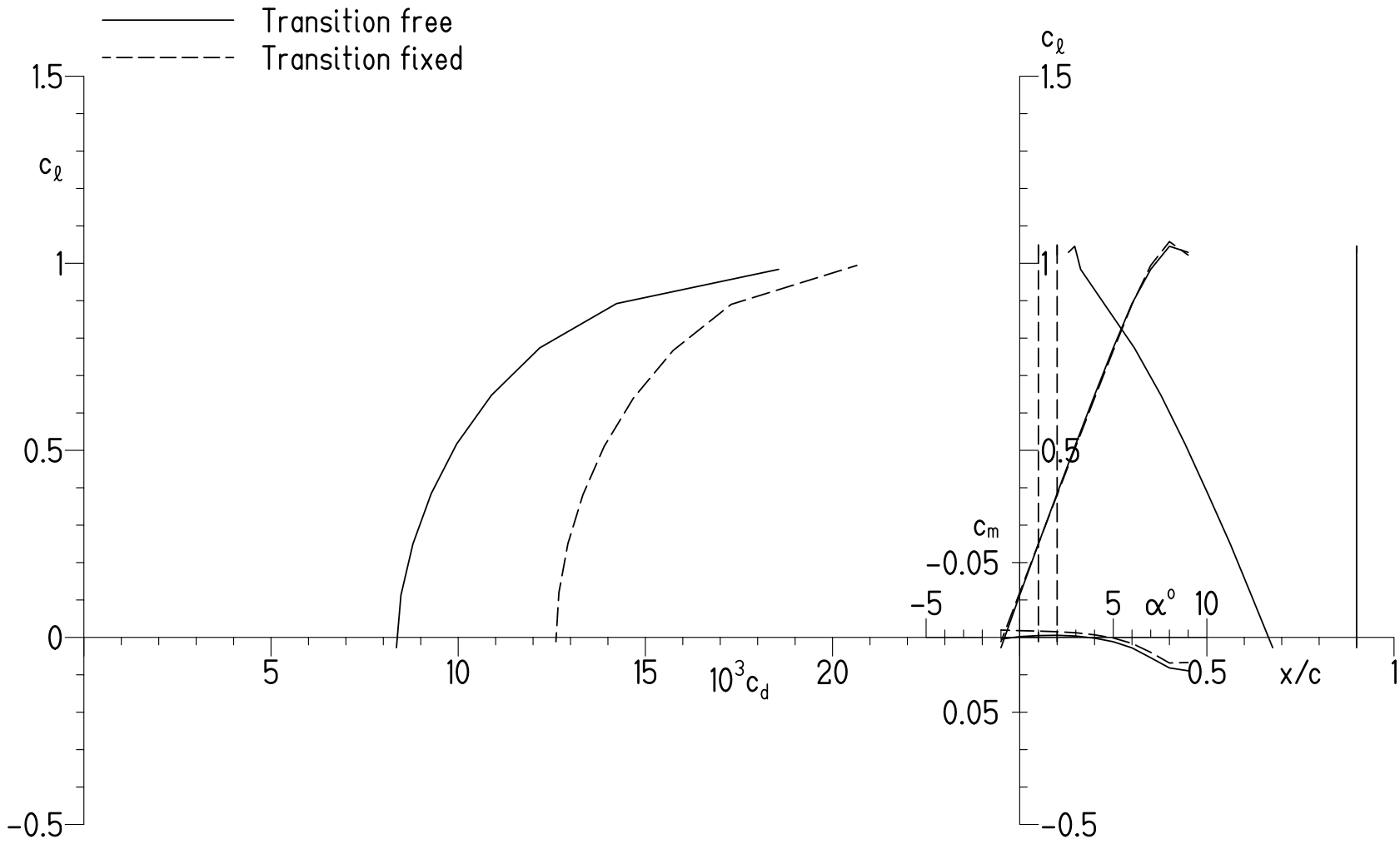

(a) M = 0.55 and R = 303,000.

Figure 12.- Effect of fixing transition on section characteristics of S409 airfoil predicted using method of reference 11.

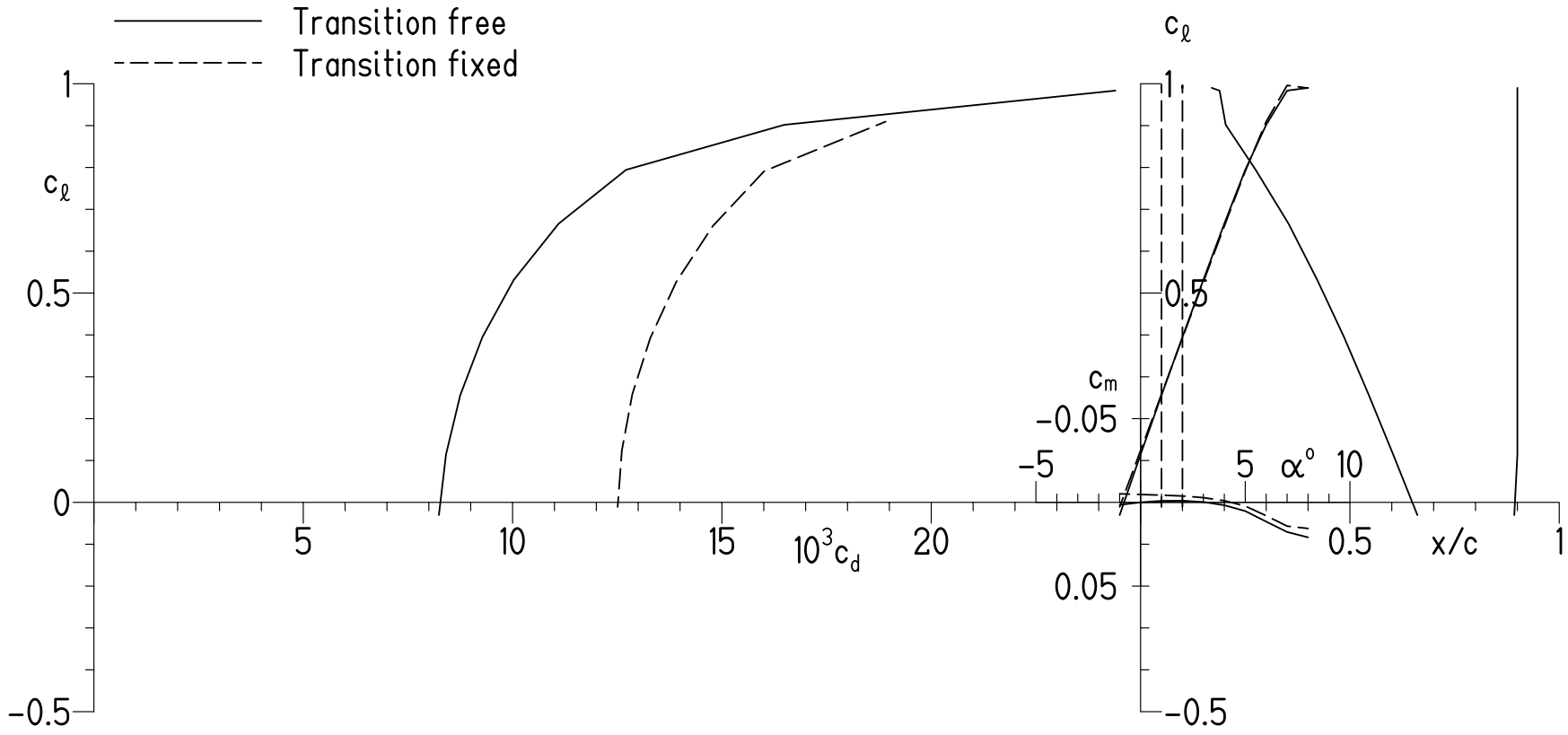

(b) M = 0.58 and R = 319,000.

Figure 12.- Continued.

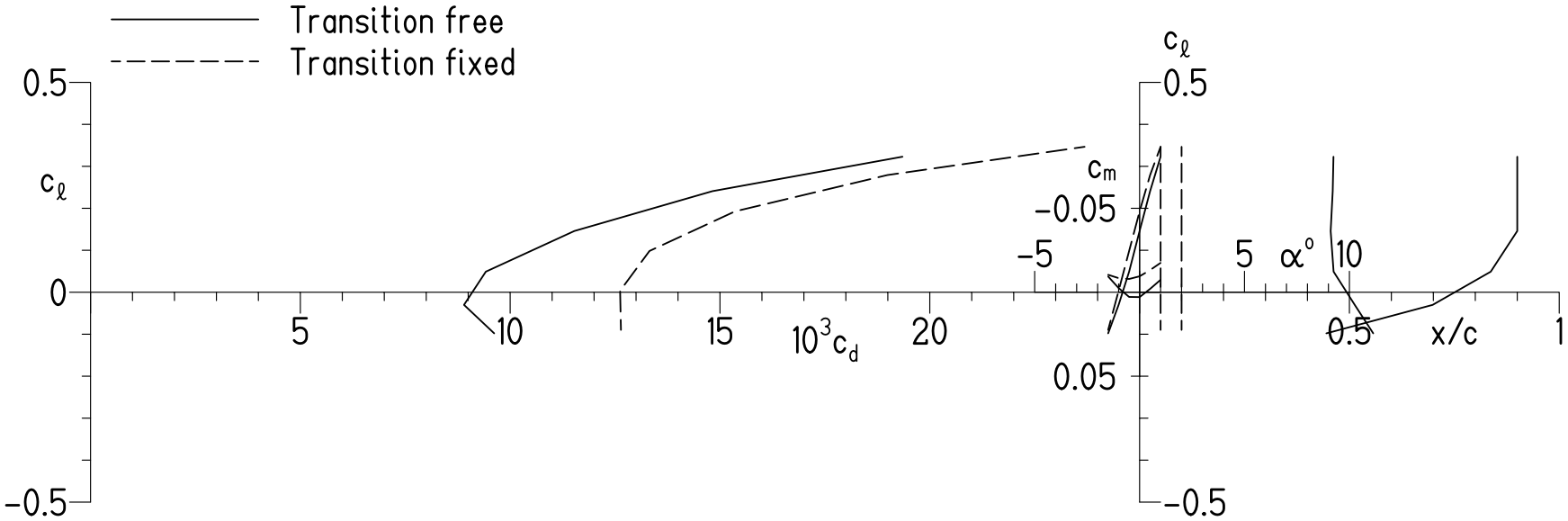

(c) M = 0.76 and R = 409,000.

Figure 12.- Concluded.

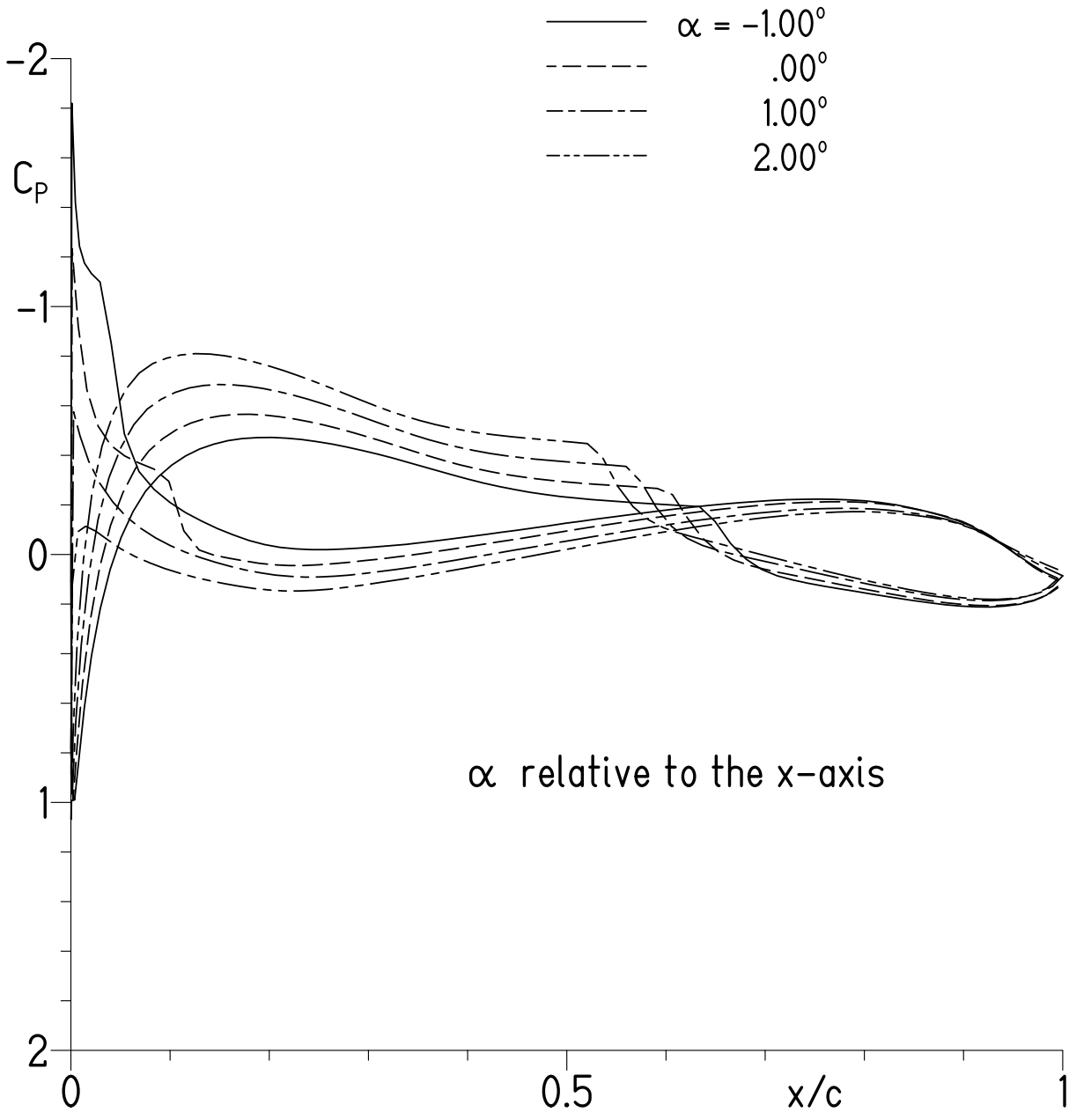

(a) $\alpha = -1.00°$, 0.00°, 1.00°, and 2.00°.

Figure 13.- Pressure distributions for S410 airfoil at M = 0.18 and R = 185,000 with transition free.

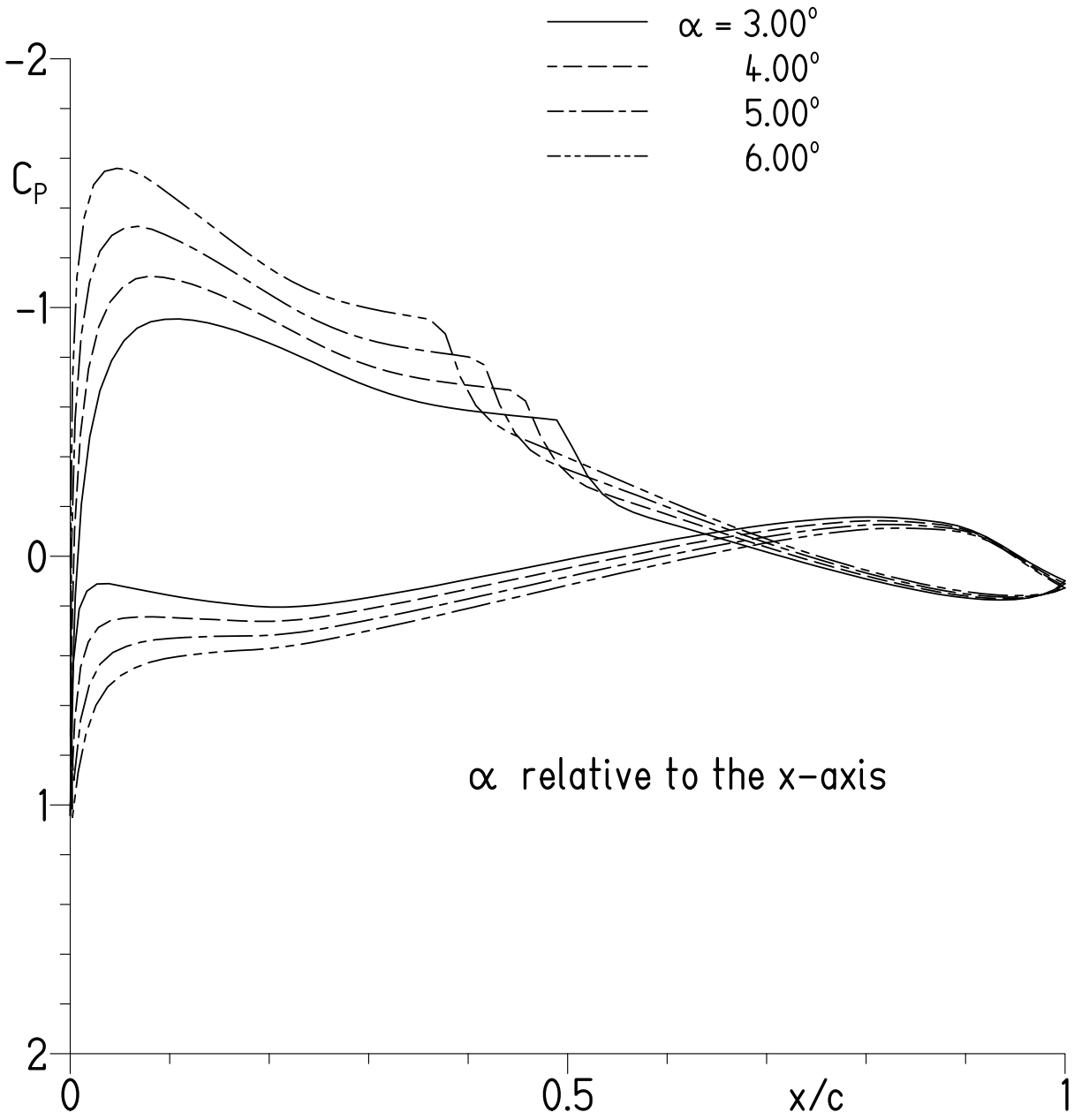

(b) $\alpha = 3.00°$, 4.00°, 5.00°, and 6.00°.

Figure 13.- Continued.

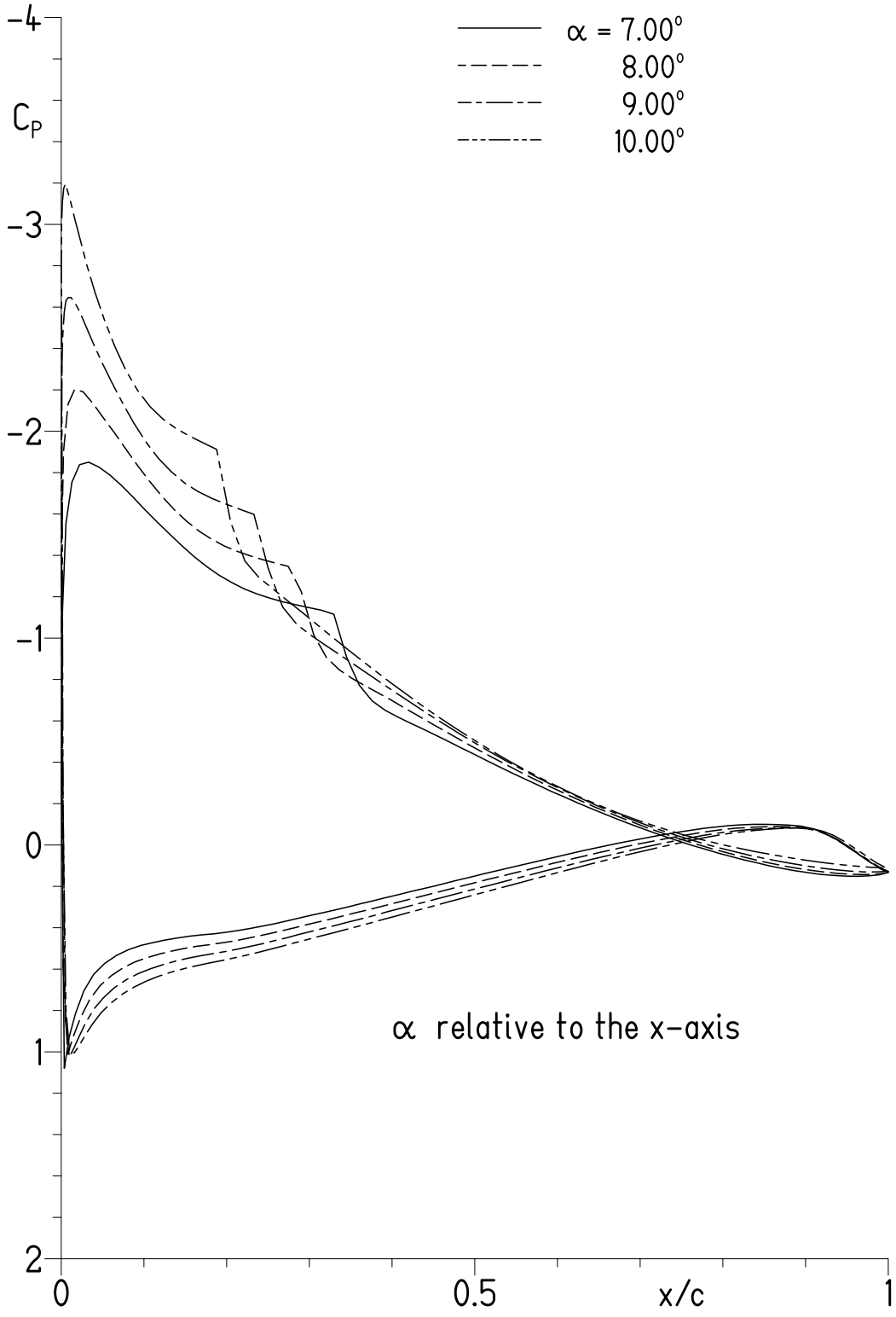

(c) α = 7.00°, 8.00°, 9.00°, and 10.00°.

Figure 13.- Continued.

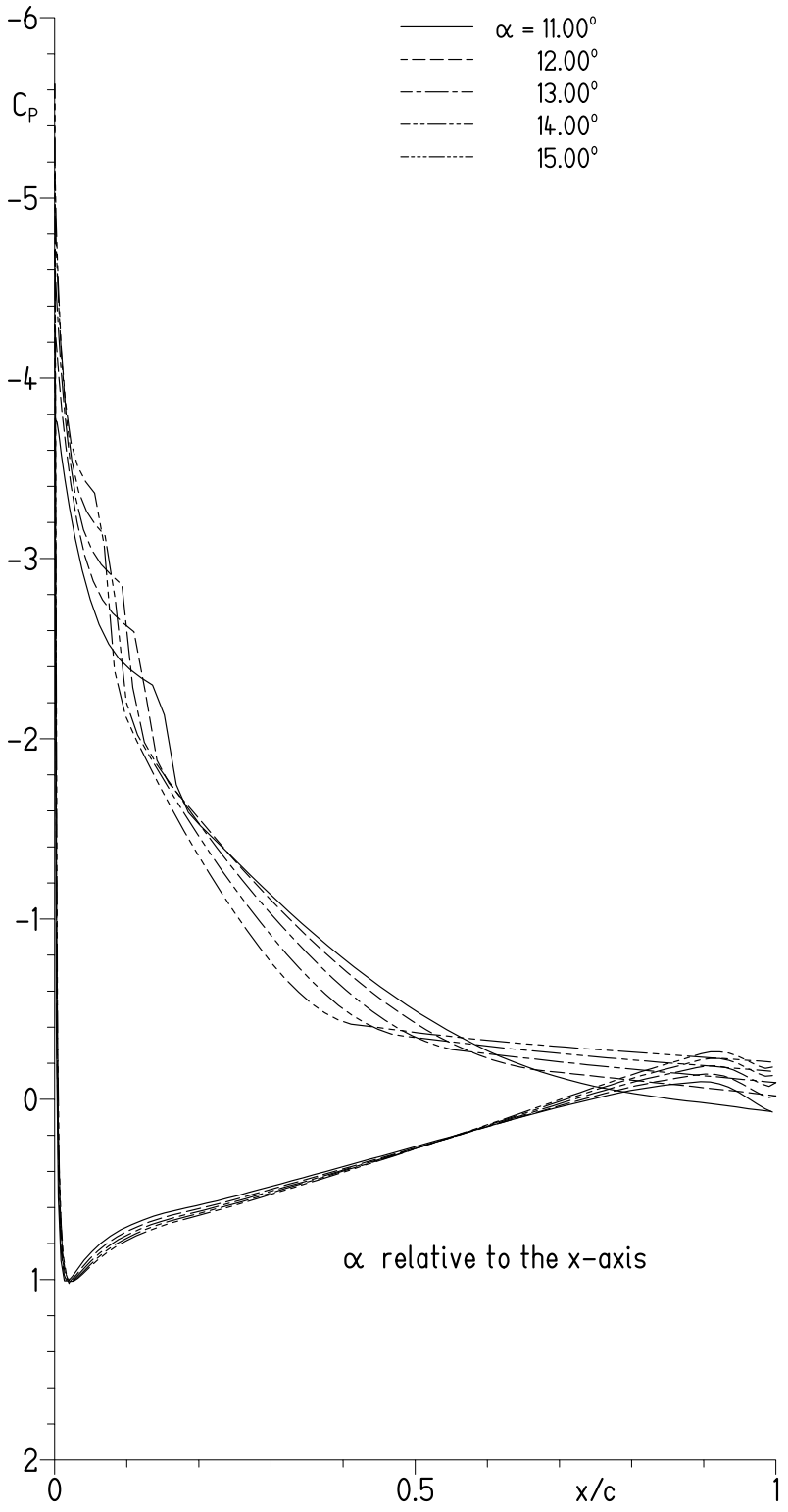

(d) $\alpha = 11.00°, 12.00°, 13.00°, 14.00°$, and $15.00°$.

Figure 13.- Concluded.

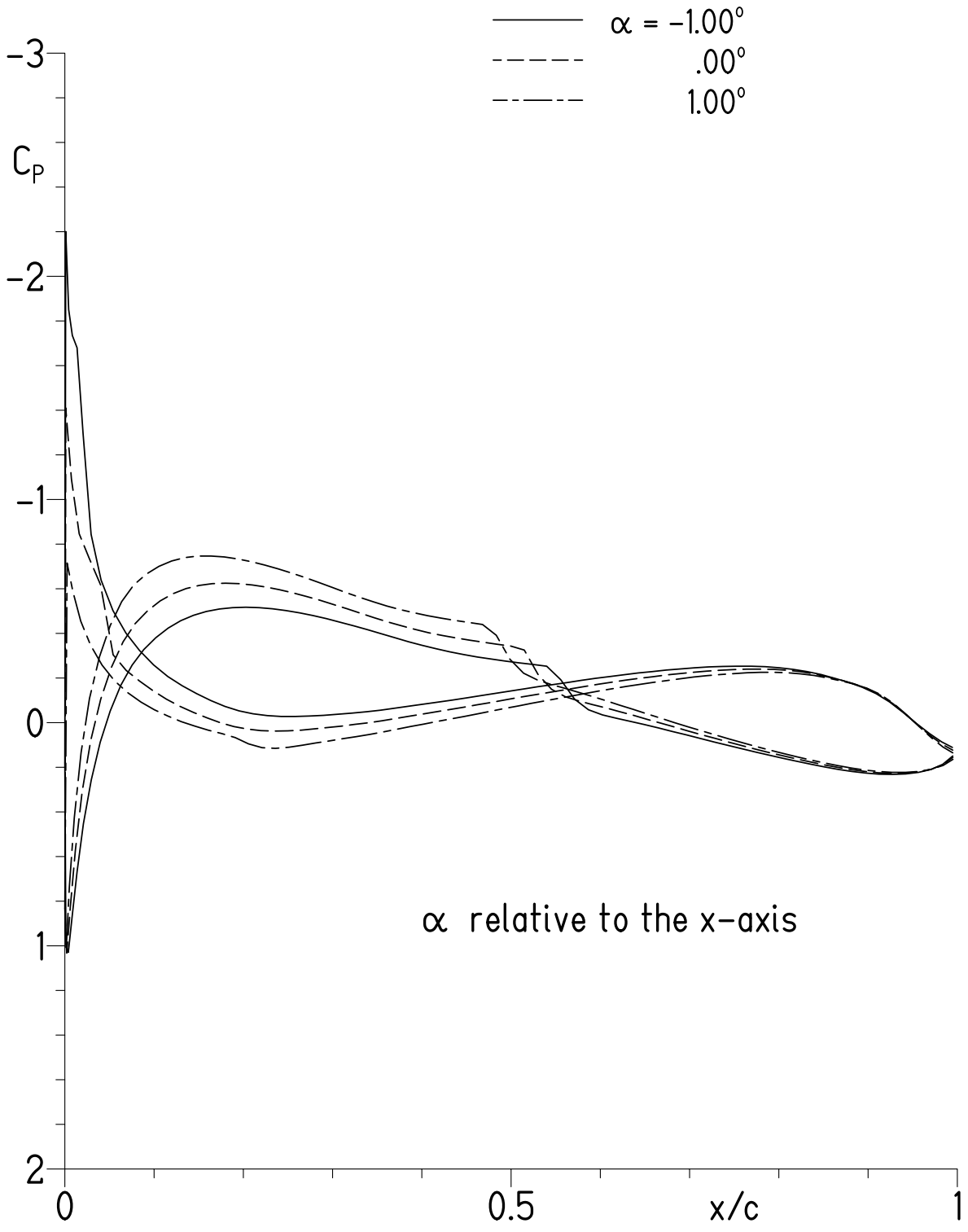

(a) $\alpha = -1.00°$, 0.00°, and 1.00°.

Figure 14.- Pressure distributions for S410 airfoil at M = 0.425 and R = 437,000 with transition free.

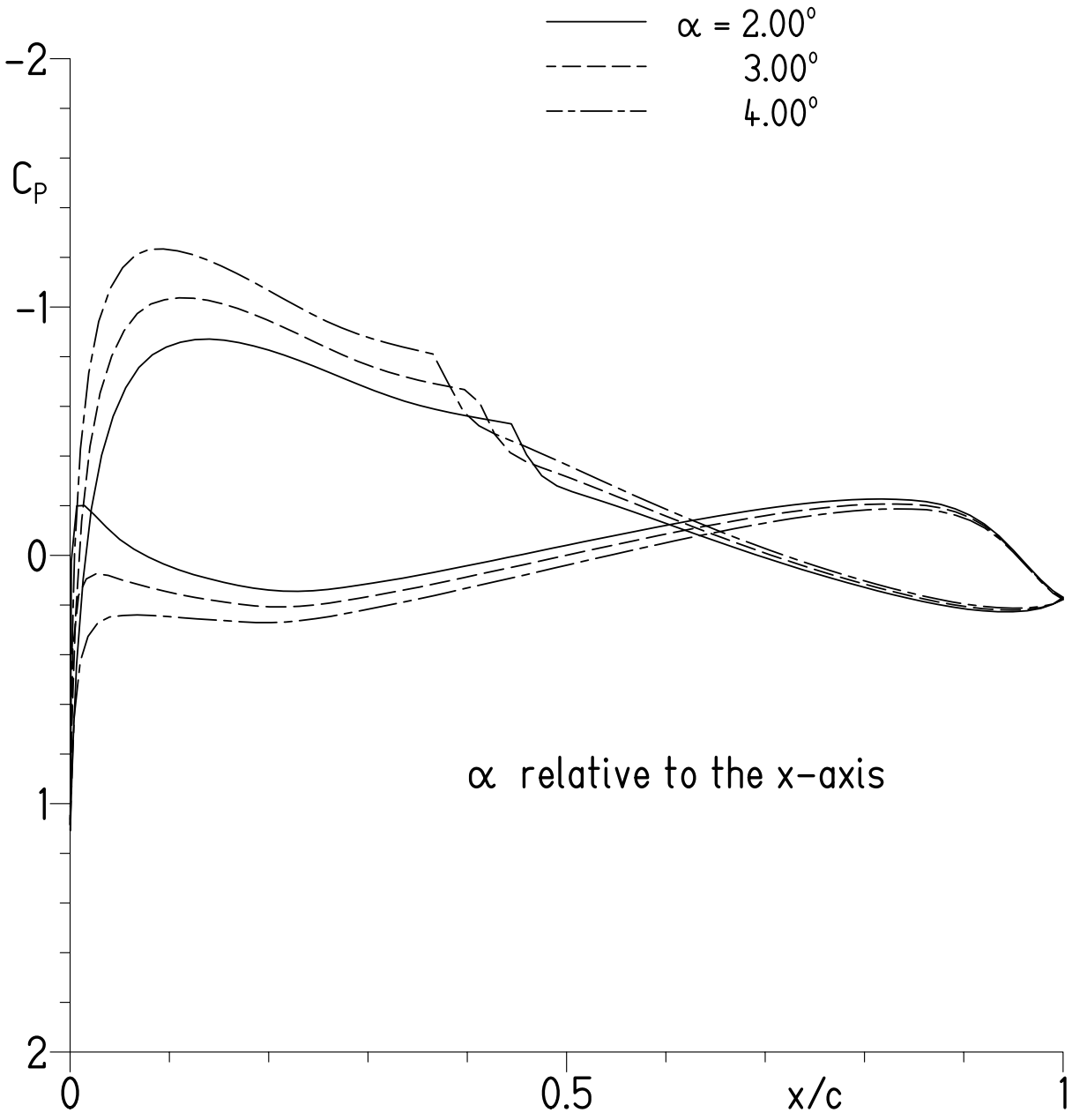

(b) $\alpha = 2.00°$, 3.00°, and 4.00°.

Figure 14.- Continued.

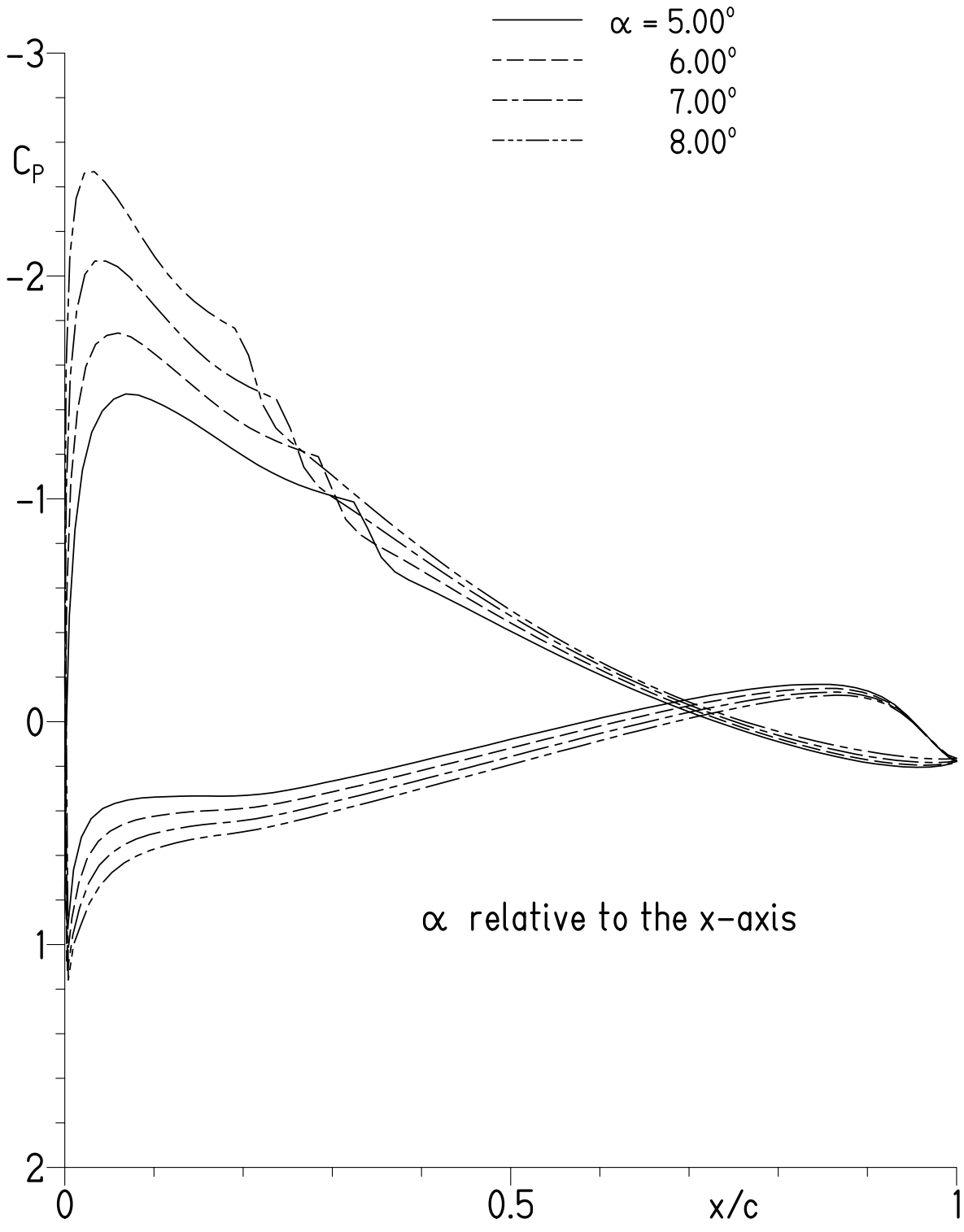

(c) $\alpha = 5.00°$, 6.00°, 7.00°, and 8.00°.

Figure 14.- Concluded.

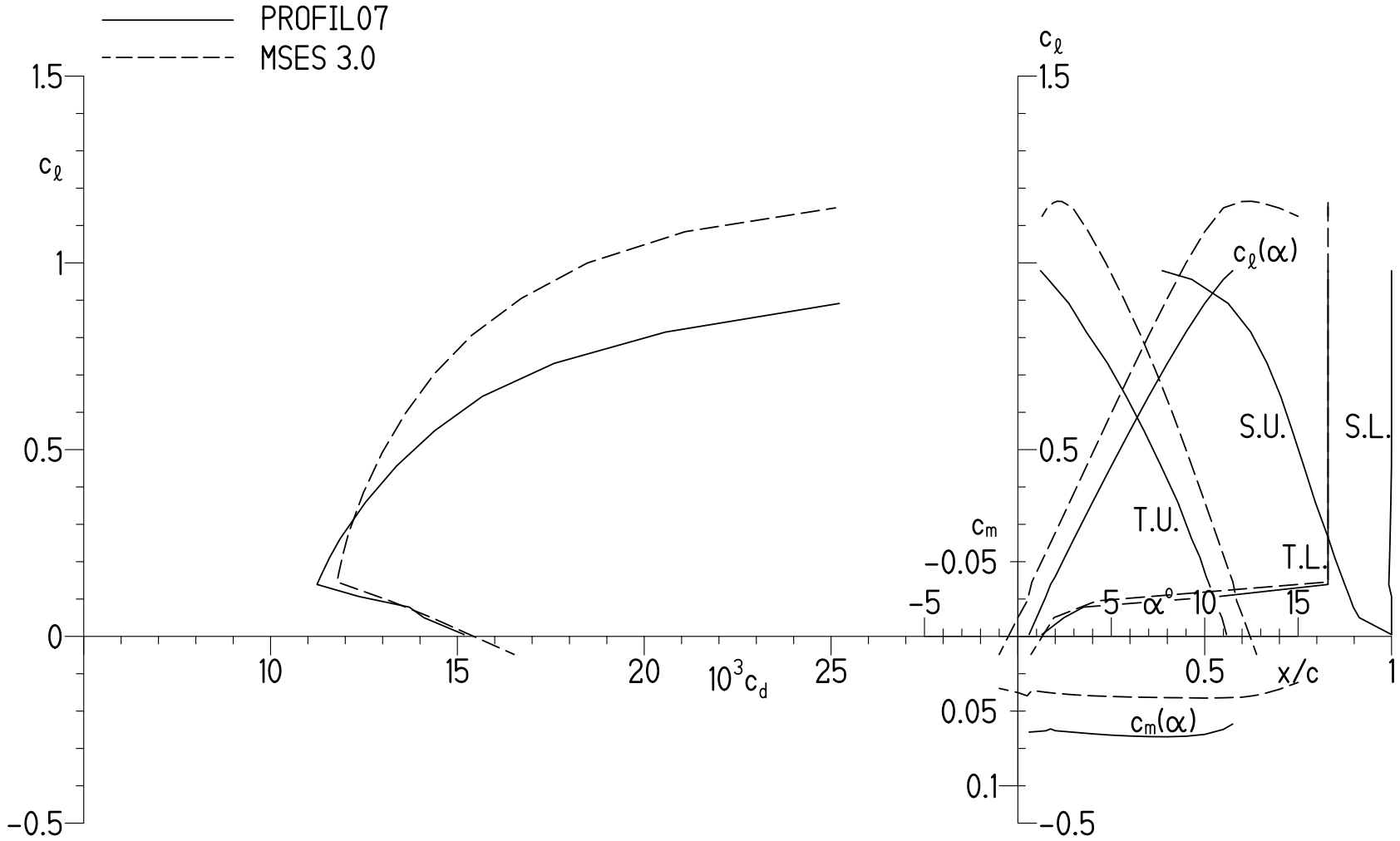

(a) M = 0.18 and R = 185,000.

Figure 15.- Section characteristics of S410 airfoil with transition free.

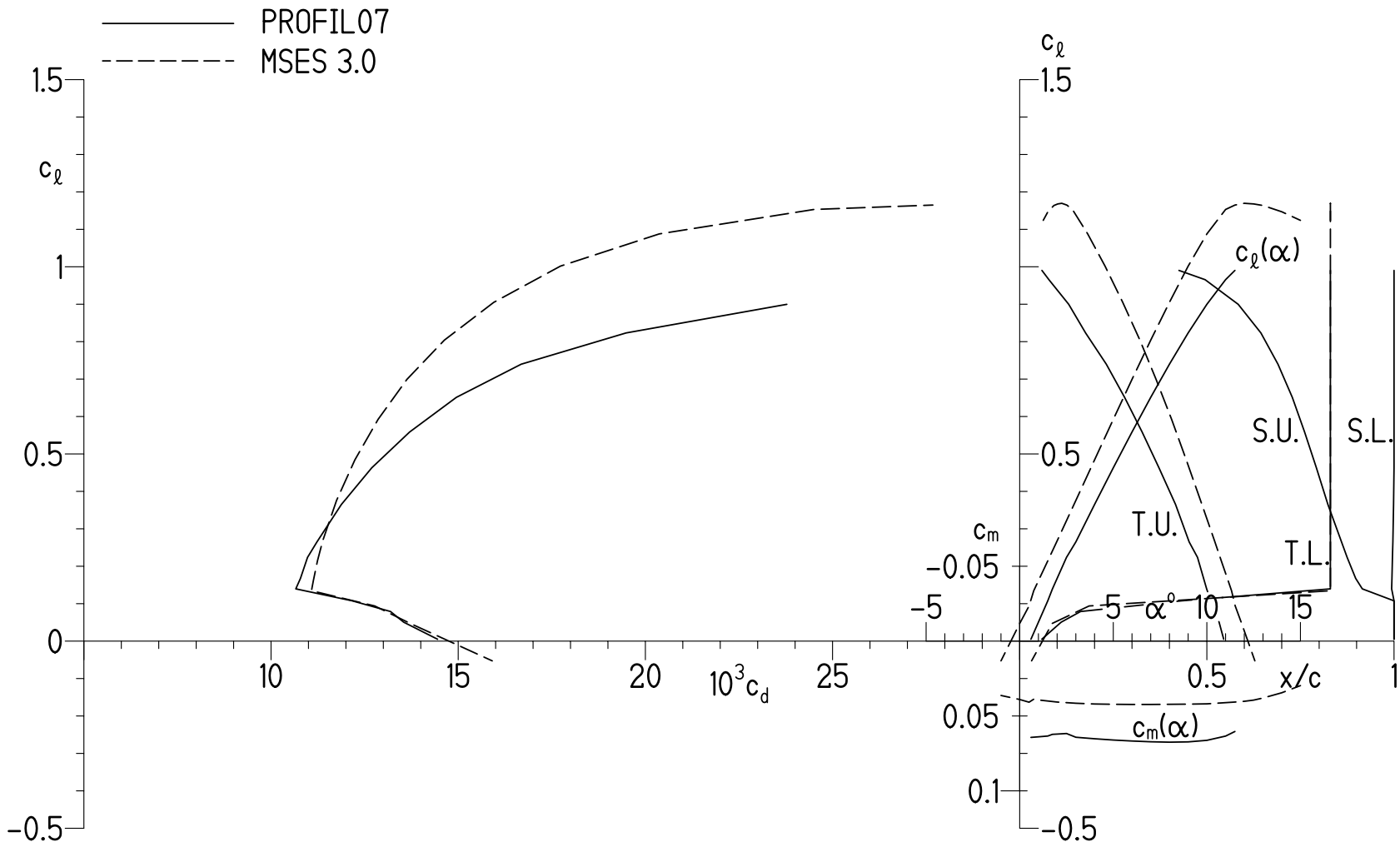

(b) M = 0.20 and R = 206,000.

Figure 15.- Continued.

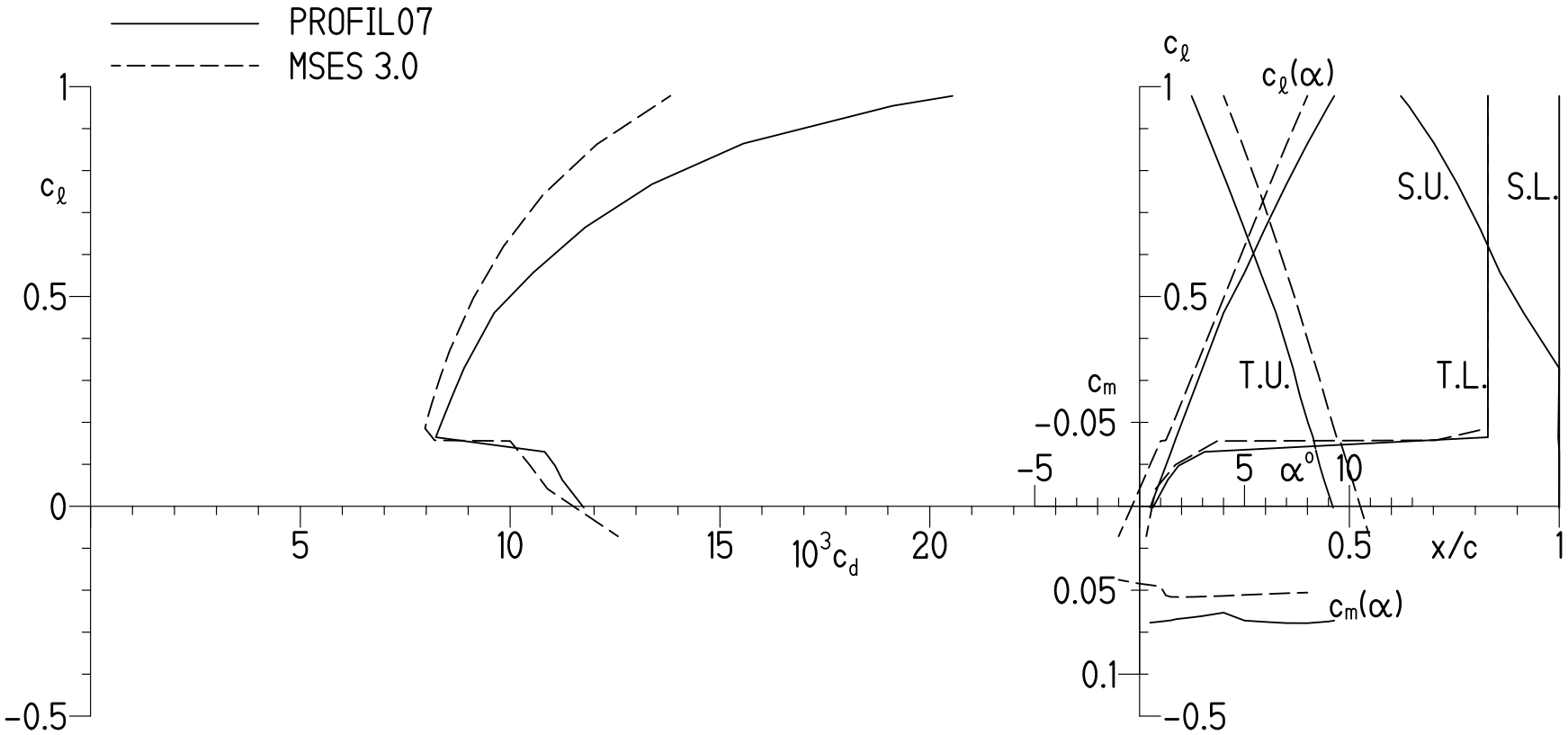

(c) M = 0.425 and R = 437,000.

Figure 15.- Concluded.

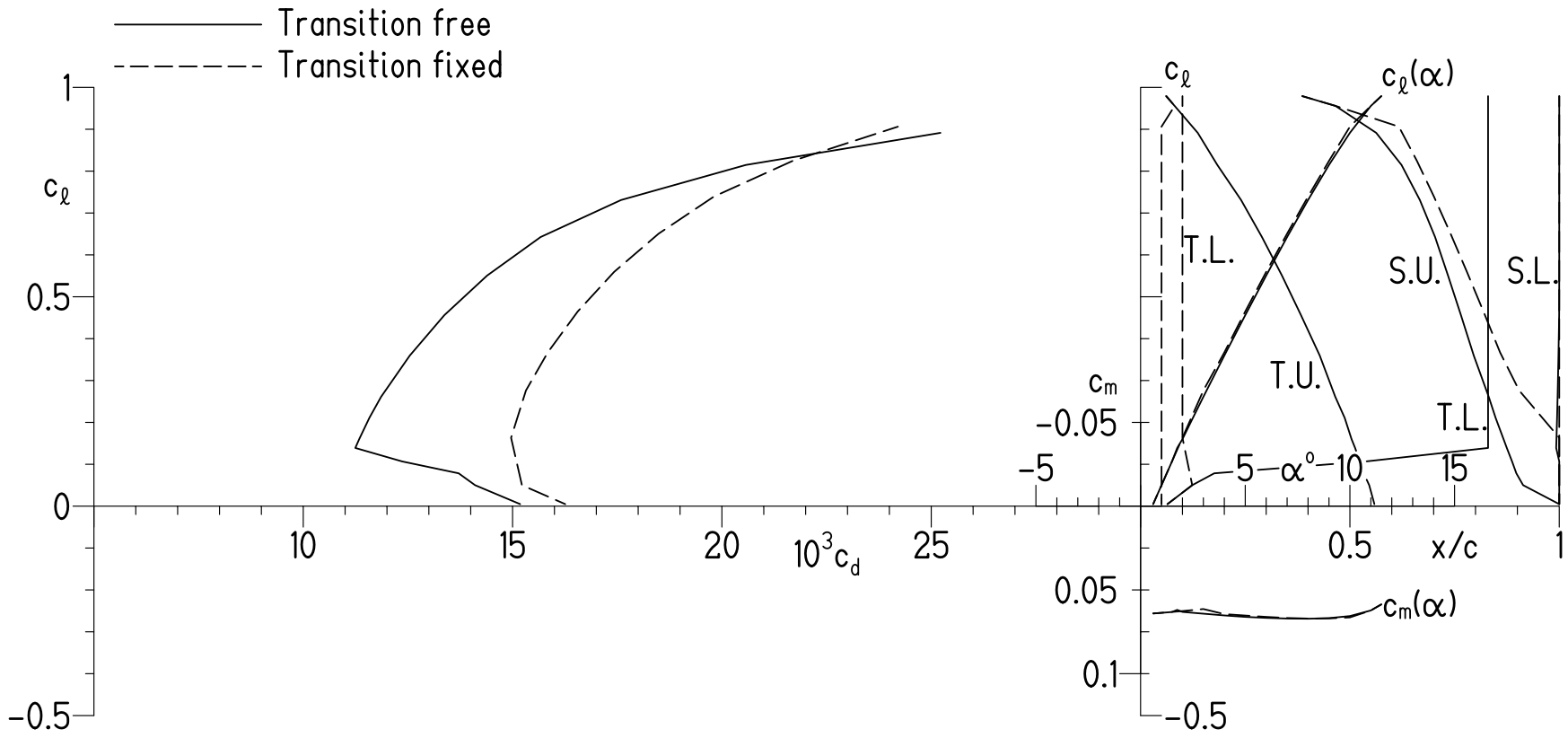

(a) M = 0.18 and R = 185,000.

Figure 16.- Effect of fixing transition on section characteristics of S410 airfoil predicted using method of references 8 and 9.

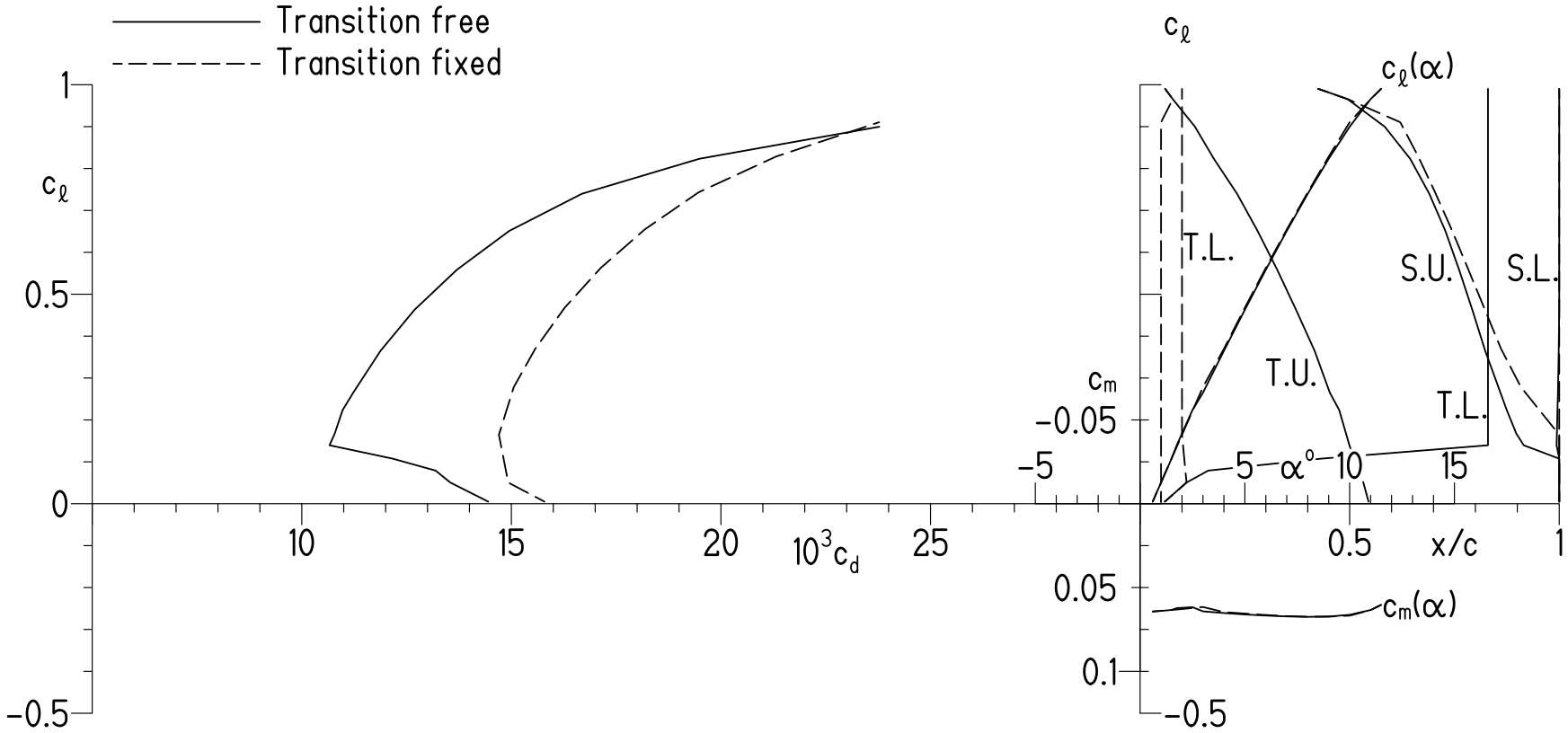

(b) M = 0.20 and R = 206,000.

Figure 16.- Continued.

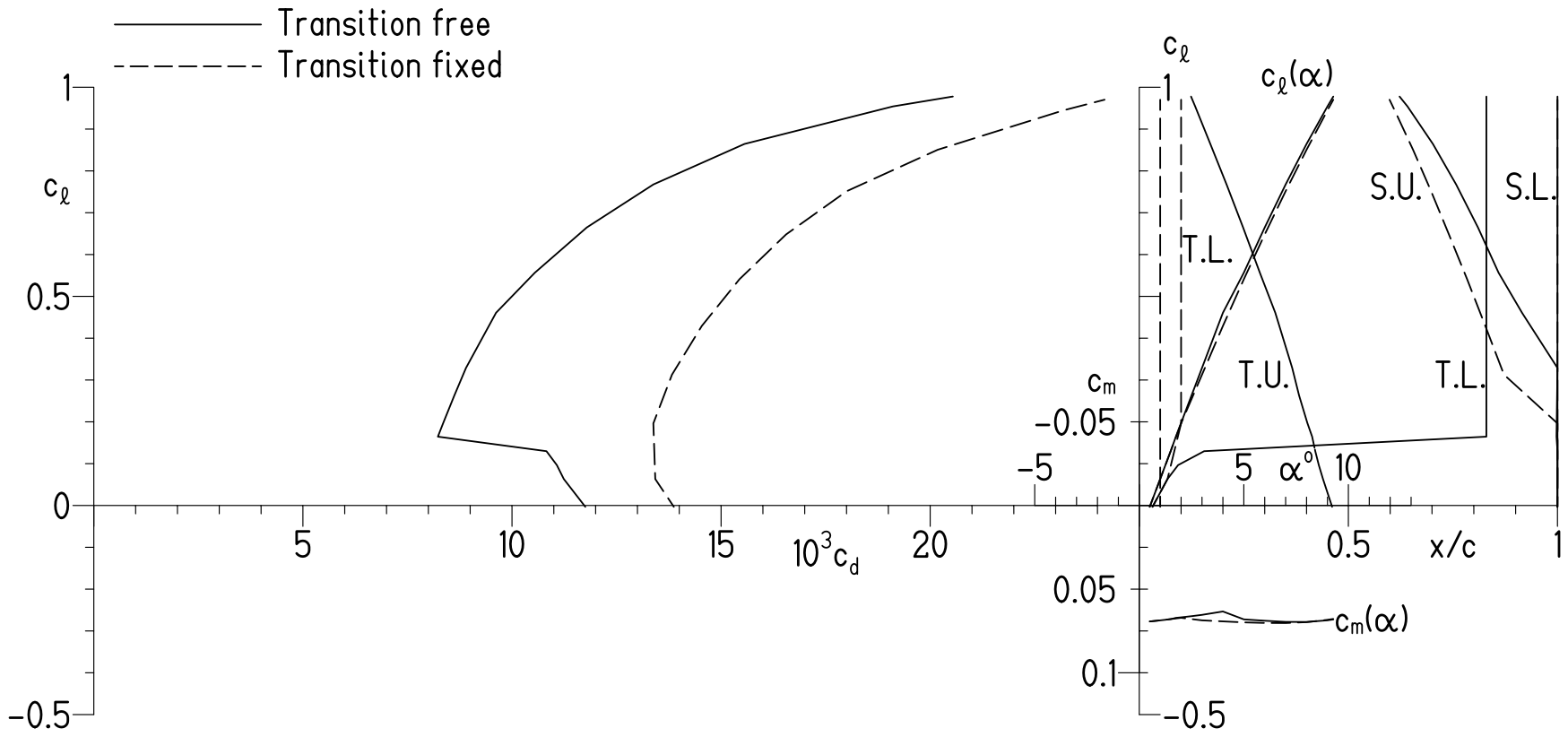

(c) M = 0.425 and R = 437,000.

Figure 16.- Concluded.

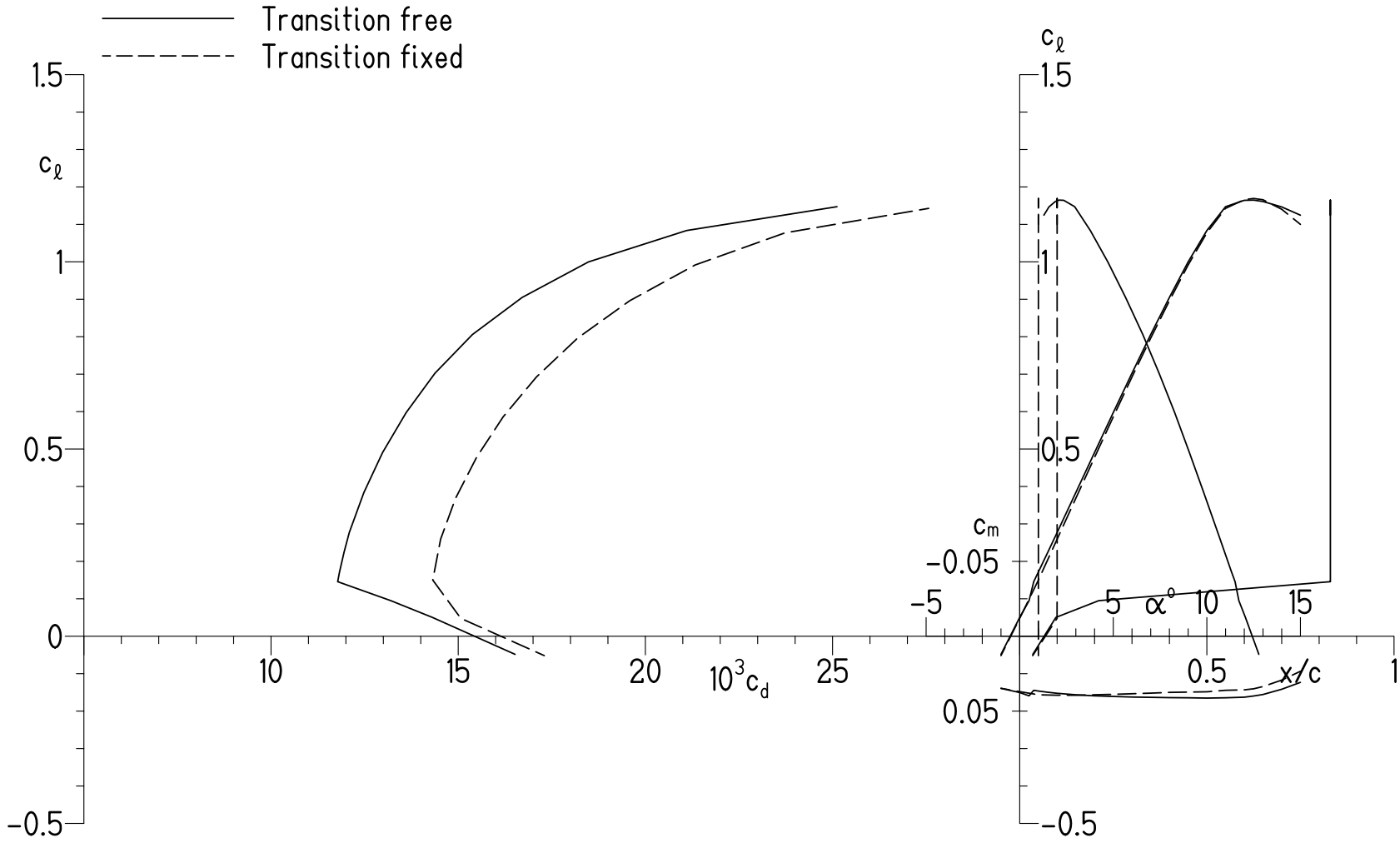

(a) M = 0.18 and R = 185,000.

Figure 17.- Effect of fixing transition on section characteristics of S410 airfoil predicted using method of reference 11.

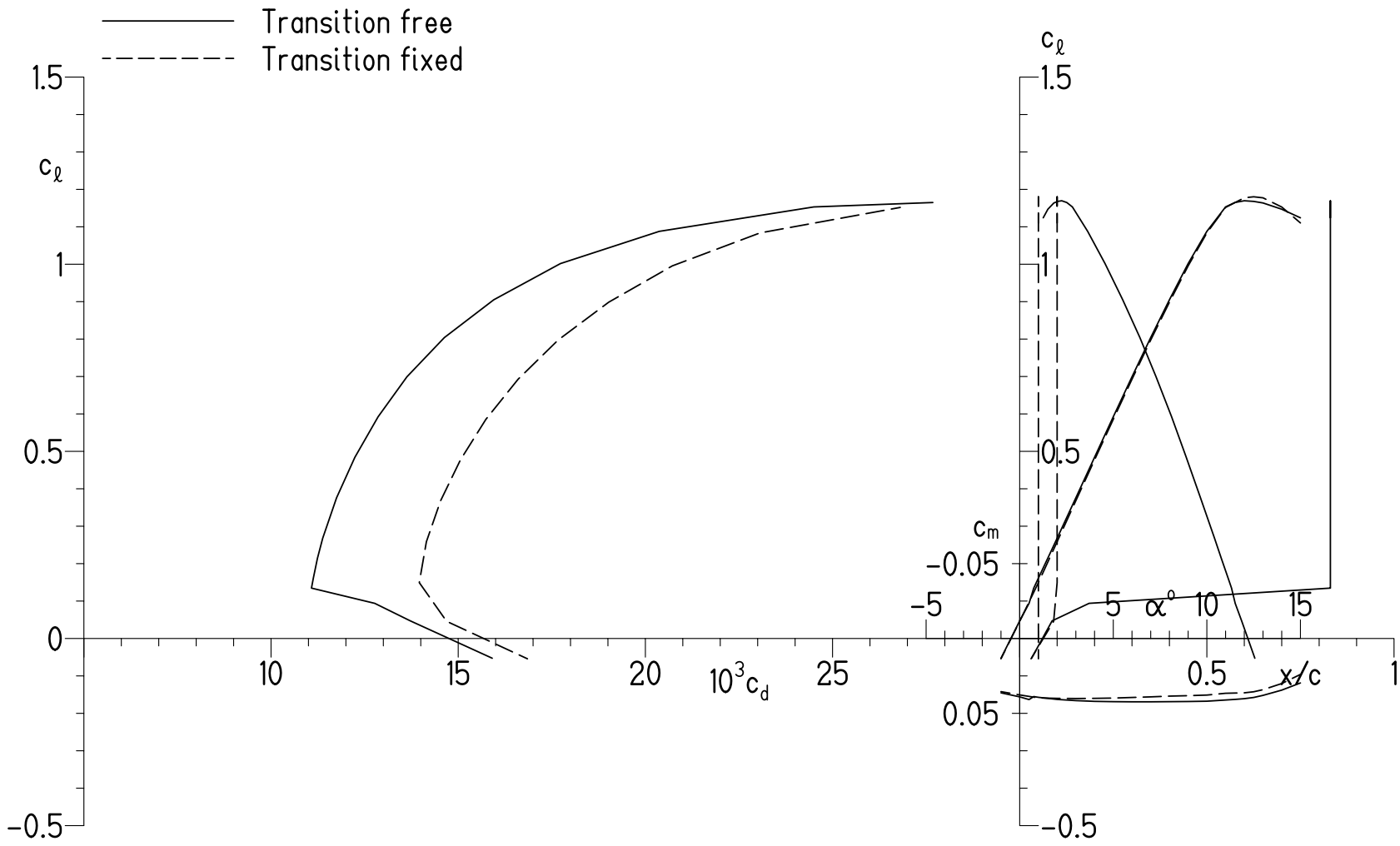

(b) M = 0.20 and R = 206,000.

Figure 17.- Continued.

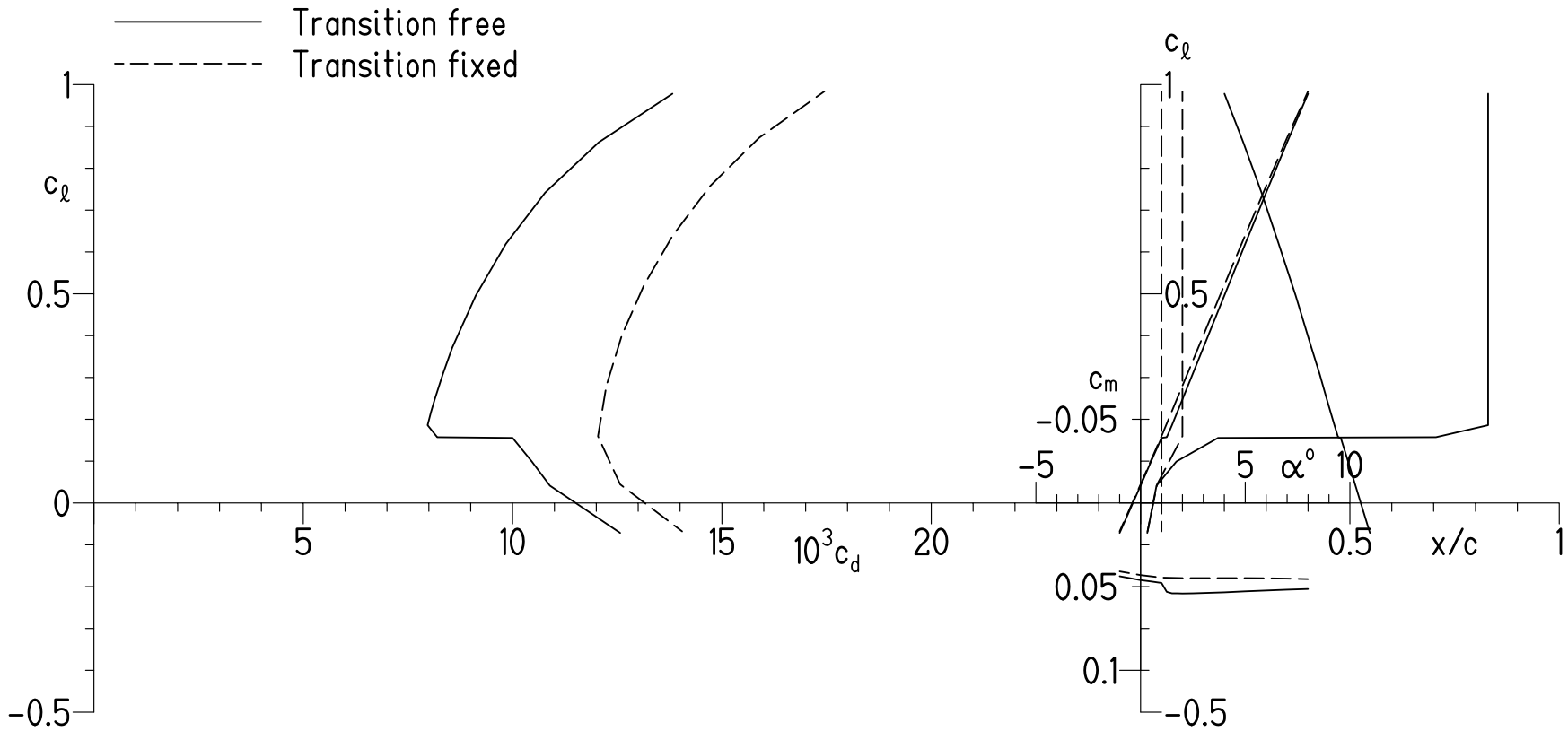

(c) M = 0.425 and R = 437,000.

Figure 17.- Concluded.

REPORT DOCUMENTATION PAGE

Form Approved
OMB No. 0704-0188

1. REPORT DATE *(DD-MM-YYYY)*	2. REPORT TYPE	3. DATES COVERED *(From - To)*
xx-08-2010	FINAL REPORT	Sep 2007 - Jun 2010

4. TITLE AND SUBTITLE

The S407, S409, and S410 Airfoils

5a. CONTRACT NUMBER
W911W6-07-C-0047

5b. GRANT NUMBER

5c. PROGRAM ELEMENT NUMBER

6. AUTHOR(S)

Somers, Dan M.

5d. PROJECT NUMBER

5e. TASK NUMBER

5f. WORK UNIT NUMBER

7. PERFORMING ORGANIZATION NAME(S) AND ADDRESS(ES)

Airfoils, Incorporated
Attn: Dan M. Somers
122 Rose Drive
Port Matilda PA 16870-7535

8. PERFORMING ORGANIZATION REPORT NUMBER

SBIR Topic Number A06-006
Proposal Number A2-2972

9. SPONSORING / MONITORING AGENCY NAME(S) AND ADDRESS(ES)

US Army Aviation Research, Development and Engineering Command (RDECOM)
Aviation Applied Technology Directorate (AATD)
Fort Eustis VA 23604-5577

10. SPONSOR/MONITOR'S ACRONYM(S)

11. SPONSOR/MONITOR'S REPORT NUMBER(S)
RDECOM TR 10-D-108

12. DISTRIBUTION / AVAILABILITY STATEMENT

Approved for public release; distribution is unlimited.

13. SUPPLEMENTARY NOTES

UL Note: No proprietary / limited information may be included in the abstract.

14. ABSTRACT

A family of airfoils, the S407, S409, and S410, intended for a high-altitude, tandem-rotor helicopter has been designed and analyzed theoretically. The two primary objectives of high maximum lift, relatively insensitive to roughness, and low profile drag have been achieved. The constraints on the pitching moments and airfoil thicknesses have been satisfied.

15. SUBJECT TERMS

Airfoils, rotorcraft, laminar flow

16. SECURITY CLASSIFICATION OF:			17. LIMITATION OF ABSTRACT	18. NUMBER OF PAGES	19a. NAME OF RESPONSIBLE PERSON
a. REPORT	b. ABSTRACT	c. THIS PAGE			Dan M. Somers
unclassified	unclassified	unclassified	UU	66	19b. TELEPHONE NUMBER *(include area code)* (814) 357-0500

Standard Form 298 (Rev. 8-98)
Prescribed by ANSI Std. Z39.18